QATAR UNIVERSITY

COLLEGE OF ARTS AND SCIENCES

THE INFLUENCE OF SHEAR STRESS ON NANOMATERIAL'S UPTAKE BY CANCER CELLS

BY

Samar H. Shurbaji

A Thesis Submitted to

the Faculty of the College of Arts and Sciences

in Partial Fulfillment of the Requirements for the Degree of

Masters of Science in Material Science and Technology

January 2020

COMMITTEE PAGE

The members of the Committee approve the Thesis of
Samar Shurbaji defended on [15] [December][2019].

Dr. Ahmed Elzatahry
Thesis/Dissertation Supervisor

Dr.Huseyin Cagatay Yalcin
Co- Supervisor

Dr.Talal Mohammed Altahtamouni
Committee Member

Dr.Asad Zeidan
Committee Member

Dr. Nader AL-Dewik
Committee Member

Approved:

Rashid Al-Kuwari, Dean, College of College of Arts and Sciences

ABSTRACT

SHURBAJI, SAMAR, H.,Masters : January : [2020,]

Material Science and Technology

Title: The influence of shear stress on nanomaterial's uptake by cancer cells

Supervisor of Thesis: Ahmed,A, Elzatahry.

Recently, nanotechnology products have been used for a variety of applications including the medical field. Two dimensional (2D) nanomaterials have attracted a growing interest due to its unique properties and ultrathin structure. One common example is MXene, which can be used for cancer photothermal therapy. In this study, two 2D nanomaterials, MXene and MXene/Au nanocomposite were fabricated as photothermal agents. To mimic physiological tumor microenvironment, nanocomposites were tested on MDA-231 breast cancer cells under fluid shear stress (~ 0.1 Dyn/cm^2) using a perfusion setup. The uptake of these nanomaterials was tested under fluid flow compared to static culture. The uptake was assessed using confocal microscopy, scanning electron microscopy (EDS) and transmission electron microscopy. Furthermore, viability assessment was performed after exposing the treated cells to laser at different power densities and durations by live/dead assay. This study revealed that there is no difference in cellular uptake under fluid flow compared to static culture. Although MXene alone could increase the temperature up to 100 ° C, its cellular uptake is very low (~ 3 ug/ml) which can only increase the temperature up to 44 ° C which is not sufficient to induce protein denaturation and cellular damage.

DEDICATION

To my Father...

ACKNOWLEDGMENTS

First and foremost, I would like to express my sincere gratitude to the Material Science Department at Qatar University and Biomedical Research Center for giving me the opportunity to conduct this research. I would like to thank my supervisor Dr. Ahmed El-Zatahry as well as Dr. Huseyin Yalcin for their continuous guidance and patience. Secondly, I would like to thank Dr. Talal Altahtamoni, the coordinator of material science program for providing me support and help during my master thesis. I extend my heartfelt thanks to Dr. Fatiha, for her ongoing assistance and being always by my side. I would like also to thank Qatar Biomedical Research Institute (QBRI) and Qatar Environment and Energy Research Institute (QEERI as sample preparation for electron microscopy was performed by the research team in the lab of Dr. Abeer Al-Shammari at QBRI. Transmission Electron Microscopy was performed by the Imaging and Characterization Core labs at QEERI. Special thanks to my family and friends for their unconditional support and well wishes. They have played a key role in keeping me motivated in putting forth my best in this project. Last but certainly not least, I would like to express my endless thanks to my special and lovely friend Duaa Al-Sadeq for her kind presence in my life.

TABLE OF CONTENTS

LIST OF TABLES

LIST OF FIGURES

CHAPTER 1

INTRODUCTION AND LITERATURE REVIEW

1 Introduction & Literature review

1.1 Introduction

Cancer is a lethal wide-spreading disease of no definitive treatment. Researchers have been working on cancer therapy for decades; with some improvements; yet, many limitations[1]. Malignant tumors are categorized into, solid-localized tumors or metastatic tumors[2]. Localized tumors like in breast cancer, are mostly removed by surgery combined with chemotherapy or radiation therapy[3]. Although these are the most applied treatments, they are limited by the incomplete removal of the tumor by surgery which leads to tumor recurrence[4]. Furthermore, chemotherapy and radiation therapy suffer from many side effects like hair loss, nausea and bowel issues. To overcome these limitations, nanomaterials were extensively studied as targeted drug delivery for cancer therapy[5]. One of these materials is Ti2C3 also known as MXene, which is a 2D material where M stands for an early transition metal, X is carbon or nitrogen and -ene is just like in graphene which is the first 2D material discovered. MXene was studied for many biomedical applications including tumor detection (i.e. as contrast agents), cancer therapy, drug delivery, and antimicrobial effect[6]. Additionally, MXene was shown to have a photothermal effect, which means that they can convert laser light energy to heat energy by surface plasmon resonance effect. MXene was studied for cancer photothermal therapy by many researchers, who focused on killing cancer cells by heat leading to protein denaturation and eventual cell death[7,8]. Many of these studies were conducted using cells in static culture, and did not consider the tumor biophysical microenvironment, which is associated with fluid flow and shear stresses[9]. The oversimplified system in static culture might lead to misleading results, which in most cases contradict results obtained from an animal model. This is because

cells under fluid flow behave differently than in static culture due to activation of flow responsive pathways that might influence their cellular adhesion and nanomaterial uptake[10,11]. Photothermal therapy, which kills the cancer cells by heat, might remove the tumor completely hence more superior compared to surgical removal. However, photothermal therapy can still induce side effects, if the material is not fully internalized by cancer cells[12]. Although MXene showed a good photothermal efficiency which makes it a good candidate for photothermal therapy, MXene internalization by cancer cells was not studied extensively. Fluid flow in cell culture can influence the way that the cell uptake the nanomaterials. It has been shown by some studies that under fluid flow, material uptake becomes more than in static culture which enhances the therapeutic approach[13].

In this work, MXene and MXene/Au nanocomposite were prepared and characterized for photothermal ablation application. Their uptake by MDA-231 breast cancer cells was studied for static and dynamic cultures.

Chapter 1 includes a literature review about cancer, MXene as a photothermal agent and cell behavior under fluid flow in terms of nanomaterials uptake. Chapter 2 has experimental section on how this research was conducted. Lastly, chapter 3 comprises the results and discussion.

1.2 Objectives

The main objectives of this thesis are as follows:

- To produce and characterize MXene and MXene/Au nanocomposites and compare their photothermal efficiency.
- To compare MXene internalization by MDA-231 breast cancer cells under fluid flow and static culture
- To test the viability of shear exposed cancer cells after MXene and laser irradiation under different conditions.

1.3 Nanobiotechnology- overview

It has not been long after Richard Feynman`s lecture about nanotechnology in 1959 in which he gave a foundation about nanotechnology and miniaturization of materials [14]. Since then, nanotechnology products i.e. nanomaterials have been used and studied extensively for various applications, including the medical field [15]. Nanotechnology does not have a specific definition, but it can be described as the technology that deals with nanometer-sized objects (10^{-9th} of meter) [16]. When the power of nanotechnology for instance nanomaterials are used for biomedical applications, it is termed as nanobiotechnology or bionanotechnology to indicate the combination of nanotechnology with the biological system [17]. Nanobiotechnology was applied in many medical branches including drug delivery by the production of nano-pharmaceuticals, contrast agents for magnetic resonance imaging, tissue engineering as well as photothermal therapy for cancer treatment. Nanomaterials are mostly used due to their extremely small size and high surface area to volume ratio, which enable these nanomaterials to penetrate cells and tissues. Furthermore, they have a better surface interaction. additionally, nanomaterials usually have enhanced properties like mechanical and optical properties [18]. One major disease that can potentially benefit significantly from nanobiotechnology is cancer, for which the current therapy suffers from low efficiency and specificity.

1.4 Cancer and solid tumors

1.4.1 Overview of cancer

Cancer creates an uncontrolled division of abnormal cells in part of the body. Each healthy cell is subjected to differentiation, division or cell death as a part of normal cell life. These processes are highly controlled by certain signals in the cell cycle. In some situations, these signals are disregarded; resulting in the uncontrolled division of unhealthy cells, which can rapidly grow and form lumps and localized tumors. Cancer cells in localized tumors can then spread to other body parts in a process known as metastasis. Metastasis is usually associated with poor prognosis, which makes the treatment more difficult. These cancer cells are characterized by their immortality, metastasis, resistance to cell death and they induce new blood vessels formation which is also known as "angiogenesis"[19].

Cancer is not a new disease, as there are evidence of bone cancer in ancient Egyptian mummies 1600 B.C. Also, a description of breast cancer was reported in ancient Egyptian book 1500 B.C. The term cancer was first called by Hippocrates – a Greek physician 460-370 B.C. Hippocrates named the diseases cancer to mean a "crab" due to the finger-like projections of spreading cells [20]. Nowadays, cancer is the second leading cause of death after cardiovascular disease with 9.6 million related deaths worldwide based in 2018 statistics [21], and in 2014, there were approximately 1,412 patients diagnosed with malignant cancer in Qatar only[22].

1.4.2 Cancer pathogenesis (disease development)

There are different types of cancers, all the types share common characteristics such as cancer cells being immortalized, and for continual growth and division. Around 85% of cancers are solid tumors. Some of these solid tumors start growing in one region of the body, and then some cancer cells travel through blood stream and grow in another region. There are other types of cancer that are not solid, for example Leukemia which

is also known as blood cancer[23].

Cancer is influenced by both environmental and genetic factors. It can occur when a normal healthy cell, acquire a mutation and change in the normal DNA sequence. These mutations are acquired due to different factors, including genetic and environmental factors such as exposure to carcinogens or smoking. These cells will continue growing, and will appear morphologically normal at the beginning. However, after some time, they will gain additional mutation that makes them out of control as they will grow indefinitely. Cancer cells depend on normal blood vessels when they are small in number, but as the tumor starts growing, cancer cells will release factors to induce new blood vessel formation to satisfy the tumor survival needs (oxygen and nutrients), which is known as angiogenesis [23] **Figure 1**.

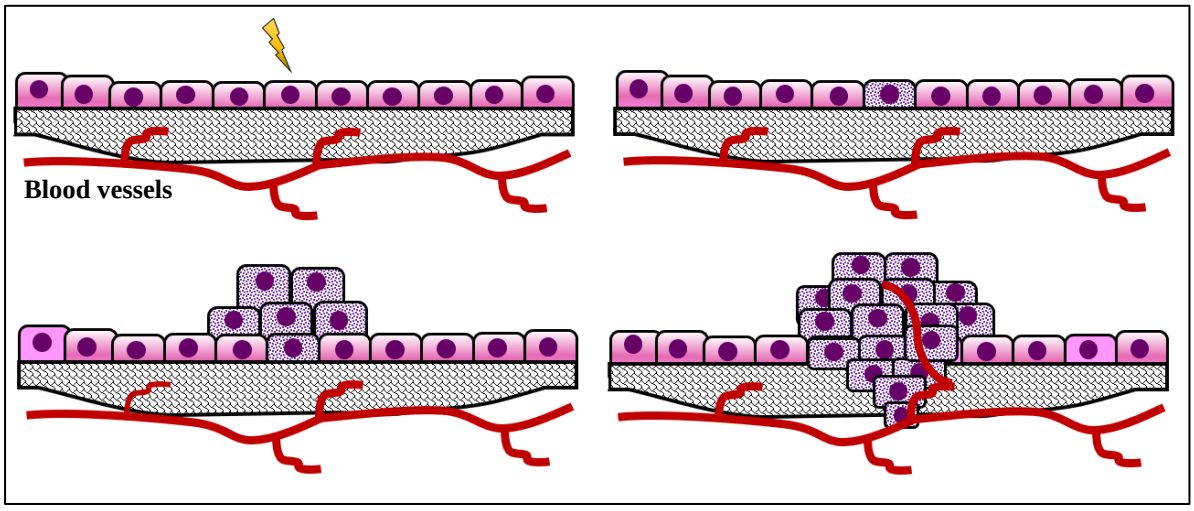

Figure 1: *Stages of cancer development****(A&B)*** *A cell or group of cells acquire mutation.****(C)****The mutated cells will grow in number.****(D)*** *Cancer cells will uncontrollably grow and induce new blood vessels formation.*

Cancer cells in a localized tumor can travel through the blood stream to other sites and form another solid tumor. The delay in tumor diagnosis will lead to tumor spread, worsening the condition, as for 90% of cancer-related deaths are due to metastasis. The mechanism in which cells can travel to other sites is not well understood. In most cases cancer cells physically break away from the original tumor and lodge the lumina of blood vessels [24].

1.5 Cancer therapy approaches

Currently, cancer is mainly treated by surgery, chemotherapy or radiation. Surgery is effective for localized tumors. However, it is difficult to assess complete removal of tumor with surgery. [25]. Surgery is limited to its invasiveness also it is associated with cancer reoccurrence if the tumor is not removed completely [7].Chemotherapy is another approach for cancer treatment. Chemotherapy involves administration of chemical drug through blood circulation. These chemicals kill highly dividing cells; mostly cancerous cells, but it also has toxicity to normal cells which divide at high rate such as hair follicles. Thus, chemotherapy has many side effects such as hair loss and anemia. Moreover, cancer cells can develop resistance to the drug [26]. Radiation therapy is often used as a complementary treatment with chemotherapy. It mainly depends upon the use of source of high energy ionization particles such as x-rays or gamma rays to destroy cancerous cells [27]. Both chemotherapy and radiation are limited as the tumor site is poorly vascularized and the drug cannot reach the tumor site homogenously[23].

Photodynamic therapy is a new approach to treat cancer, mainly by using a photosensitizer (i.e. a dye that can be converted to another molecule when exposed to light at certain wavelength). When a photosensitizer gets excited by light, it will interact with another molecule such as lipids or polymers. This interaction will transfer the hydrogen atom via radical mechanism, thus producing free radicals. In the availability of oxygen, these free radicals will interact with oxygen, producing reactive oxygen

species which can destroy cancerous cells by oxidative damage. This approach is limited as the cancerous microenvironment is poorly vascularized and highly hypoxic, which means that the oxygen content is limited which restrict the formation of reactive oxygen species [28].

1.5.1 Photothermal therapy for cancer treatment

Temperature is an important parameter in human body. Normally, cells function at 37 ºC and an increment in body temperature can lead to cellular damage. Hyperthermia (i.e. high temperature) has been known as a treatment of multiple diseases for several decades[29]. In fact, Hippocrates- a Greek physician- mentioned about burning the tumor as a cancer treatment. He mentioned that if the tumor cannot be burned, then it has no cure[30]. Moreover, it was shown that, when cancer patients get fever, their tumor decrease in size[29].

Photothermal therapy (PTT) is the destruction of cancer cells by heat. PTT involves two techniques: hyperthermia and thermal ablation. The difference between these two techniques is the temperature range and the exposure time. While hyperthermia involves increasing the temperature up to 42 °C for a long time, thermal ablation involves the increment of temperature to more than 42 °C for only few minutes. It was shown that cancer cells can be killed when they are kept at at 42 °C for 15 minutes to 1 hour. This can be improved by increasing the temperature to more than 50 °C for few minutes[31].

There are different energy sources that can be used to induce thermal ablation, such as radiofrequency, microwave and laser. Laser-induced thermal ablation was used previously but it is considered as a non- reliable technique because it is difficult to direct the laser to the tumor without influencing the nearby tissues. To improve the selectivity of photothermal therapy, a photothermal agent should be used.[32]

1.5.2 Photothermal agents

A photothermal agent (PA) is a material that can convert light into heat. This material must be biocompatible as it should not induce toxic effect to the body. Furthermore, it should be able to absorb near-infrared radiation (NIR). There are several PA, and they can be classified as organic and inorganic materials[33].

Inorganic materials include several substances, but most commonly metallic materials like gold (Au) and carbon-based materials such as carbon nanotubes. The organic materials include polymeric based nanoparticles and organic dyes[34]. Metallic nano-materials have a phenomenon known as localized surface plasmon resonance (LSPR) which enables them to generate heat upon light exposure[35].

1.5.3 Examples of PA

Au based nanomaterials

Silver nanoparticles are considered as strong PA but, they are not used for PTT due to their high toxicity in biological system[36]. However, gold nanomaterials in their different forms (nanoparticles, nanotubes, and nanocages) are highly efficient and safe for the human body, and they were used for a variety of biomedical applications[37,38,39]. Au nanoparticles were used for plasmonic effect applications since the 1970s. The surface plasmon resonance (SPR) frequency is dependent on the size and shape of the gold-based nanomaterial. For example, it was theoretically simulated the photothermal efficiency of gold in different shapes and sizes. It was found that, the most efficient is gold nanospheres with a diameter of 30-40nm[40] . Gold nanorods were also efficient with a length of 15-70 nm. Au based nanomaterials must be designed to absorb light in these regions (650-850nm) or (950-1350nm) [37]. These wavelengths can penetrate through tissue to reach Au NPs in tumor without affecting the normal tissue. Au NPs can efficiently absorb light in these wavelengths and induce the photothermal effect[29]. Different studies tested the efficiency of Au based nanomaterials. For example, Pattani

and coworkers, tested the photothermal efficiency of Au nanorods on human colorectal carcinoma cells after applying laser in the NIR region. They found that, Au nanorods have a maximum killing competence of cancer cells, which is related to the internalization and plasmonic effect of these particles[36]. In another study conducted by Okuno and colleagues, Au nanorods were tested on tumor tissue in mice. It was found that, treatment with Au nanorods led to partial destruction of the tumor, as the tumor is viable and able to regrow [41].

MXene

MXene is a new family of 2D materials that were produced first by Drexel University scientists in 2011[42]. It was designed by etching the aluminum from a MAX phase using hydrofluoric acid (HF) or HF containing etchants, to break the strong bond between M and A elements **Figure 2**.MAX phases are layered ternary carbides and nitrides, which are the precursors in which MXene is produced. Here, M is an early transition metal, A is group 13 or 14 from the periodic table, and X is carbon or nitrogen. MXenes have a general formula of $M_{(n+1)}X_n$, the suffix -ene is added to indicate the similarity between the material and graphene. The resultant 2D MXene from the chemically etched MAX phase has a functional group of -OH -F and -O with a formula of $M_{(n+1)}X_nT_x$ [43]

Ti_3C_2 MXene was recently used for biomedical applications, as their surfaces can be functionalized to be used for certain applications. For example, MXenes produced by HF etching have (-OH) group in their surface, which can be used to adsorb positively charged molecules such as drugs. Therefore, MXenes can be used for drug delivery [44].

MXene has an excellent absorption in the NIR region, thus can be used for biomedical applications especially for PTT [45].Ti_3C_2 has a 100% photothermal

conversion efficiency when laser sources of 473 and 785 nm are applied[46].

Lin, Chen, & Shi tested MXene modified with soybean phospholipid on breast cancer cells (4T1). They found that MXene induced major cell death in the treated group at a power density of 1 W/cm^2 when incubated for 4 hours at a 100ug/ml concentration. They tested different concentrations upon laser exposure, and found that viability was reduced as the concentration of MXene increased, An in-vivo study in mice demonstrated a size regression on the tumor after the laser exposure, which suggests that MXene can be used in the future as an PTT agent.. Lin, Chen, & Shi compared the PT property of soybean phospholipid modified and non-modified MXene, and suggested a nonsignificant difference in PT activity between both materials[48].

Another study by Liu et al., showed, injection of Doxurbicn" DOX "(cancer drug) loaded MXene resulted in a complete tumor regression as compared to less efficient effect when MXene or DOX was used alone[44].

Mixing of Mxene with other materials were shown to improve the acticity.. For example, MXene prepared with Polyvinyl alcohol and carbon nanotubes were used for energy storage applications[49]. Au/MXene nanocomposite was prepared by Rakhi, Nayak, Xia, & Alshareef for glucose biosensor applications[50]. However, there is no study on MXene composites for PTT applications. As both MXene and Au are considered as good photothermal agent when hybridized, MX/Au nanocomposites are expected to have an enhanced photothermal efficiency, which was tested in this work.

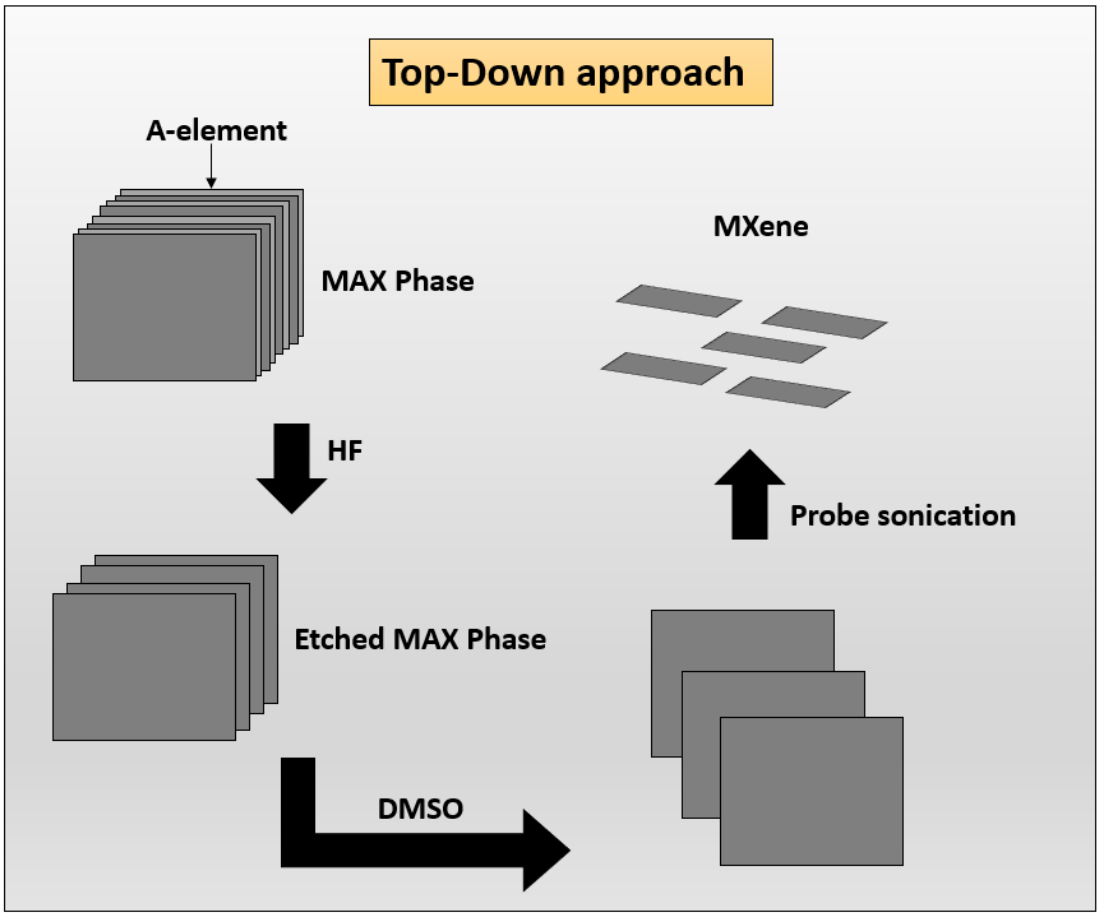

Figure 2: *Top down approach for MXene production.*

1.5.3 Principle of photothermal therapy

LSPR is present in metallic nanoparticles such as Au, Ag and Cu[51]. It occurs due to the oscillations of the conductive free electrons because of the electric field of the incident light. These oscillations lead to charge separation and formation of dipole oscillation **Figure 3** [40]. The oscillations can reach maximum at a certain frequency, which is also known as the surface plasmon resonance (SPR). These SPR support the light absorption of the noble metal nanoparticles[37].

When the photothermal agent absorbs the light energy (near-infrared NIR between 650 and 900nm), the free electrons in the conductive band gain energy and get excited. These electrons move from the ground state to the excited state, which

is followed by a non-radiative relaxation. This leads to heat generation in the medium surrounding the photothermal agent as the kinetic energy is increased. The generated heat will lead to tumor cell death and tissue damage due to protein denaturation **Figure 4** [52].

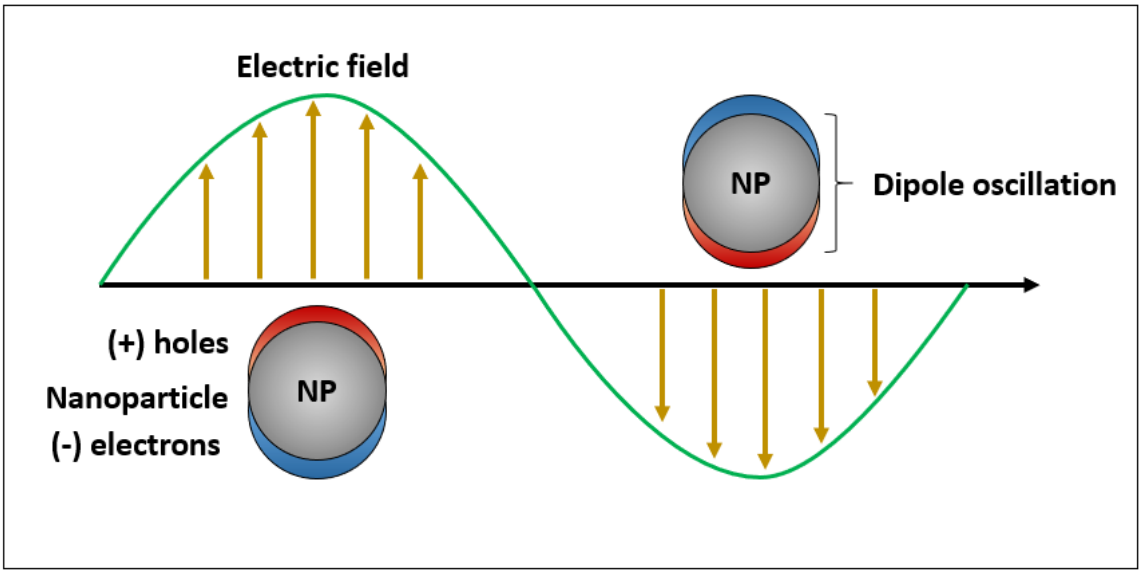

Figure 3: *LSPR and formation of dipole oscillation when exposed to light or electric field*

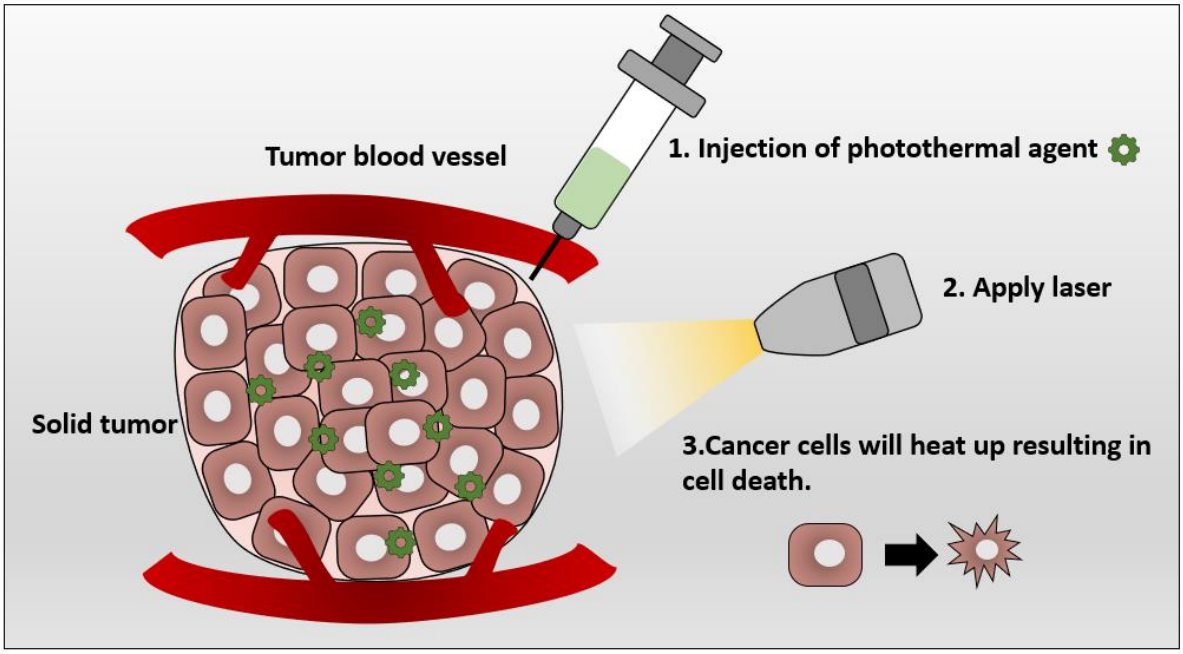

***Figure 4**: the general principle of PTT*

When PT agents are produced, they are tested initially using in-vitro cell culture (static culture). The problem with this approach that it lacks the realistic physiological tumor environment such as fluid flow and shear stresses. These parameters influence the cell mechanics and can change cell behavior towards nanomaterial's uptake and toxicity.

1.6 Cancer cell mechanics

1.6.1 Tumor biophysical microenvironment

Cancer cells undergo different forces and mechanical stresses, such as compressive forces due to tumor growth. Additionally, interstitial pressure and shear stress due to blood and interstitial fluid flow [53]. The biophysical microenvironment of tumor cells is different from what normal cells experience. For instance, blood flow in cancer microenvironment is irregular in comparison to normal circulation. This causes the tumor to be less oxygenated as the tumor

grows[54]. Furthermore, the tumor site (extracellular fluid) is more acidic compared to normal tissues [55]. The extracellular environment accompanying the tumor has an influence in which tumor cells interact with their surroundings. For example, shear forces in the extracellular environment can activate some cellular processes as well as influence the way in which cells uptake certain drugs and nanomaterials[56].

Fluid shear stress (FSS) is the frictional force experienced by the cells due to fluid flow. In biological systems, FSS, can occur as a result of blood flow, interstitial fluid flow, or lymphatic fluid flow. Cancer cells mainly encounter interstitial fluid flow in localized tumor at first and blood flow in case of metastasis[57]. Tumor cells can also encounter other body fluids, for example, shear stress in peritoneal cavity due to fluid flow in ovarian cancer[58].

1.6.2 Shear stress due to blood flow

Circulating tumor cells (CTC) or metastatic cells are cancer cells that shed from the localized primary tumor and migrate to another body site through blood stream[59]. These cells experience FSS due to blood flow [60,61]. Studies showed that, CTC can be influenced by FSS in two ways, either the cell cycle will be arrested in these cells due to mechanical force[62] or FSS will activate certain cellular processes, resulting in migration of these cells and invasion of other organs[63].

1.6.3 Shear stress due to interstitial fluid flow

In normal tissues, the way that cells get nutrition is through diffusion of the blood plasma to the stromal space near the cells (known as the interstitial space). The cells excrete wastes by diffusion of waste products to the nearby lymphatics to be drained in the venous blood stream[64] **Figure 5.**

In normal situations, the flow of interstitial fluid is only by diffusion of nutrients from blood stream to the interstitial space, and waste products from the cells to the interstitial space, to the lymphatic vessels. This mechanism prevents the fluid

accumulation in interstitial site. The situation is different in cancer microenvironment. As cancer cells keep growing, it becomes difficult for cancer cells to support good waste drainage, so the fluid will be absorbed from the blood vessels, but it will not be drained back to the venous system. This fluid accumulation will result in pressure difference between cancer microenvironment and healthy tissue, resulting in fluid flow from cancerous tissue towards surrounding tissues [64]. The flow of interstitial fluid was shown to induce FSS to the cancer cells within the localized tumor[65] with a shear rate of 0.1 (dyn/Cm^2)[56].

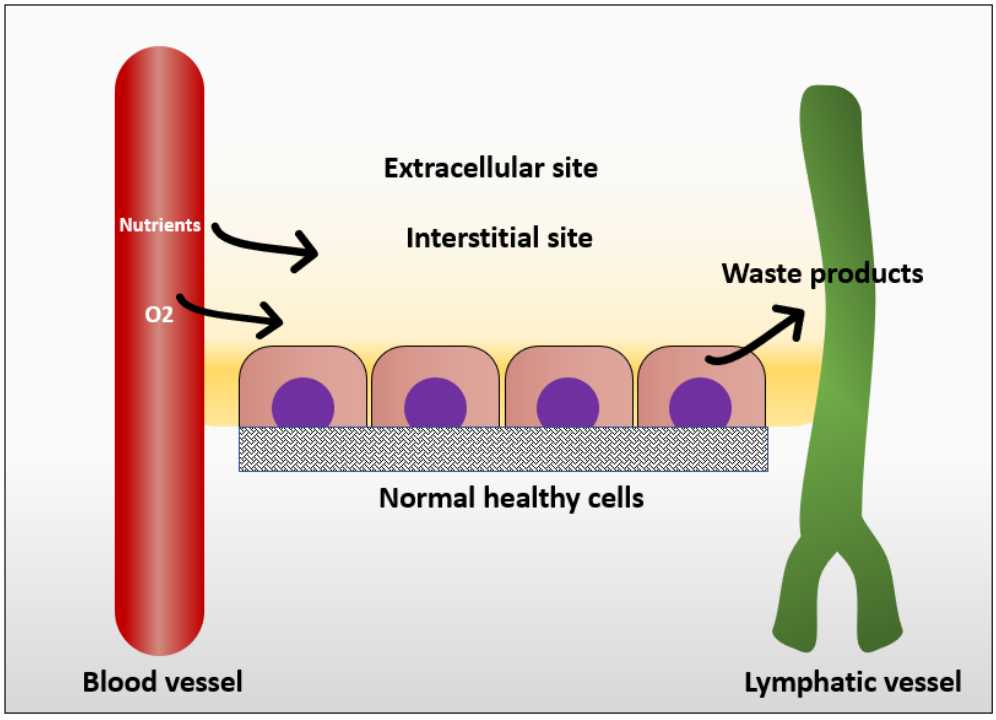

Figure 5: *Mechanism in which normal cells get their nutrients and excrete their wastes.*

Interstitial flow is different from blood flow in that it occurs at much slower velocities. The interstitial flow velocity ranges from 0.1-4 um/s compared to blood flow at 0.6-0.9m/s in pulmonary artery. **Figure 6.** Although this velocity is very slow, it influences many cellular processes such as migration, differentiation[66] as well as cellular uptake of drugs and nano-pharmaceuticals[56].

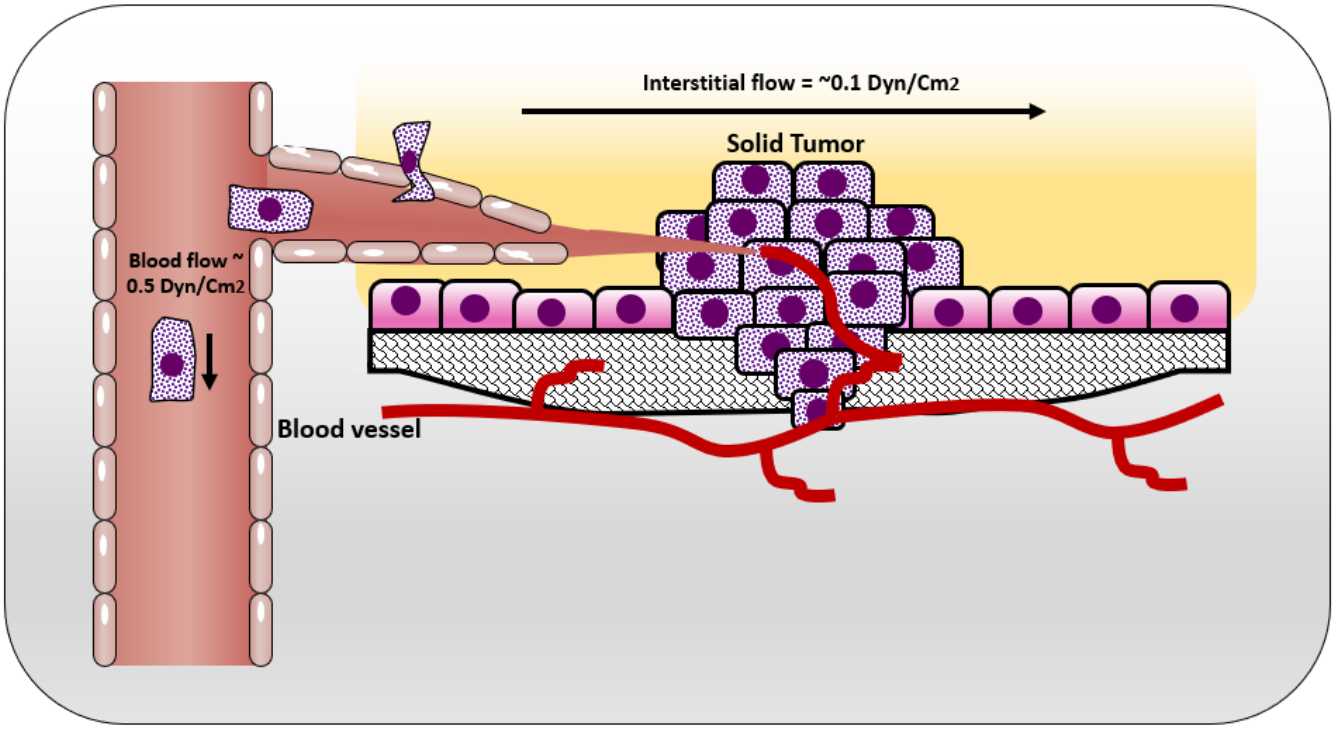

Figure 6: *Shear stresses experienced by cells in solid tumor and circulating tumor cells.*

It is ideal to test nanomaterials i.e. nanoparticles, or photothermal agents, on animal models for cancer therapy. However, using animal models is limited to ethical guidelines, also it is more time and labor intensive[67]. To avoid the uncritical testing on animals, in-vitro systems can be used as preliminary testing due to its low cost, simplicity and simple control of the experimental conditions. In most cases, there are

discrepancies in viability and nanomaterial uptake for in vitro systems when compared to in vivo conditions. The reason for these discrepancies is related to the fact that real cells are under the influence of many factors in physiological states. For example, FSS is one of the most important parameter that has to be taken into account. To mimic the physiological in vivo environment using an in vitro system, FSS can be induced to cultured cell by using microfluidic devices[68].

1.7 Inducing FSS in in-vitro systems

FSS is the force experienced by cells due to the flow of viscous fluids [60]. FSS can be applied to cells using parallel plate flow chambers (PPFC), cone plate chambers or microfluidic chambers. Different chambers are used based on the site where FSS is intended to be mimicked. For example, cone-plate chambers are used to mimic FSS in abdominal aorta and brachial artery due to resemblance of the geometry [69].

PPFC were commonly used to mimic FSS in cancer microenvironment. These systems were also used to study the cellular uptake of some nanomaterials by cancer cells [70,71].One of the first PPFC was developed in 1995 by Ruel et al. A typical PPFC has an inlet port, an outlet port, silicon gaskets to form the flow channel and a coverslip where cells are grown on [72]

These flow chambers are mostly connected to a syringe or peristaltic pumps, that can pump a certain fluid (mostly cell media) at specific flow rates. The shear rate can be calculated using the Hagen-Poiseuille equation. This equation is used for Newtonian fluids under steady and laminar flows.

$$Q = \frac{\tau . w . h2}{6 . \mu}$$

Here Q represents the fluid flow rate, τ is the shear stress acting on the cells, w

and h are width and height of the flow chamber respectively and μ is the viscosity of the fluid which is the cell medium is kept at [73]. **Figure 7** illustrates a typical chamber setup representing the flow of the fluid in a closed circuit.

PPFCs offers a model that is not as simple as static cell culture, but not as complex as animal models; thus, cellular interactions and nanomaterials uptake can be studied in a practical and reliant manner **Figure 8**[74].

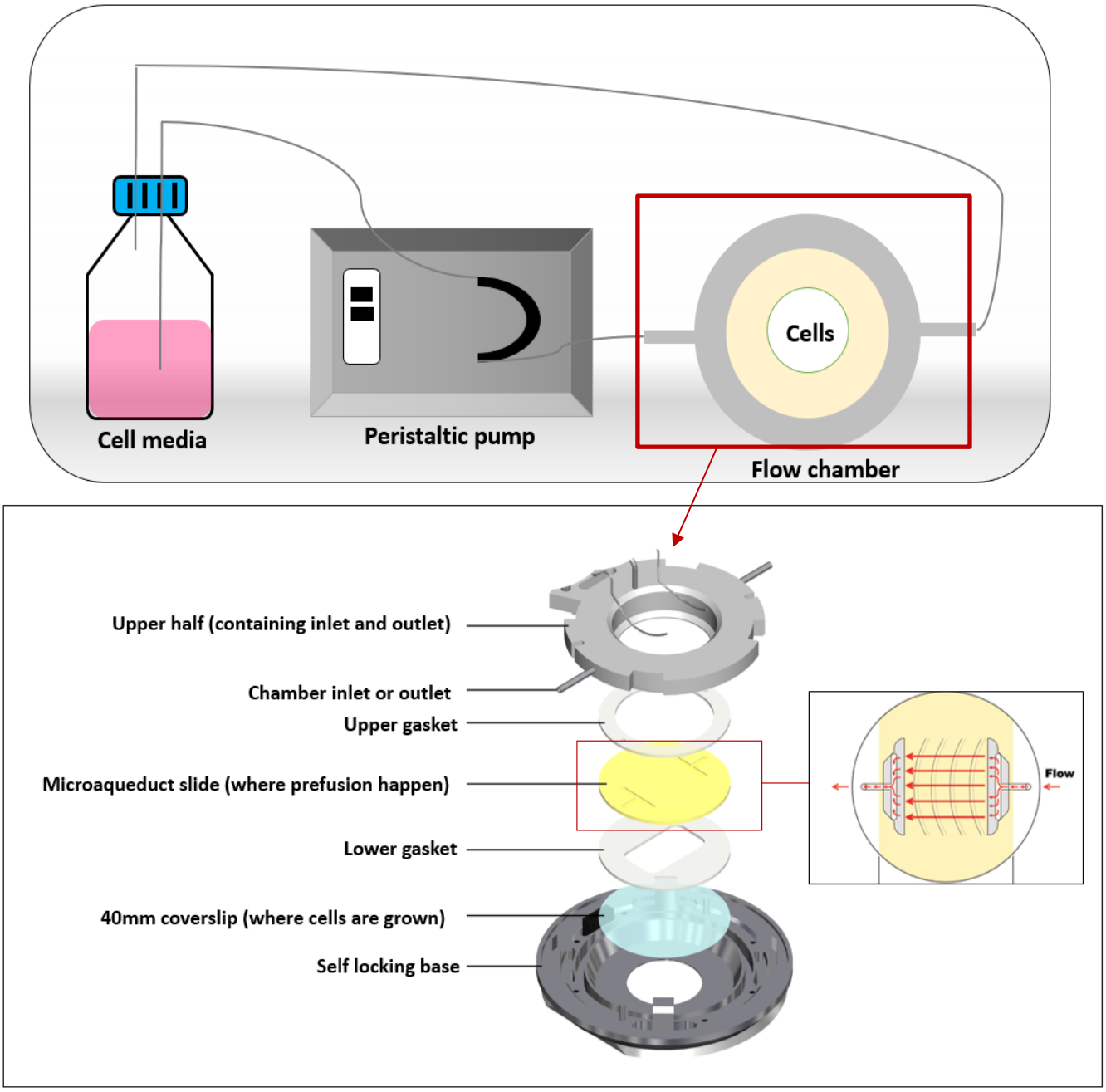

Figure 7: *A typical flow chamber setup. Adapted from http://www.bioptechs.com/product/fcs2-system/*

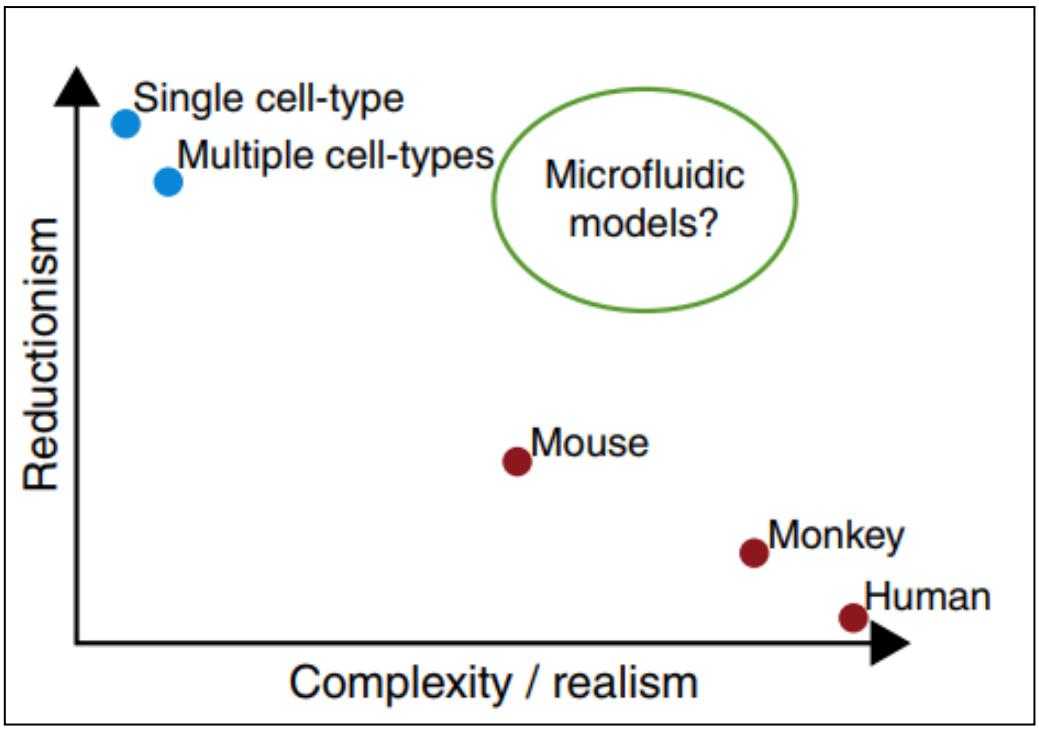

Figure 8: *microfluidic devices as a model. From Engineering and evaluating drug delivery particles in microfluidic devices.*

1.8 Nanoparticle cell interaction

The way that nanomaterials interact with cells is different in static culture and in dynamic culture. These differences include production of reactive oxygen species (ROS)[75], viability and uptake of these nanomaterials by cells[76]. Dynamic culture is more relevant to physiological conditions present in an animal model or in human body, as the biological system is complex and dynamic[56]. Usually, it is easier to study the influence of nanomaterials using static culture, but the results might be misleading and contradictory when compared to animal model or dynamic culture. For example, Nanomaterials tend to sediment and settle down in static culture, inducing stress on cells. Furthermore, nanomaterials form aggregates in static culture, which might alter their uptake by the cells, and therefore, the viability will be altered as explained in **Figure 9**. [75]

When nanomaterials form aggregates, the aggregate size should be much smaller than the cell size for uptake. There are different mechanisms by which cells uptake nanomaterials, these include: diffusion or passive penetration through the plasma membrane, and endocytosis which involves pinocytosis and phagocytosis. Pinocytosis involves internalization of molecules or fluid by formation of small vesicles whereas phagocytosis involves the engulfment of large materials by the formation of intracellular phagosomes[77]. It was reported that the uptake of nanomaterials is size dependent, and in some cases, it is easier for the cells to uptake larger nanomaterials by endocytosis, than smaller nanomaterials by diffusion. Moreover, the formation of aggregates and sedimentation of nanomaterials will alter the real concentration of nanomaterials delivered and affecting on the cells[78].

Therefore, nanoparticle aggregation is not a good affect for nanoparticle studies and should be prevented in most cases. To uniformly distribute the nanomaterials to

cells in culture without aggregate formation or sedimentation, it is suggested to use dynamic culture, and grow the cells under flow conditions using flow chambers [68].

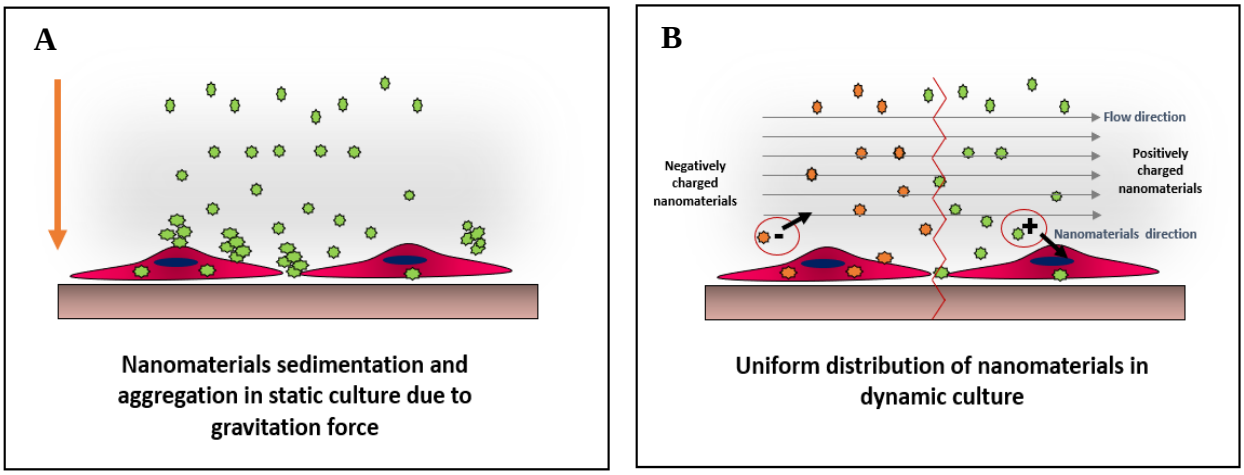

***Figure 9**: comparison between nanomaterials distribution under static **(A)** and dynamic conditions **(B)**.*

It was reported that, the uptake of nanomaterials is altered under flow conditions and these changes are due to material's surface charge, size and shape. Cells can uptake nanomaterials in two steps: the first step is binding to cell membrane due to electrostatic interactions affected by the physico-chemical properties of the nanomaterial, mostly surface charge. As the cell membrane is negatively charged, it is more favorable for positively charged materials to interact with its surface than neutral or negatively charged particles. The second step is the internalization of the nanoparticle from the cell membrane. After nanomaterials interaction and binding to the cell`s surface by electrostatic interactions, it can then be internalized by different uptake approaches[79]. Although surface charge is considered as an important contributor to higher uptake, other parameters as well are influencing the cellular uptake such as the material shape

specially under flow conditions [80]. Under flow conditions, the alignment of non-spherical nanomaterials can be different than in static culture, thus altering the uptake. It has been reported that fibrous or 2D materials have a flow aligning effect, which affect their cellular adhesion and uptake [74] **Figure 10.**

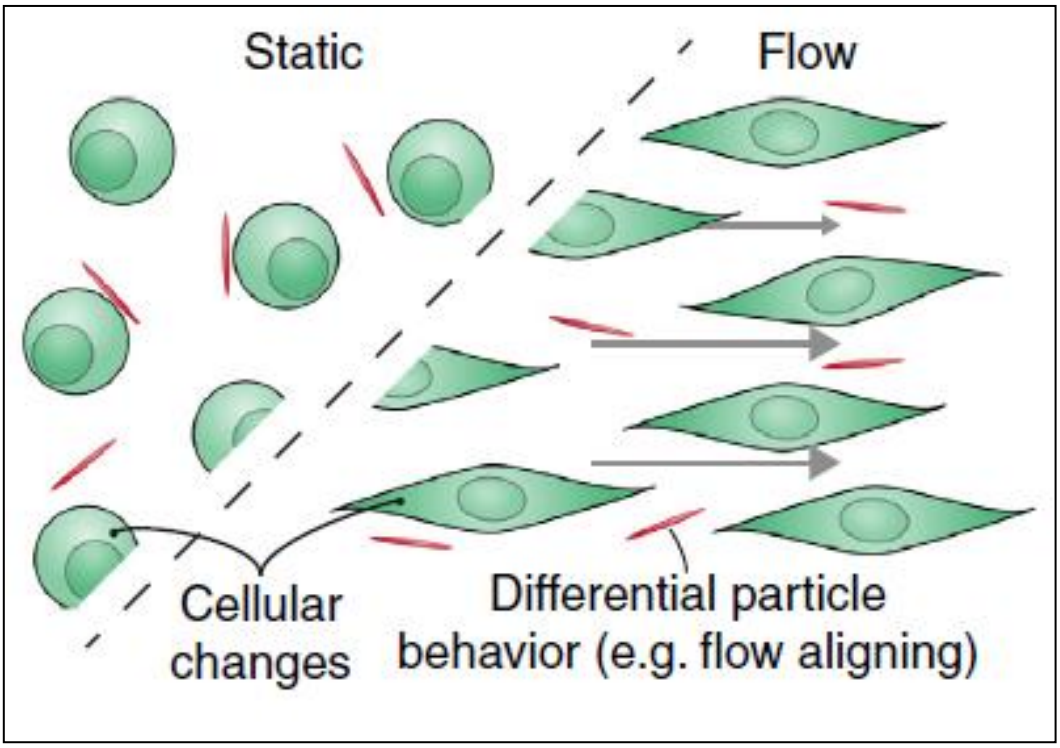

Figure 10: *Material shape effect on the nanomaterial- cell interaction under flow conditions.adapted from Björnmalm, M.; Yan, Y.; Caruso, F. Engineering and Evaluating Drug Delivery Particles in Microfluidic Devices. J. Control. Release 2014. https://doi.org/10.1*

1.9 Shear stresses and nanomaterials uptake

Owing to the effect of the dynamic environment in different biological processes, tissue engineering, and drug-delivery [81,82], many studies have been devoted to investigate the role of FSS in the interaction between cells and nanoparticles [83–85]. One of these significant interactions is the cellular uptake of nanoparticles. To illustrate, the uptake of the applied nanomaterials by cells is considered an important aspect especially in drug-delivery and other therapeutic purposes, which require sufficient uptake by the targeted tissue. More interestingly, the surface charge of nanoparticles has been reported to play a significant role on the cellular uptake in the absence and/or the presence of FSS. For instance, the interaction of endothelial cells with both negatively charged nanoparticles has been scrutinized by Samuel et al. by application of varying levels of FSS on cells [86]. The authors revealed that the cellular uptake increased with low shear stresses (0.05 Pa) when compared to high shear (0.5 Pa), resulting in less cellular uptake of the negatively charged nanoparticles. In static conditions (0 Pa), cellular uptake was lower compared to low shear stress (0.05). The higher uptake of these particles under stress was mainly attributed to the formation of cytoskeletal stress fibers and membrane ruffles which enhance endocytosis. These changes in the cytoskeleton was not observed in the non-shear exposed cells.

Additionally, Rigau and Städler [87] correlated between the uptake of nano-sized drug delivery systems and the subsequent therapeutic effect using skeletal mouse myoblast cell model (C2C12) in the absence or presence of FSS. They concluded that the liposomes with positively- charged lipids ended up to higher cellular interaction in the presence of shear, in contrast to those contained negatively charged lipids or zwitterionic ones. Furthermore, the authors investigated the therapeutic effect, in terms of cell viability, after treatment with the positively charged liposomes carrying a small cytotoxic molecule in static and dynamic conditions. Their findings stated that there

was a higher therapeutic response (i.e. higher cell mortality) in the case of dynamic conditions, which demonstrates the relationship between the higher cellular association of positive carriers and more effective therapy in the presence of shear.

Toe et al.[88] studied the cell response to modified liposomes with and without FSS using two cell lines. The former cell line was the immortalized skeletal mouse myoblast (C2C12), a tumor cell model, which is important to estimate the activity of the applied liposomes as drug carriers in drug delivery systems. While the latter cell model is a liver cell line (HepG2), was chosen to investigate the efficiency of hepatic clearance of the drug delivery nanoplatforms from the body. To illustrate, the authors fabricated PEGylated poly (dopamine) coated liposomes and quantified their cellular uptake by myoblasts and hepatocytes using flow cytometry in both static and dynamic conditions. The results manifested that the hepatocytes response in the dynamic conditions was significantly higher after 30 minutes only, while the myoblasts demonstrated a significant increase after a relatively longer time (4 hrs). The authors explained these findings as the nature of the two cell lines is different; the hepatic cells are concerned with clearance, so their response is instantaneous in the presence of physiological shear. On the other hand, the cancer cell model needed longer time to show a response in that low shear stress (0.146 dyn/cm2).

Applying different FSS is considered a paramount factor for deep investigation of the effect of dynamic conditions on cellular response, where the cellular uptake could be determined in charge of all applied FSS levels. Hence, more relevant correlation between the cell response and the stress level can be stated. For instance, Kona and co-workers developed a novel drug delivery system that imitates the natural platelet adhesion to the injured vascular walls under different shear flow rates.[89] Their results implied that at high shear stress levels, 20dyn/cm2, the cellular uptake fell dramatically

by three folds when compared to the control static group. The authors explained their findings through computational model revealing that the high shear rates induce huge dislodging forces able to detach the adhered particles.[90,91]

Moreover, Klingberg & Oddershede studied the effect of FSS on the uptake of spherical 80 nm gold nanoparticles (Au NPs) by human umbilical vein endothelial cells (HUVEC). They categorized the cells into two groups, one group cultured in static conditions for 24 hours (non-adapted group), while the other cultured for 24 hours under 10dyn/cm2 shear stress (shear adapted group). Then, both groups were exposed to 5ug/ml Au NPs for 3 hours either under flow or static conditions. A slight reduction in uptake of Au NPs was observed for groups that were exposed to shear before or with the treatment in comparison to static culture. [92]

One more study was conducted by Fede, Albertin, Petrelli, & Caro to reveal the effect of FSS and size of spherical citrate stabilized gold nanoparticles on HUVEC. They have tested two batches of gold NPs (Batch 24nm and Batch 13nm). It was observed that, the viability is significantly more when testing gold NPs under flow conditions in comparison to static culture, regardless of NPs size or concentration. They measured the NPs concentration in two methods, one based on the surface area per unit volume, while the other based on the number of NPs per unit volume. They found that the cells are less viable when increasing the surface area per unit volume irrespective to NPs size. [67]

Yazdimamaghani, Barber & Moghaddam studied the effect of silica NPs density and flow conditions on cell cytotoxicity, uptake and sedimentation. They produced 4 types of silica NPs with different densities and surface charges and they tested cytotoxicity and uptake on RAW 264.7 macrophage cells after 24 hours incubation with the cells, in static or under flow conditions. They found that, the cell viability is better

under flow conditions, compared to static culture. Moreover, none of the 4 particles showed a toxic effect on macrophage cells up to 250ug/ml in dynamic conditions. Also, particles sedimentation is less in dynamic conditions, and the distribution of particles is more homogeneous. Yazdimamaghani et al. also found that, cellular uptake of silica NPs is more in static compared to dynamic conditions. Furthermore, low density particles, showed a lower uptake under flow conditions compared to high density particles.[93]

Particle shape and size dependent uptake under physiological shear stress was reported by Jurney et al. They produced negatively charged rod shaped PEG NPs with different aspect ratios and assessed their uptake by HUVEC under flow conditions at different incubation times (1,12 and 24 hours). In all the cases, it was found that larger particles are uptaken more than smaller ones under flow in comparison to static culture. Whereas, smaller particles are internalized more in static than in flow conditions. The trend of larger NPs being internalized more under flow is contradictory with what was reported in literature with similar sized spherical NPs. This indicates that particles with higher aspect ratios interact more with cells under flow conditions. [94]

Additionally, the uptake of lipidic NPs by MCF-7 breast cancer cells and Hela human cervical cancer cells was reported by Palchetti et al. under flow conditions. Authors produced two types of lipidic NPs, one with surface modification (PEGylated) while the other without modification. They incubated the cells with particles at two incubation times (5 and 90 minutes). For unmodified NPs, MCF-7 cells showed a significantly lower uptake in dynamic culture in comparison to static condition at both incubation times. Whereas Hela cells showed a higher NPs cellular uptake after 90 minutes incubation in dynamic culture. On the other hand, a non-significant difference of uptake by MCF-7 was observed for modified NPs either under flow or static

conditions. But still a higher NPs uptake at dynamic conditions by Hela cells. They clarified that shear stress can affect the protein corona (protein corona is formed when NPs absorb biomolecules when they interact with cells and biological system) which changes its surface chemistry and properties, which in turn affect their uptake by cells.[95] I another relevant study by Rinkenauer et al. was performed to investigate the effect of FSS on the uptake of co-polymers (negatively charged PMMA -co-PMAA with different ratios of MAA (3%,5%,8% and 13%) and positively charged PMMA-co-PDMAEMA with 20% PDMAEMA) by different cell lines. They found that, increasing the negative charge (MMA) increases the uptake by different cells under static conditions. However, the uptake is not as efficient as positive particles (20 % PDMAEMA). Similar trend was observed in different cell lines, but not in co-culture which reduced the cellular uptake due to cellular interactions. When the uptake was assessed under flow conditions (0.7,3,6,10 Dyn/cm2) it was observed that, increasing shear stress is positively correlated with cellular uptake. Nevertheless, compared to static culture, 13% PMMA showed more efficient uptake compared to positively charged 20% PDMAEMA. This is probably related to the differences of surface receptors patterns observed under flow conditions which can alter the cellular uptake [71]

As seen from these multiple studies, normal cells and cancer cells behave differently with respect to nanomaterials uptake. There are several important factors such as the material size, surface charge and shape. Contradictory findings from different studies necessitates further investigations for cell-nanoparticle interactions.

CHAPTER 2

MATERIALS AND METHODS

2 Experimental

2.1 List of Materials

Here is the list of materials used to conduct this study

- Aluminum Titanium Carbide powder (Ti3AlC2, or MAX phase) (Carbon-Ukraine limited).
- Hydrofluoric acid (HF, 48%) (Merck Schuchardt OHG, Germany).
- Ethanol absolute (Sisco Research Laboratories, Mumbai, India).
- Dimethyl sulfoxide (DMSO) was obtained from Honeywell Riedel-de Haën®, Germany.
- Tetrachloroauric acid, HAuCl4 powder (Sigma-Aldrich).
- NaBH4 fine granular solid (Merck Schuchardt OHG, Germany).
- RPMI Medium 1640 (Gibco® Laboratories, Thermo Fisher Scientific, USA).
- 1 X phosphate buffer saline (PBS)
- Water was purified using a Milli Q system (Millipore, Molsheim, France).

Alexa Fluor® 488 Phalloidin- Thermo Fisher Scientific

- Live/Dead cell viability assay – Thermo Fisher Scientific
- Paraformaldehyde – Sigma Aldrich
- 50% glutaraldehyde solution

2.2 List of Equipments

Below is the list of equipments used to conduct this study

- Scanning electron microscope (SEM): NOVA NANOSEM 450
- Transmission electron microscope (TEM): Talos (FEI)
- PAN analytical X-Ray diffractometer
- Atomic force microscope (AFM)
- Confocal microscopy
- ZetaSIZER NANO -Malvern
- FLIR C3 Thermal camera
- Olympus fluorescent microscopy
- 808 nm high power multimode pump laser (Shanghai Connet Fiber Optics Company)
- UP400S Ultrasonic Processor (hielscher Ultrasound Technology, Germany)
- Oven
- Magnetic Stirrer
- Autoclave
- Strong Magnet
- 60 mm petri dishes
- Bioptechs micro-perfusion peristaltic pump
- Tygon tubing- Bioptechs
- 40 mm coverslips - Bioptechs
- Bioptech flow chamber
- Hemocytometer
- Pipettes and micropipettes

2.3 Methods

2.3.1 Synthesis of nanocomposites

2.3.1.1 Synthesis of MXene nanosheets

MXene was synthesized following the instructions and guidelines provided by Dr.Yury Gogotsi from Drexel university where MXene was first produced [42]. Below, these steps are briefly explained.

Chemical etching of MAX phase

This reaction was performed to remove Al from the MAX phase. Here, Ti_3AlC_2, etching is required due to the strong chemical bond between Ti and Al which cannot be eliminated by mechanical exfoliation. For each gram of MAX powder, 10 ml of 48% hydrofluoric acid (HF) was added slowly as the reaction is exothermic. This reaction was done in a chemical fume hood, with stirring overnight. A plastic bottle was used for this reaction, which was covered after the addition of MAX powder and HF.

washing and drying process

After etching, washing process was performed to remove residual acids and reaction salts, as well as to achieve a safe PH. Washing was performed by adding 100 ml of deionized water to the reaction bottle. The mixture was centrifuged at 3500 rpm for 15 minutes**.** After that, the supernatant was discarded, and the pellet was resuspended in deionized water, vortexed and centrifuged again. This process was repeated multiple times until a safe PH was reached (PH=5-6). After the last wash, the supernatant was removed, and the tubes were placed in the oven at 40 C until complete drying.

Intercalation and delamination

Intercalating compounds are used to increase the interlayer spacing between the flakes and for weakening the interactions between the 2D layers, to produce single 2D sheets. Here, Dimethyl sulfoxide (DMSO) was used as an intercalating agent. For each gram of etched MAX phase, 12 ml of DMSO was added and kept for overnight stirring. After that, free DMSO was removed by washing the mixture with deaerated water few times. Following that, deaerated water was added to the intercalated MXene. For each gram of etched MAX, 300 ml of deaerated water was added. The mixture was sonicated for one hour under argon gas flow, followed by one-hour centrifugation at 3500 rpm. Thereafter, the supernatant was kept at the desired 2D MXene. The concentration was measured by drying and weighing a certain amount of the produced MXene.

2.3.1.2 Synthesis of MXene/Au nanocomposite

MXene/ Au nanocomposite was produced with a ratio of 1: 0.1 by reduction of $AuCl_4$ solution with 1 molar sodium borohydride ($NaBH_4$). To prepare this solution, AuCl4 and NABH4 were mixed with MXene solution while stirring. This is followed by Argon gas purge for 5 minutes. After that, the mixture was sonicated for 2 hours and then centrifuged (10000rpm for 30 minutes) and washed 3 times with deaerated water. The resulting pellet is the desired MXene/Au nanocomposite, which is then dried and weighed **Figure 11.**

The resulting nanomaterials were characterized using scanning electron microscopy (SEM), transmission electron microscopy (TEM) and X-ray diffraction (XRD).

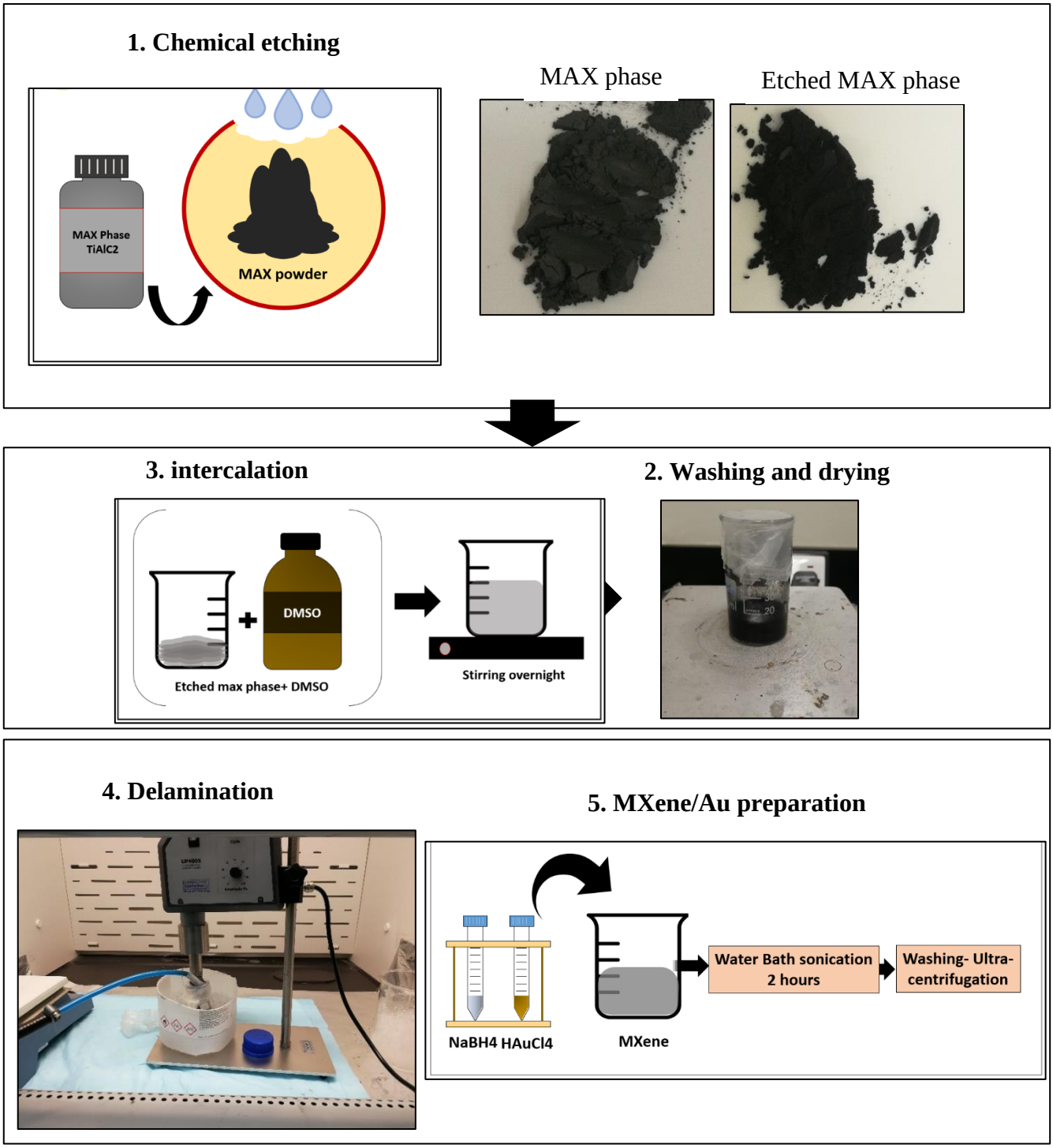

Figure 11: *general outline to produce MXene and MXene/Au nanomaterials*

2.3.2 Material Characterization

2.3.2.1 Scanning Electron Microscope SEM

Surface morphology and elemental analysis were assessed using NOVA NANOSEM 450 (N-SEM) and energy dispersive spectrometer EDS respectively. A voltage between 500 V to 30 kV was applied with 10 mm distance between the sample and electron source, which is satisfactory to obtain good images. The Scanning Electron Microscopy uses a field emission gun as a source of electrons. The electron beam travels through the column while being adjusted by different lenses till reaching the sample. The electrons interact with the sample producing secondary electrons and characteristic X-rays that can be detected by special detector to produce electron image and elemental spectra respectively.

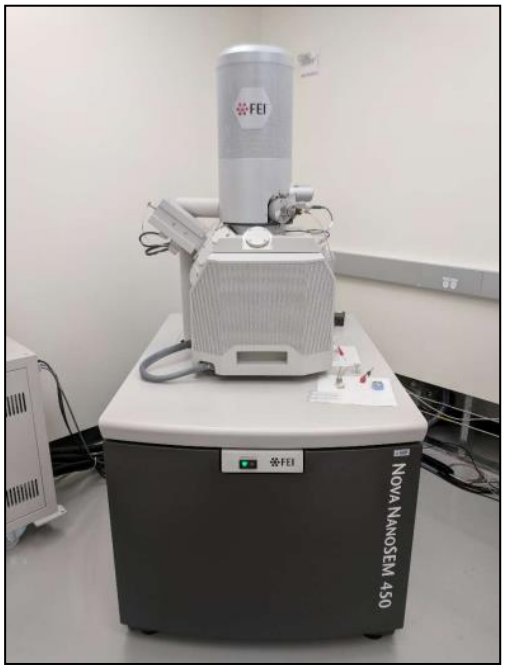

Figure 12: *NOVA NANOSEM 450 (N-SEM) instrument*

2.3.2.2 Transmission Electron Microscope TEM

TEM is an extremely powerful instrument for characterizing materials and imaging, as it uses a higher voltage in comparison to SEM. This provides images with higher magnification and resolution, also the electron beam can penetrate through the sample which provides more information about the internal structures and composition. Here, Talos Transmission Electron Microscope (FEI) was used to characterize the produced nanomaterials. After sample preparation, MXene and MXene/Au were sonicated for 15 minutes and then were subjected to imagining. To get the image, the microscope was operated at 200Kv. A very thin layer of the sample was placed in carbon coated grid, and then positioned on electron beam produced by the electron gun. The produced electrons were accelerated and focused by the electromagnetic lenses which penetrate the sample and produces the image.

Figure 13: *Talos Transmission Electron Microscope (FEI) instrument*

2.3.2.3 X-Ray diffraction XRD

The main principle of X-ray diffraction is based on electron scattering. Since electrons are the lightest component in an atom, they can scatter light when an electric field or x-ray beam are applied. The wavelength of X-ray is similar to the distances between atoms. This is the reason for using X-ray diffraction instead of visible light, as when X-ray beam hits an atom the electrons will oscillate with the same frequency of the x-ray beam. Diffraction will occur for certain planes with specific directions in a crystal. There will be a constructive interference, and a diffraction pattern will be formed. The diffraction pattern can give a clue about the atomic arrangement within a crystal structure of a certain material.

PAN analytical X-ray diffractometer was used to assess the crystal structure. X-ray diffractometer is an instrument that is basically composed of three parts: X-ray source, sample holder and a detector. The X-ray source sends a beam to the sample and the detector collects the diffracted radiation. Both source and detector move until a wide range of angles of incident are measured. The X-ray beam is focused into the sample by X-ray optics. There are variety of slits like the anti-diversion slit and the anti-scatter slits to eliminate the unwanted beams of Kβ and to focus the desired beams like Kα onto the sample, which is more intense.

Figure 14: *PAN analytical X-Ray diffractometer*

2.3.2.4 Atomic force microscopy (AFM)

The AFM device MFP-3D at CAM, (Asylum research, USA) equipped with a Silicon probe (Al reflex coated Veeco model – OLTESPA, Olympus) was used for measurement under ambient conditions using the Standard Topography AC air (tapping mode in air). Here, AFM was used to measure the exact dimensions of MXene sheets. To do that, MXene solution was sonicated and diluted to 20ug/ml. Samples were then placed on silicon wafer and allowed to air dry before measurements.

2.3.2.5 Zeta potential measurement

ZetaSIZER NANO -Malvern hosted at CAM was used to assess the surface charge of MXene. The device can find the Zeta potential by using electrophoretic light scattering. MXene absorbance and refractive index was collected from literature [46] [96]. MXene solution was diluted to 5ug/ml before obtaining the measurements, and it was placed in disposable folded capillary cell to be processed by the device.

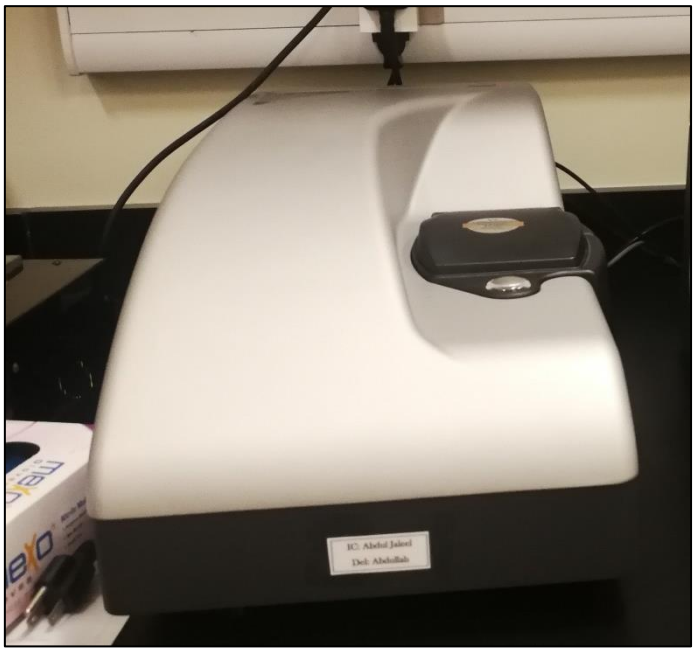

Figure 15: *ZetaSIZER NANO analyzer.*

2.3.2.6 Heat measurements

FLIR C3 thermal camera and Go Temp Probe thermometer (with Logger Lite software) was used to assess the temperature of MXene samples upon laser irradiation. The thermal camera has a special lens that allows infra-red energy to pass through it. The focused light is detected by a sensor, which renders the light information into

thermogram. Thermogram then processes the colored image that has a color scale which represents the amount of infra-red present. FLIR thermal camera can measure temperatures up to 150 ºC. The electronic probe thermometer assesses the temperature by putting voltage across the probe and measures current flow through it. Heat that is generated creates a condition of low current flow, which is represented by resistance. Resistance of electrons is measured and converted to a measurable value. To assess the temperature, different dilutions of MXene were prepared and exposed to laser at different power densities. Data was collected by taking images or by the program (Logger Lite).

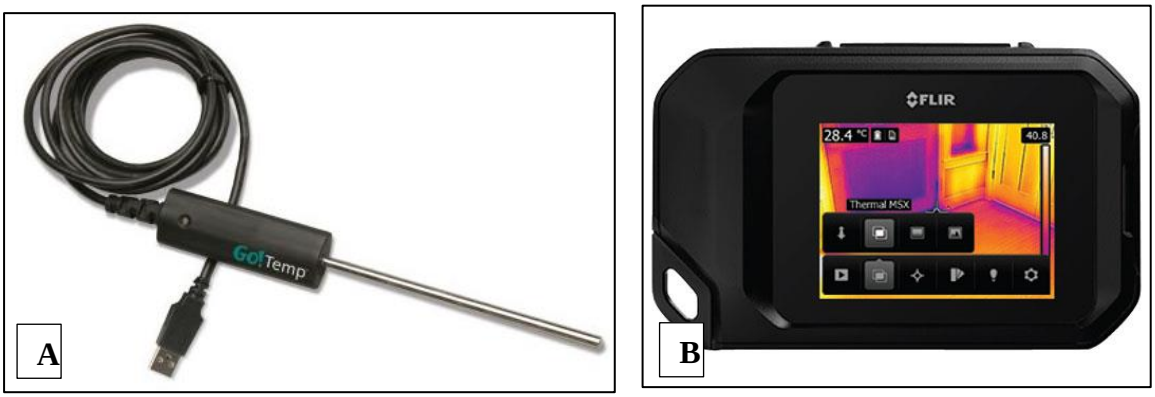

Figure 16: A) *Go Temp probe thermometer* ***B)*** *C3 FLIR thermal camera*

2.3.3 Cell culture and *in-vitro* testing

Cell culture is the technique by which cells are maintained outside human body, under artificial controlled sterile conditions. Cell culture can be used for a variety of tests, for example: vaccination, cancer research and testing new pharmaceuticals as well as nanomaterials. It is considered as a first-line or preliminary testing, before doing further research in animal models[97].

Static cell culture is a beneficial tool for research, as it simplifies complex systems, also it is easy to cultivate and control the culture conditions. However, results obtained from static culture are sometimes contradictory when compared to animal model due to its oversimplified design and its lack of consideration of other factors for example cells are in dynamic conditions due to presence of shear stresses in different body organs due to fluid flow[78].

Cells that can be used in such experiments can be classified as primary cells and immortalized cells. Primary cells are isolated from an animal or human for research purposes. These cells can be grown in culture for a limited time. Immortalized cells are engineered cells to be programmed for proliferation indefinitely. Primary or immortalized cells are isolated from specific organs. In most cases, these cells can be purchased from commercial sources. A specific type of cells comes in a cryopreserved tube, which is then thawed and cultured in specific culture flasks or Petri dishes, providing cells with culture medium depending on the cell type. These cells can grow until the culture flask or the Petri dish if full (confluency). After the cells reach confluency, they can be sub-cultured to another flask to provide space for these cells to grow. During subculturing, Trypsin enzyme is used to detach the adherent cells from the culture plate. . [98].

2.3.3.1 Culturing MDA-MB- 231 cells

MDA- MB-231 are epithelial breast cancer cells, that were first obtained from a 51 years old Caucasian woman who had metastatic adenocarcinoma. These cells are known to be highly aggressive and invasive, and it has limited treatment options.[99] Protocols from ATCC (the company from which they were purchased) were followed to culture MDA cells. The preparation for an experiment starts by harvesting (subculturing) 80% confluent cells in T25 culture flask, by washing the cells twice using phosphate buffered saline (PBS) followed by trypsinization for 5 minutes using 0.25% trypsin solution until the cells are fully detached (floating cells). After that, complete cell media RPMI medium supplemented with 10% fetal bovine serum FBS and 1% antibiotic and antifungal solution were added to the trypsinized cells to stop the action of trypsin as FBS contains protease inhibitors. This is followed by 5 minutes centrifugation at 1000 rpm. Thereafter, the supernatant is removed, and 1 ml complete media is added to the pellet and mixed thoroughly[100]. These steps are followed by cell counting. Here, two different methods of counting were used: manual counting using hemocytometer and automated counting using Tali cell counter. For manual counting, 10 µl of the cell suspension was added to 10 µl trypan blue stain, which can penetrate dead cells only and stain them blue. The mixture was mixed thoroughly and kept for few minutes. After that, 10µl of the mixture was inserted in on side of hemocytometer groove. Only the cells in the 4 squares at the edges were counted under a light microscope [98] **Figure 17.**

After counting, 10,000 cells were seeded in 40mm diameter circular coverslips kept in 50 µm diameter petri dishes. This was achieved by adding the desired number of cells to complete cell media and then incubating the cells in cell incubator at optimum conditions (37C, 5% Co_2 and 95% air). The following equations were used to seed the desired number of cells:

Total cell count = (Average number of cells) X $(dilution\ factor)$ X (10^4)

Equation 1

Here, 10^4 is the hemocytometer constant

Equation 2

$$The\ desired\ cell\ volume = \frac{Total\ cell\ count/ml}{Final\ volume X\ desired\ cell\ concntration}$$

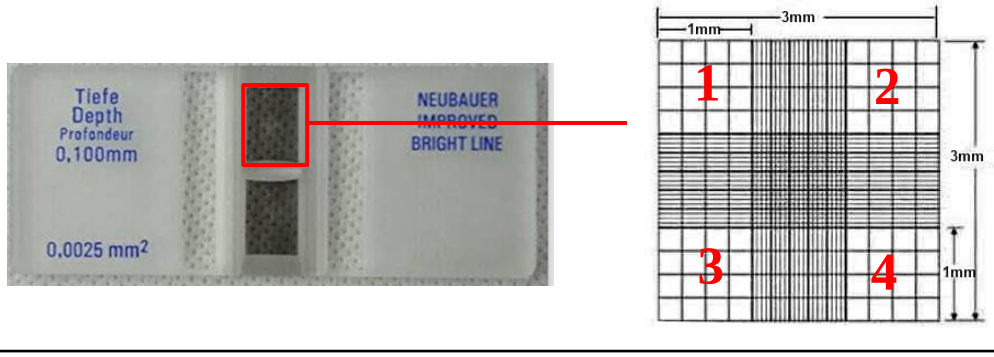

Figure 17:*Hemocytometer, for manual cell counting*

40 mm circular coverslips were used to seed cells on them so they can be assembled in the flow chamber. The coverslips were sterilized by autoclaving at 121 C for 30 minutes and then by UV sterilization for 15 minutes.

All the steps were performed in biosafety level 2 cabinet (BSL2) and under sterile conditions. When 10,000 cells are seeded, the plates will be 80% confluent after 4 days of their harvest. A static culture of MDA-MB-231 is achieved this way.

2.3.3.2 Creating a dynamic condition in cell culture

PPFC are mostly used to create dynamic conditions for cultured cells. These chambers are connected to different types of pumps for generating physiological flows over cells. Here we used FCS Micro perfusion peristaltic pump. We first calibrated the pump by allowing a known volume of fluid to pass through the pump at certain speeds. For each speed, the time by which total volume of fluid delivered was measured, and from this measurement, flow rate was calculated. **Figure 18** shows the linear relation that was obtained between the pump speed (machine-specific) and flow rate (ml/hour).

Thereafter, based on the desired shear rate, the flow rate can be set if the fluid viscosity (cell media) and the flow chamber parameters are known. In this experiment, we calculated flow rate using the Hagen-Poiseuille equation for a Newtonian fluid. A shear rate of 0.1 dyn/cm^2 was used to model the interstitial flow FSS over cultured cells [56]. **Table 1** shows calculation of flow rate.

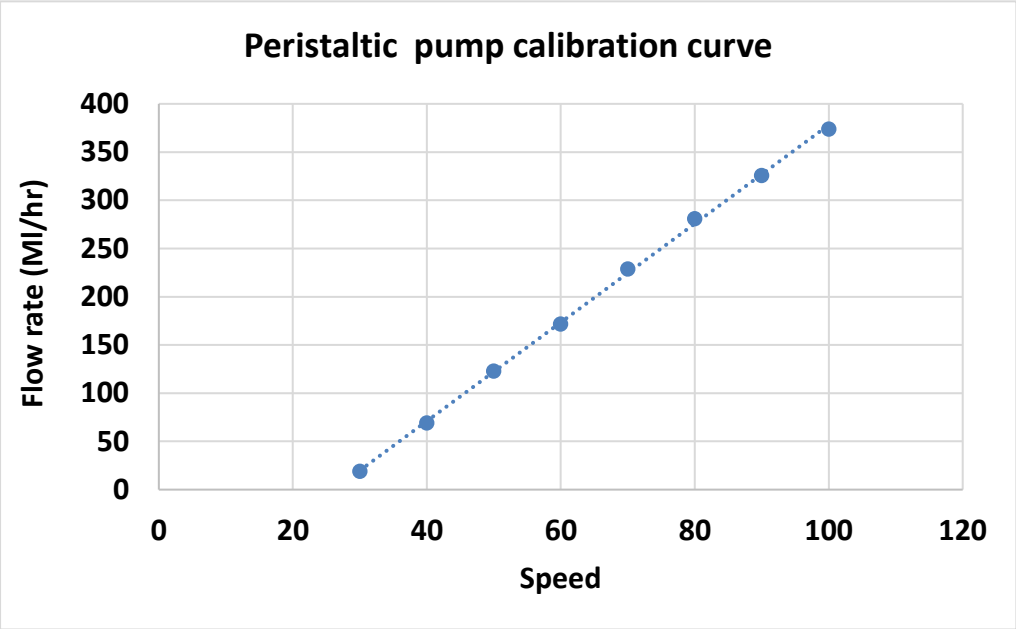

Figure 18: *the relation between speed and flow rate (ml/hr)*

Table 1*:Flow rate calculations*

Hagen-Poiseuille equation	τ [dyne/cm^2] = (6 μ Q) ÷(bh^2)
Dynamic viscosity (μ) of cell medium	*0.00096*
Chamber parameters (mm)	Width =15
	Thickness = 1
	Length =25

After pump calibration and speed calculation, the pump was connected to Tygon tubing connecting the pump to the flow chamber in a closed-circuit **Figure 19**. MXene was sonicated, then diluted in cell media to the desired concentration. Circular coverslip where cells are seeded was assembled in the chamber as in **Figure 19 B.** After that, the whole setup was incubated in cell incubator under optimum conditions for the desired incubation time (4 or 8 hours).

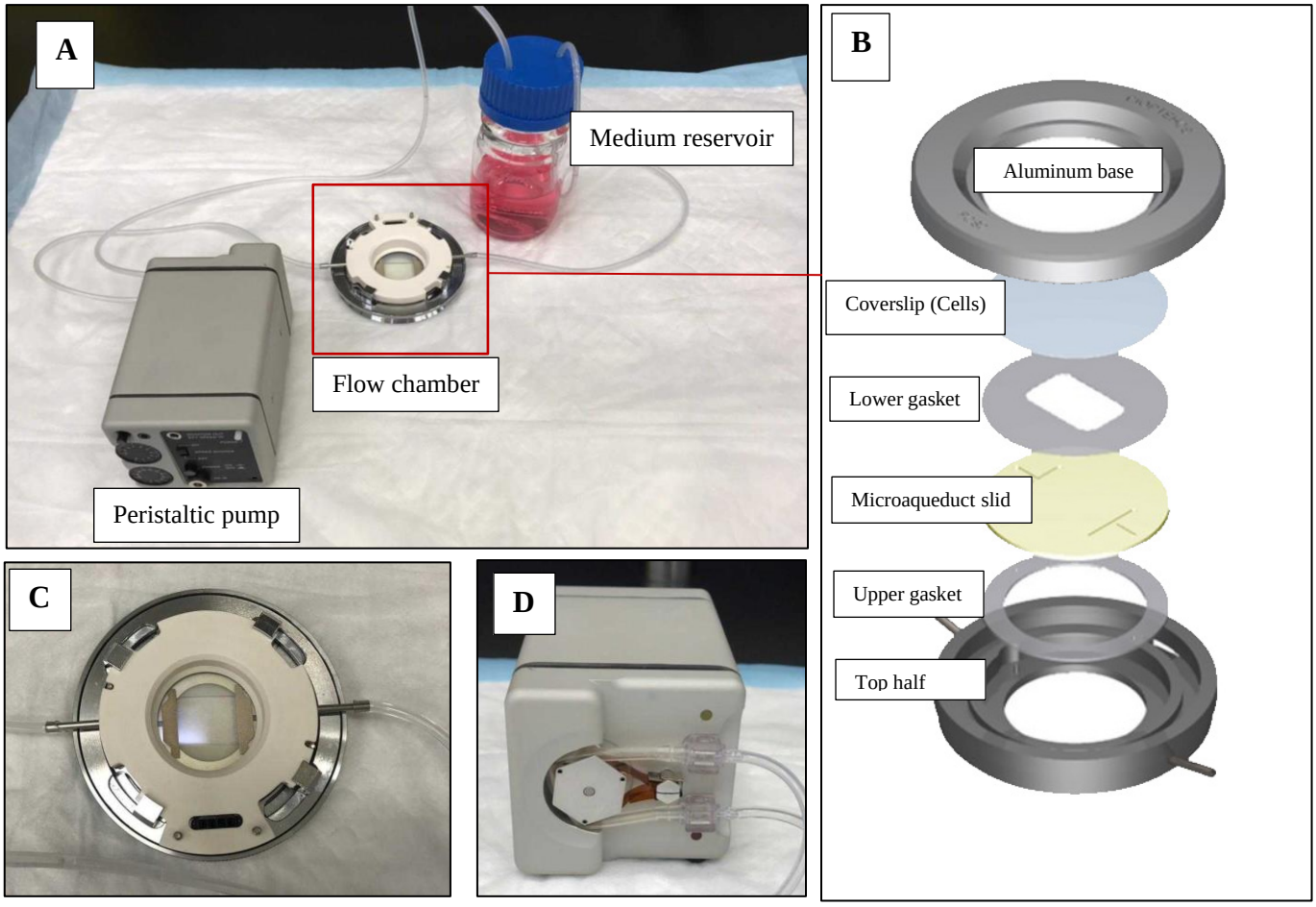

***Figure 19**: flow chamber setup. **A**) the flow chamber is connected to the peristaltic pump from one side and the medium reservoir from the other side in a closed-circuit way. **B)** Flow chamber assembly. **C)** The flow chamber -closer view **D)** Back view of the peristaltic pump.*

2.3.3.3 Exposing cells to laser

To expose laser to cells, VENUS series high stability benchtop laser with wavelength of 808 nm was used with different PDs (1,3, or 5 W/cm^2) for 3 durations (5,10 or 15 minutes).

2.3.4 Viability assessment

After exposing the cells to MXene and laser, viability was assessed using Live/dead stain. Basically, Live/dead stain is composed of two stains: Calcein and Ethidium homodimer 1. Calcein AM is a compound that is not fluorescent by itself, but it is membrane permeable. When the cell is alive, Calcein AM gets through the cell membrane and is then converted to Calcein by enzymatic reaction within the cell, which is fluorescent and membrane impermeable, keeping the solution inside the cell. Therefore, live cells, will be stained by Calcein and will fluoresce green. Ethidium homodimer-1 is membrane impermeable and can only enter the cell if the cell membrane is damaged. Ethidum homodimer-1 binds to DNA in damaged cells and stains the cell nucleus red.

To assess viability, Live/dead stain was prepared by covering 15 ml falcon tube with aluminum foil as the stain is light sensitive. 10 ml of serum-free media with 5 ul Calcein and 5 ul Ethidium homodimer-1 were added to the tube and the solution was mixed thoroughly. Around 1 ml of the prepared stain was added to each slide and the petri dish was then covered with foil. The cells were incubated with the stain for 10 minutes at room temperature. After that, fluorescent images were taken by Olympus microscope IX73. Live images were taken by GFP filter whereas dead images were taken by C3Y filter. Ten representative images were taken for live and dead cells at 10X magnification. After that, images were merged, and viability percentage was calculated with ImageJ by quantification of live and dead cells then applying the following equation:

Equation 3

$$Viability\ rate\ = \frac{\text{Number of dead cells}}{\text{Total number of cells}} \times 100$$

2.3.5 Uptake assessment

MXene uptake by cells was assessed by three different methods: confocal microscopy, EDS analysis, and TEM imaging.

2.3.5.1 Confocal microscopy

Zeiss confocal LSM microscope (hosted at Weill Cornell labs) was used for imaging along with ARIES imaging program. The slides were prepared by staining the cells with Calcein AM as in the previous section with DAPI stain. After that the slides were fixed with 4% paraformaldehyde for 15 minutes, washed twice with PBS. A gel mount was used for the coverslips to get better fluorescent signals. Stained samples were imaged where 2D and stack images were obtained at 63x magnification, using the green channel (showing cell cytoplasm stained by Calcein am), blue channel (showing DAPI stained nucleus) and phase contrast (showing the nanoparticles). Images were processed using image j to produce 3D projections, 3D volumes, and sliced 3D volumes.

2.3.5.2 SEM & EDS

After performing the experiment, the slides were fixed with 2% glutaraldehyde fixative for 24 hours at 4 C. After that, the slides were washed twice with PBS followed by a series of ethanol dehydration (50%, 70%, 80%, 90%, 95%, and 100%). Finally, the slides were allowed to air dry. All the slides were coated with Au to be conductive, so SEM and EDS analysis become possible.

2.3.5.3 TEM

After conducting experiments, cells were scraped from the coverslip surface with a cell scraper. Samples were centrifuged at 1000 rpm for 5 minutes. After that, 1 ml of 2% glutaraldehyde and 2% paraformaldehyde fixative was added. The pallets were kept at 4°C with the fixative overnight. This was followed by washing twice with Phosphate buffer buffer. After that, the samples were rinsed with cold acetate buffer for 10 minutes. The samples were stained with 0.5% uranyl acetate stain for one hour. Then, the samples were subjected to ethanol dehydration (36%,50%,70%,90% and 100%). Following that, the samples were mixed with epoxy resin and incubated in the oven at 55 °C for 10 minutes. The resin was changed three times. Following the addition of the final amount of resin, samples were incubated in the oven at 55 °C for 48 hours. Once the resin blocks were ready, they were cut to thin layers by sharp microtome using diamond knife. Then, samples were imaged by TEM at QEERI.

2.3.6 Cytoskeletal staining

Changes in cytoskeletal structure have been shown in some studies to affect the cellular uptake of nanomaterials [101]. To test that, cells were grown at 50% confluency and fixed with 4% paraformaldehyde for 15 minutes. The samples were permeabilized using Triton X solution then bovine serum albumin was added to block the unspecific bindings. Following that, Alexa-488 actin labeled phalloidin was added to the sample, which binds specifically to actin fibers in the cell's cytoskeleton. The samples were incubated overnight at 4 °C. Following that, mounting media was added to the coverslips and the samples were imaged using Olympus fluorescent microscope at 60X magnification using the GFP filter.

2.3.7 Statistical analysis

One-way ANOVA was done to finds statistical significance followed by Tuckey test to compare the significance between the sample means.

CHAPTER 3

3. Results and discussion

In this work, two nanomaterials were prepared: MXene and MXene/Au nanocomposite for photothermal cancer therapy. MXene was prepared by chemical etching followed by probe sonication. After that, gold was deposited on its surface by reduction of tetrachloroauric acid using $NaBH_4$ as a reductant. This section is categorized into three main parts: 1. Preparation and characterization of the nanomaterials. 2. In vitro viability results of MXene and MXene/Au treated cells after laser exposure. 3. Nanomaterials uptake by cells under different conditions.

3.1 Synthesis and characterization

3.1.1 SEM

3.1.1.1 MXene

Mxene was produced by wet chemical etching to remove the A layer from the MAX precursor, which binds strongly to M element. This was followed by intercalation with large molecular weight molecule (DMSO) and delamination (Alhabeb et al., 2017). As represented in Figure 20 A, MAX phase has layered into a closely packed structure, which spread out after the removal of Al resembling an accordion [103] (Figure 20 B**).** Delaminated single MXene sheets are represented in **Figure 20 C**, **and 20 D** at higher magnification. Using SEM measurements, the average sheet size was found to be 190 nm ± 35. This size is optimum for biomedical applications for PTT[104].

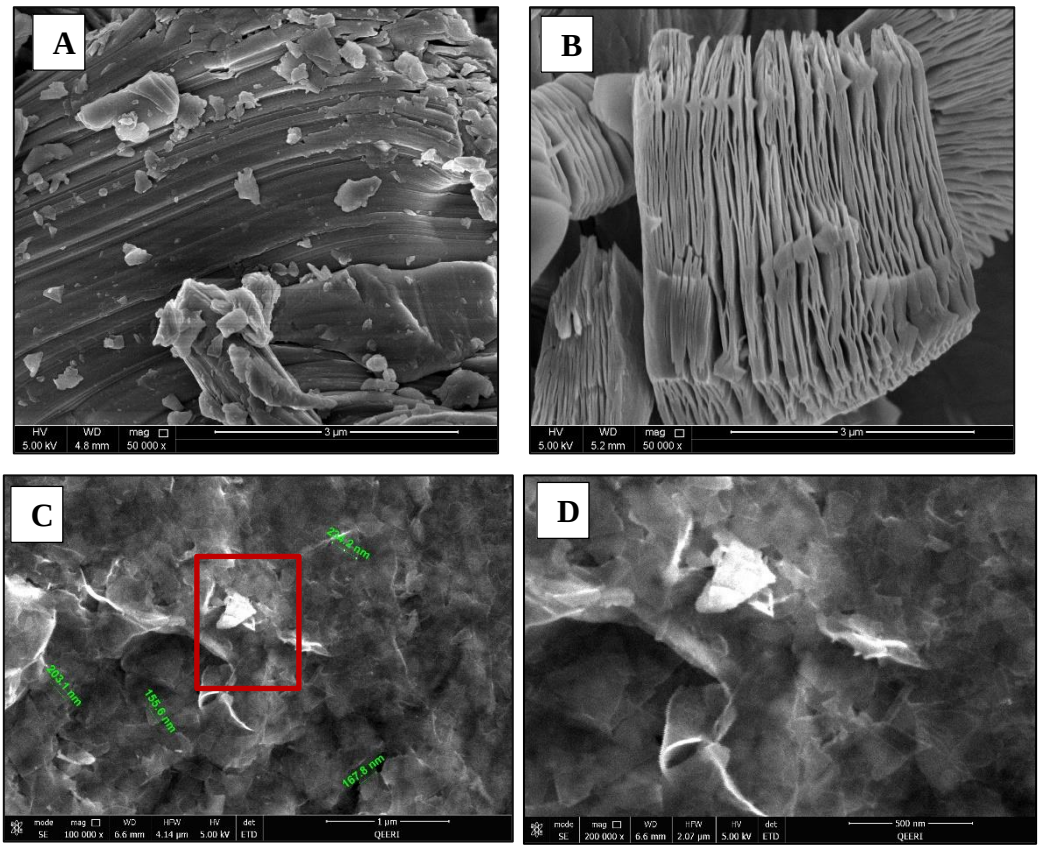

Figure 20: A) *MAX phase* ***B)*** *etched MAX phase* ***C)*** *MXene nanosheets* ***D)*** *MXene nanosheets at higher magnification.*

3.1.1.2 MXene /Au nanocomposite

Au nanoparticles were deposited on MXene surface by reduction reaction, to produce a composite with better photothermal efficiency. **Figure 21 A, B** represents homogeneous distribution of Au nanospheres on MXene sheets. The average size of MXene sheet is 190.1± 46 nm. The diameter range of Au nanoparticles is 25-30 nm. Usually, Au nanospheres have their highest photothermal efficiency at sizes ranging from 10 to 30 nm compared to nanospheres that are outside this range[105].

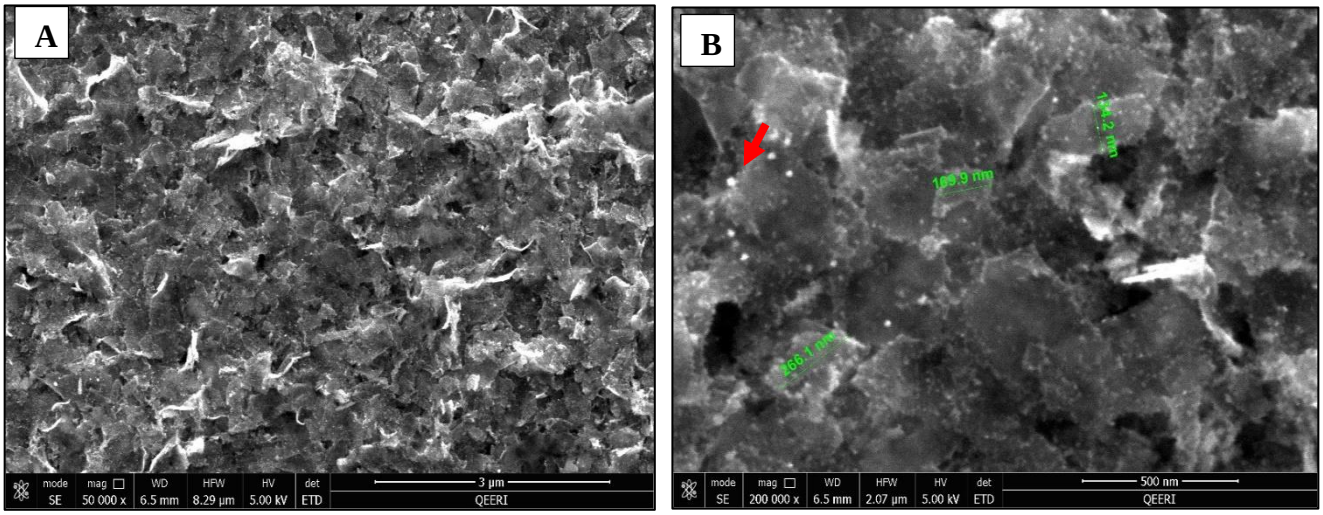

Figure 21: A) *Mxene with Au nanoparticles deposited on the surface of the sheet.* ***B)*** *MXene/Au nanocomposite at higher magnification, showing homogeneous distribution of Au on Mxene surface (red arrow represents Au nanoparticle).*

3.1.2 TEM

TEM was used to characterize MXene sheets and MXene/Au nanocomposite to visualize Au nanospheres hidden between the MXene sheets. **Figure 22 A** represents single MXene sheet with size within the average obtained from SEM. **Figure 22B** represents Au nanoparticles (black spots) coating the MXene sheet. Elemental mapping was done for MXene/ Au nanocomposite to detect the elements present in the material. **Figure 23** indicates the presence of Au (orange) as one of the elements demonstrating successful deposition of Au on MXene surface.

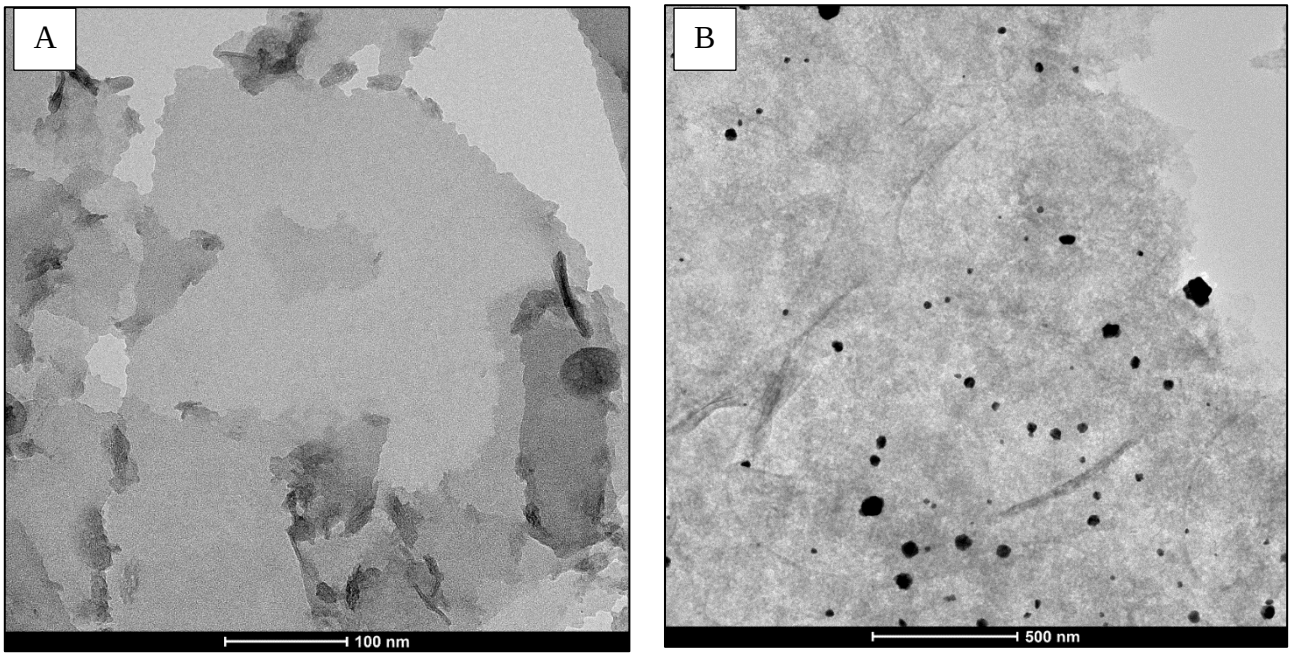

Figure 22: A) *Single MXene sheet* ***B)*** *MXene sheet with Au nanospheres coating its surface.*

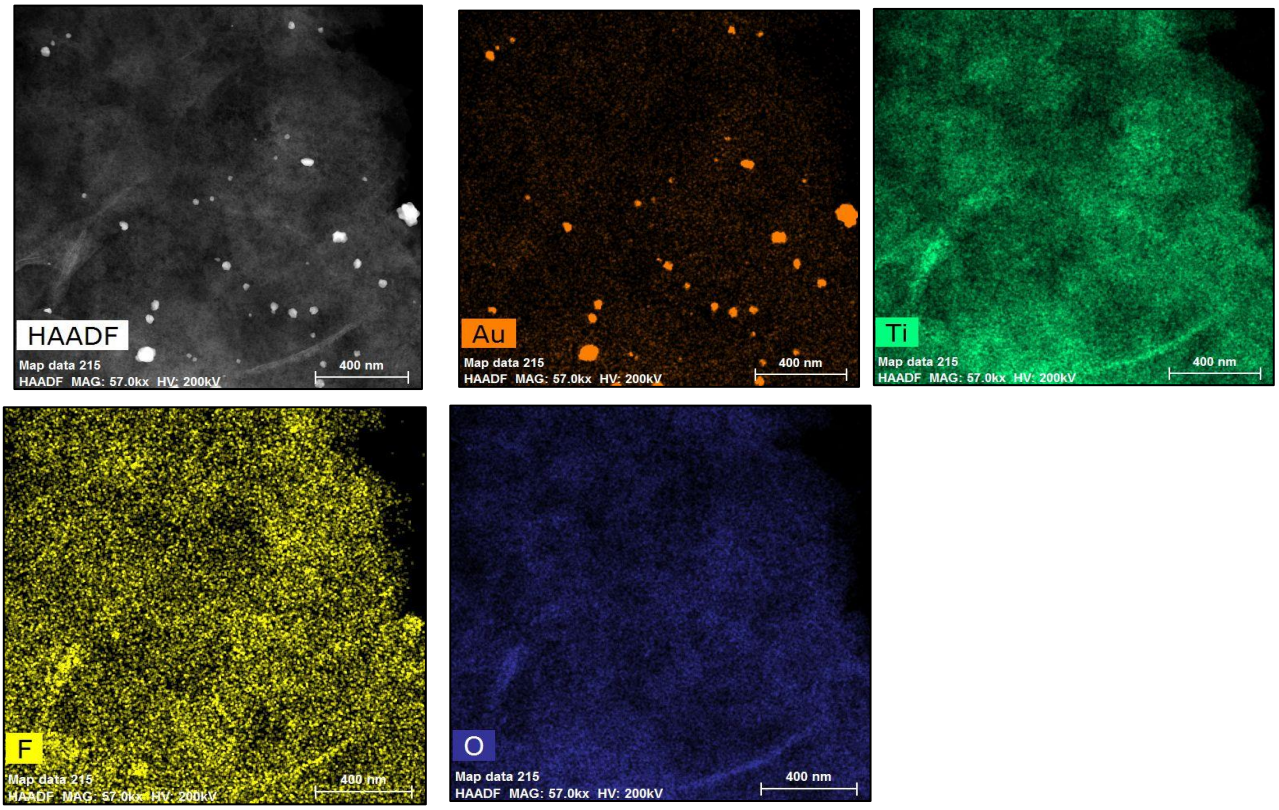

Figure 23: *elemental mapping for MXene/Au nanocomposite*

3.1.2 XRD

XRD was performed to reveal the crystal structure, also to support the material morphology obtained from SEM and TEM. **Figure 24** represents XRD peaks for the MAX phase, etched MAX, MXene and MXene/Au nanocomposite. XRD pattern for MAX phase demonstrates the purity of the MAX precursor (Ti_3AlC_2). One prevalent impurity is Ti_2AlC, which can be distinguished from Ti_3AlC_2 by the first XRD peak (002) around 9.5 in Ti_3AlC_2 and 13 in Ti_2AlC. The XRD pattern for MAX phase shows its first peak (002) at ~ 9.5 which is a satisfactory indicator that the MAX precursor is pure.

Good etching can be observed by the loss of Al peak from MAX precursor at $2\theta \sim 39°$ in both etched MAX and MXene. Comparing MAX phase to etched MAX and MXene, it can be observed that the two peaks (002) and (004) become wider and less intense with a slight shift to lower angles. Diffraction peaks from $2\theta = 35°$ to $45°$ were lost in MXene XRD which indicates delamination and loss of stacking. All of these observations were similar to MXene XRD patterns from the literature [106].

XRD pattern was obtained for MXene/Au nanocomposite and was compared to the reference file ICSD:53763 ICDD:00-004-0784 and ICDD:98-005-3763 to confirm the presence of Au. **Table 2** shows a comparison between Au NPs XRD peaks that are experimentally obtained, and those obtained from a reference file. XRD patterns obtained for the MXene/Au sample are similar to those from reference files, which confirms that the existing particles are Au NPs with cubic crystalline structure.

Table 2: *Comparison between reference and experimental diffraction angle of Au NPs*

No.	hkl	Experimental diffraction angle (2θ in degrees)	Reference diffraction angle ICDD:980053763 (2θ in degrees)
1	111	38.0185	38.078
2	002	44.1803	44.256
3	022	64.5	64.376
4	113	77.4557	77.312
5	222	81.6	81.448

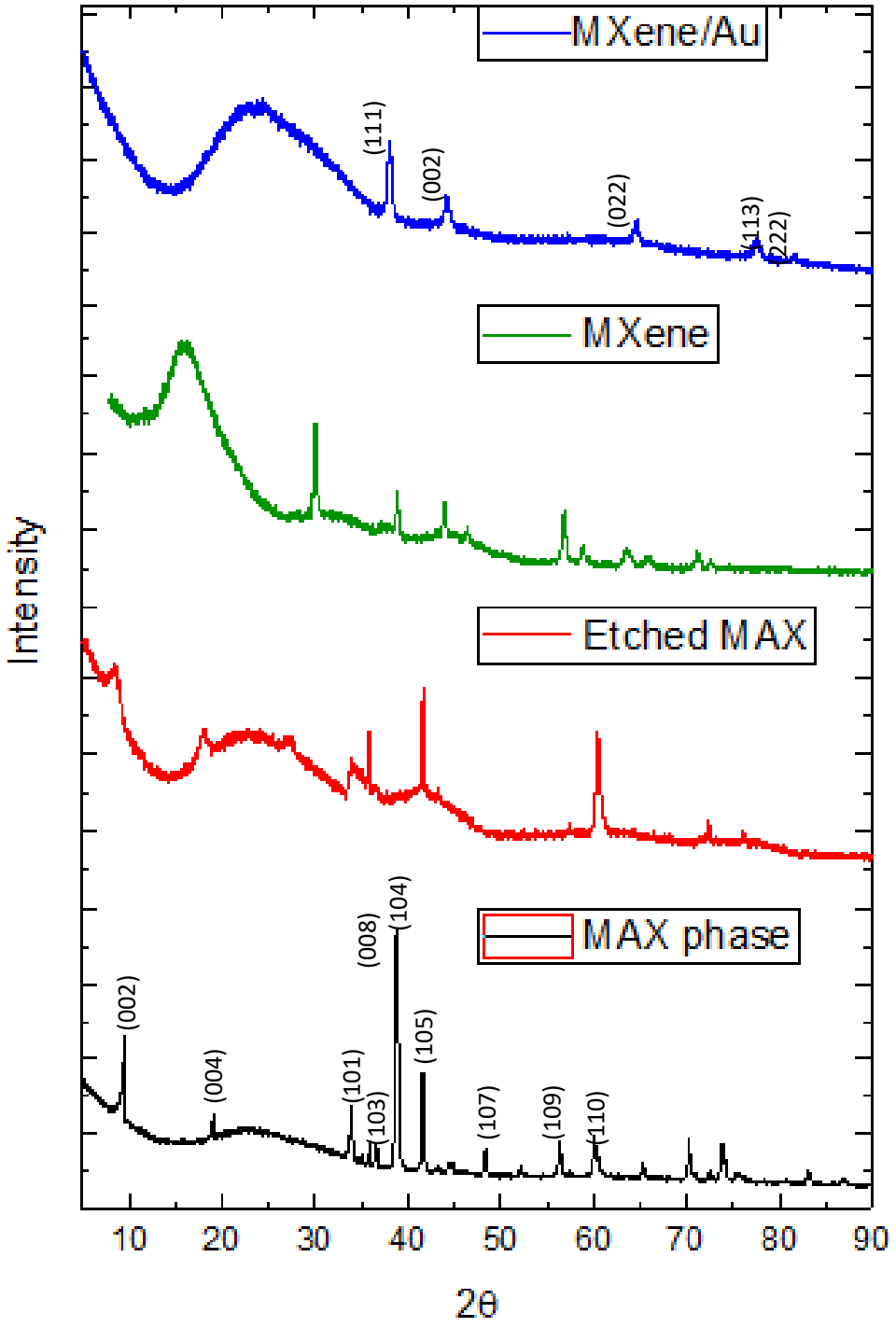

Figure 24: *XRD peaks for MAX phase, etched max, MXene and MXene/ Au nanocomposite.*

3.1.3 AFM

AFM was used to confirm the dimensions obtained by SEM and TEM, as MXene size is important for biomedical applications and cellular uptake.

Figure 25 A shows an AFM image for multiple MXene sheets with size range from 50-200 nm. Size measurements obtained from AFM are close to those obtained from TEM and SEM, although size values obtained from AFM are more accurate. This average size is still acceptable for cellular uptake.

Figure 25 B shows MXene sheet which was exposed to probe sonication for fewer time as in **Figure 25 A**, which shows a big sheet with 4 nm thickness.

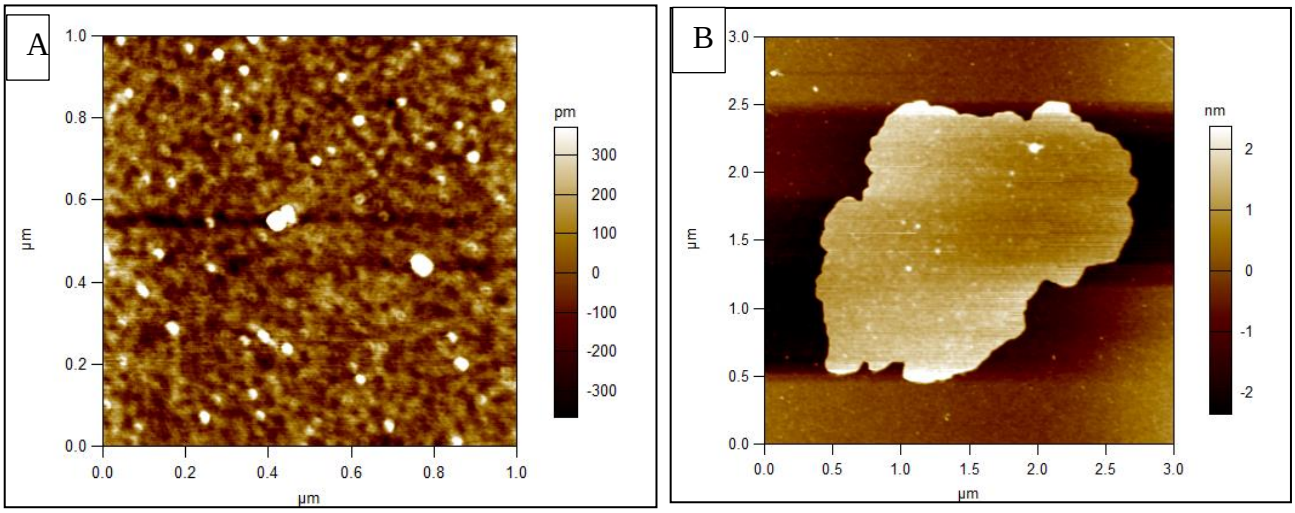

Figure 25: *AFM for measuring MXene sheets dimensions.*

3.1.4 Zeta potential

The surface charge for MXene sheets was assessed **Table 3** to know more about the material properties, so its interaction with the biological system can be predicted. MXene showed a negatively charged surface, which was expected due to the presence of negative ions as functional groups (-OH group, fluorine, and oxygen)[107,108].

Table 3:*MXene surface charge*

T (°C)	**ZP (mV)**
25	-20.8
25	-21
25	-22
Mean	-21.3
STD	0.643

3.1.5 Temperature assessment

The temperature of MXene and MXene/Au was assessed and compared after laser application at different power densities and concentrations. Two methods were used for temperature assessment (Thermometer- temperature probe and thermal camera). There is some variation in the results obtained from the two methods, the thermometer showed fewer values compared to thermal camera. As per the temperature probe blocks some of the incident laser light; having fewer measurements when using the thermometer is expected.

3.1.5.1 Photothermal comparison in MXene and MXene/Au

Temperature measurements for MXene and MXene/Au were compared at power density of 1 W/Cm^2 and at three different concentrations (50,100 and 200 ug/ml). The results showed less temperature increment in MXene/Au compared to MXene alone **Table 4**. The concentration must be doubled in MXene/Au to get temperatures closer to MXene at a certain concentration **Figure 26**. This inefficiency in MXene/Au can be attributed to the maximum absorption wavelength of Au nanoparticles (~ 540 nm for 25-30 nm Au nanoparticles) [105]**Figure 27,** which is different than the absorption wavelength in MXene (~ 800 nm) [46]. These results are similar to what obtained by Zagho et al. They mentioned that the reduced photothermal efficiency in MXene/Au might be due to the integration of Au NPs in MXene sheets. which might alter MXene properties (size) and influence the PT activity.

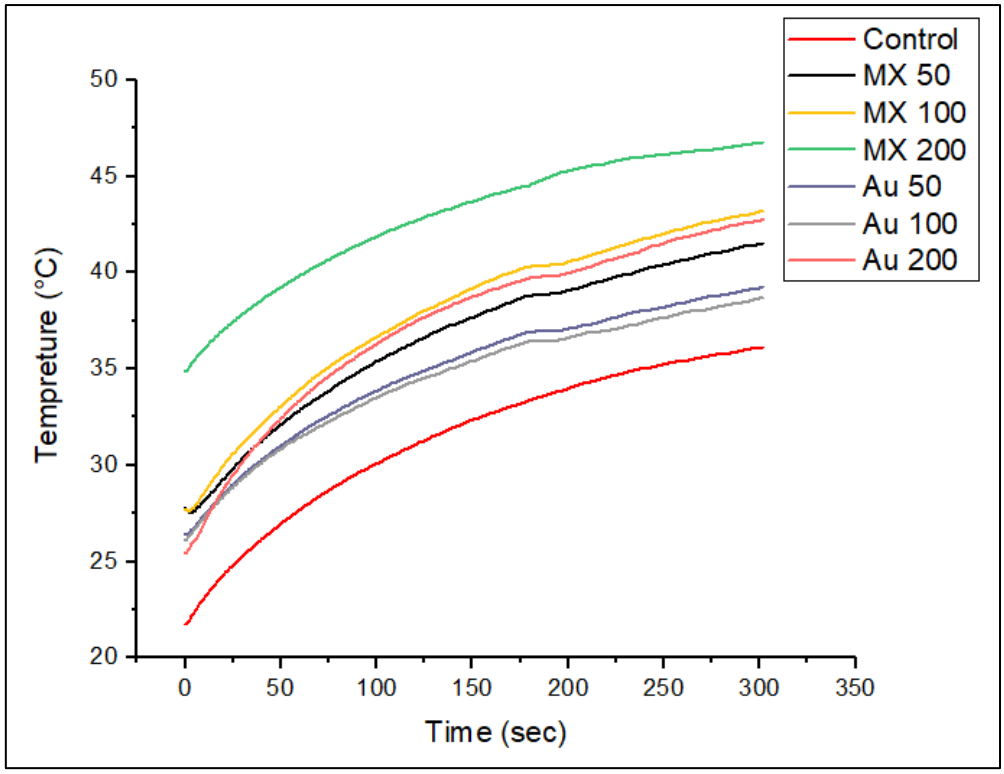

Figure 26: *Different temperature measurements for MXene and MXene/Au at PD=1 W/Cm2*

Table 4:*Comparison between MXene and MXene/Au at different concentrations, PD=1 W/Cm2*

Concentration (ug/ml)	**MXene Temperature in °C**	**MXene/Au Temperature in °C**
50	41.4 ± 0.36	38.8 ± 0.15
100	43.9 ± 0.585	40.1 ± 0.79
200	46.7 ± 0.25	42.8 ± 0.26

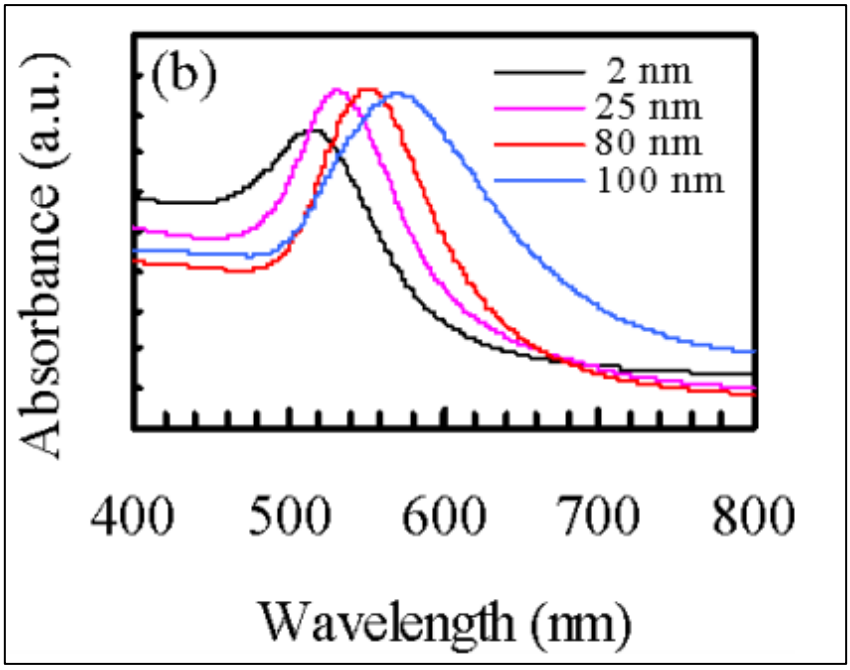

Figure 27: *Size, absorbance wavelength relationship for Au NPs*

3.1.5.2 Detailed temperature measurements for MXene

The thermal camera was used to assess the raise in MXene temperature after laser exposure. Different laser power densities were applied for two MXene concentrations (100 and 200 ug/ml). For all the cases, it took the MXene one minute to reach the maximum temperature which stays constant at the rest of the five minutes. After removing the incident laser light, it took ~ 4 minutes for the solution to reach 37 °C.

The results in **Figure 28** and **Figure 29** show a trend, as when increasing the concentration or the power densities the temperature increases. However, for power densities of 3 and 5, similar results were obtained; which can tell that this is the maximum limit that MXene can be heated, and beyond this limit (~ 99 °C) there will not be any increment in temperature even when increasing the MXene concentration.

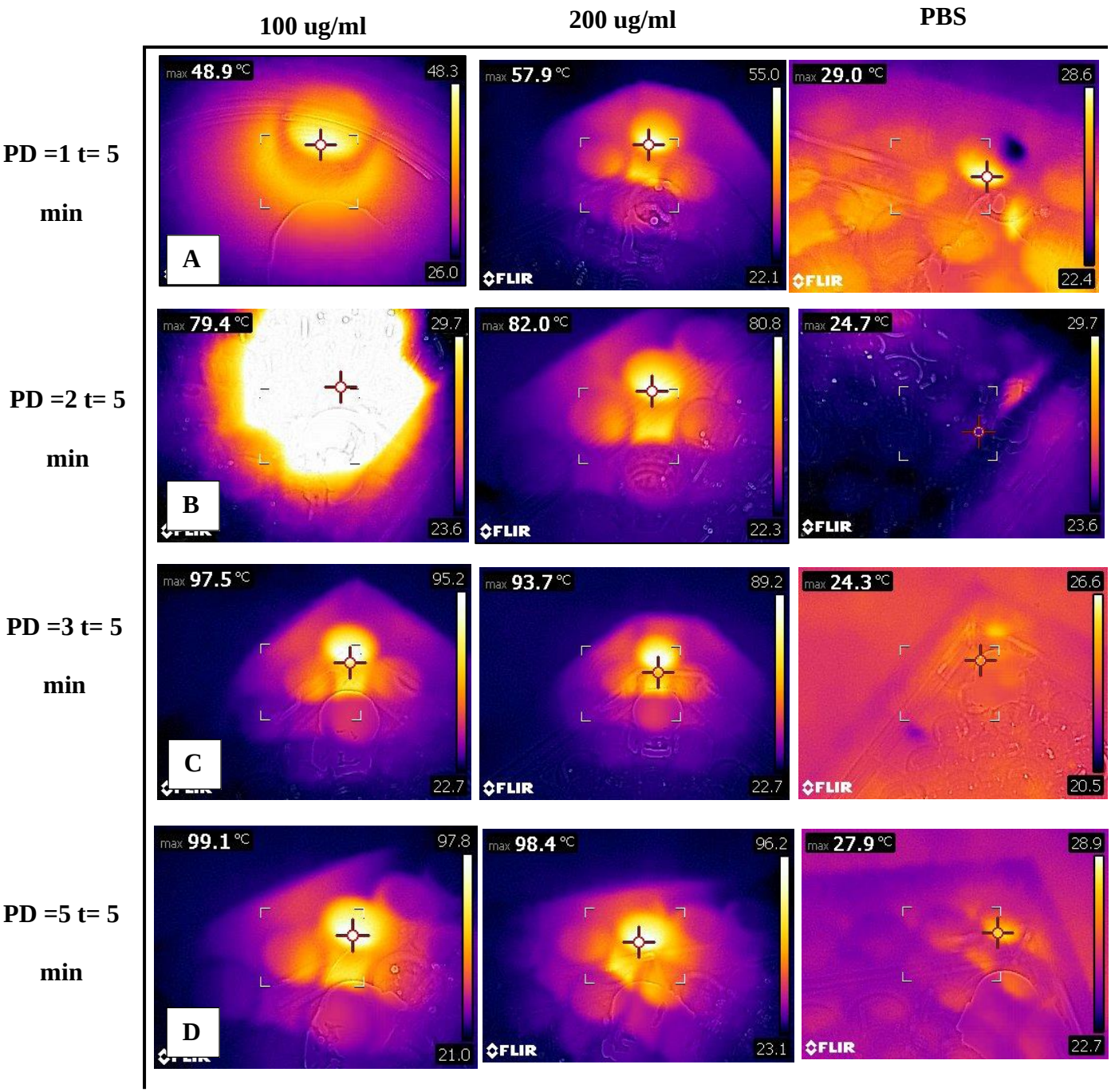

Figure 28:*Temperature measurement of MXene at different PD and concentrations. A) Temperature measurement of MXene at PD= 1 W/Cm^2 B) Temperature measurement of MXene at PD= 2 W/Cm^2 C) Temperature measurement of MXene at PD= 3 W/Cm^2 D) Temperature measurement of MXene at PD= 5 W/Cm^2*

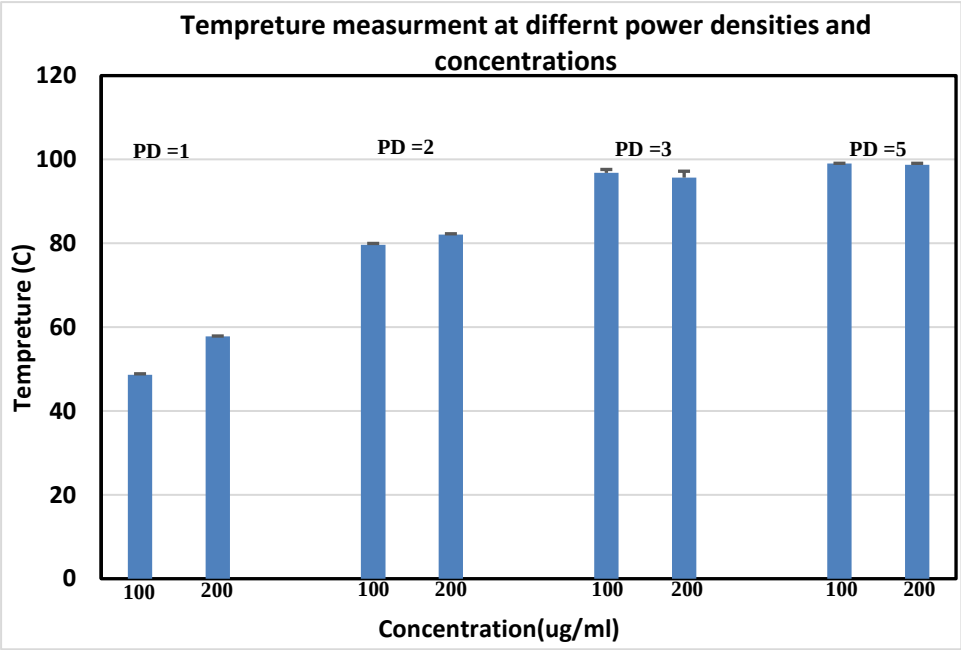

***Figure 29**:Average temperature for MXene at different PD and concentrations*

3.2 Photothermal effect- Cell viability assessment

MXene photothermal effect was assessed after exposure to breast cancer cells (MDA-231) upon laser irradiation. In this section, different conditions were tested to find out the best condition where MXene is most effective with cells being under fluid shear stress.

3.2.1 The effect of different PD and exposure times

Cells were treated with 100 ug/ml MXene under fluid flow and then exposed to laser with different power densities (1, 3 and 5 W/Cm^2) for different durations (5,10 and 15 minutes). This was done as optimization to find out the best condition where cells are damaged.

From **Figure 30** and **Figure 31** no cell death was induced in MXene and laser exposed cells at PD =1 W/Cm^2 for all durations. In this case. the treated groups resemble the control groups. When the temperature was measured after 15 minutes of laser exposure,

it was ~ 34 °C which is not enough to induce photothermal ablative effect as the optimum living condition for cells is 37 °C [110].

The same experiment was repeated but with increasing the laser PD to 3 W/Cm^2 **Figure 32** and **Figure 33**. The results suggest no difference between control groups and treated groups. The cells were completely viable in all MXene treated and laser exposed groups at all the duration. After 15 minutes of laser exposure, the temperature was raised up to 38.7 °C, which is not sufficient to induce protein denaturation and cell death [111].

When the PD was increased to 5 W/Cm^2, no cell death was noticed for the three durations. However, a temperature increment was noticed which reached up to 43 °C. This temperature is not enough to induce cell death [112] **Figure 34** and **Figure 35**.

Since none of the applied laser power densities and durations could induce cell death in MXene, MXene/Au nanocomposite was not tested. As MXene/Au showed less photothermal efficiency compared to MXene alone; it is not expected to raise the temperature and induce cell death.

To induce cell death in short period of time, the temperature must reach more than 50 °C[112]. it was reported by Nagashima & Takagi that tumor metastasis can be inhibited if cancer cells are exposed to 43 °C for longer durations (40 minutes) [113]. Here, Cells were not exposed to laser for more than 15 minutes to meet the concept of photothermal ablation i.e. exposure to high temperatures for short periods [31].

Cells did not die as the temperature was not high enough to induce cell death, this is mainly due to low MXene uptake by the cells, as MXene alone showed higher temperatures when irradiated.

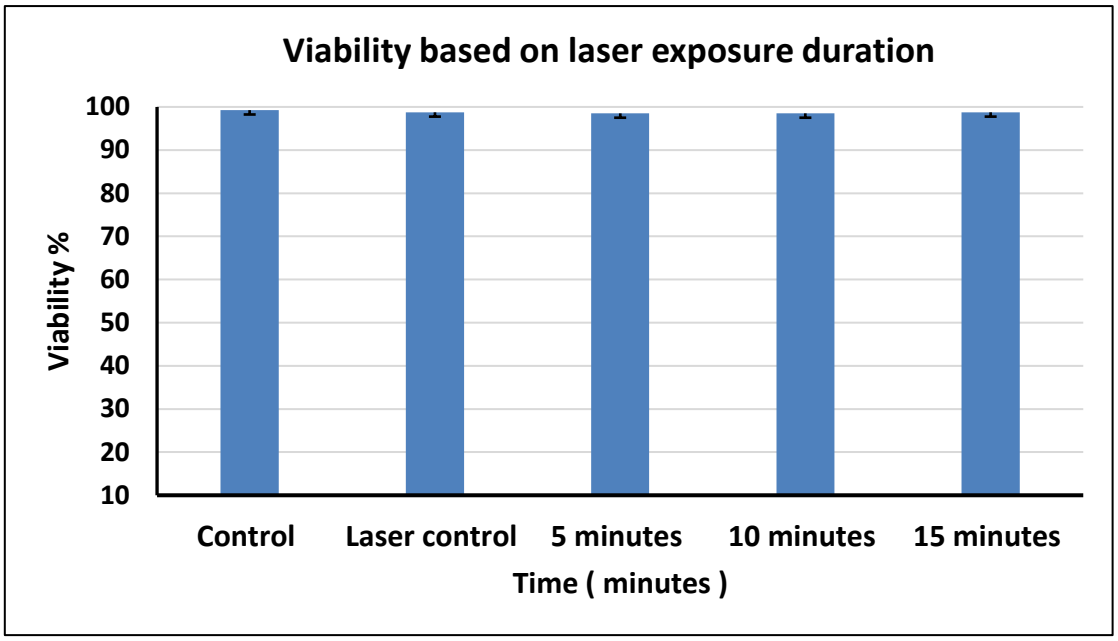

Figure 30:*Cell viability after exposure to PD =1 W/Cm2 for different durations (5,10 and 15 minutes)*

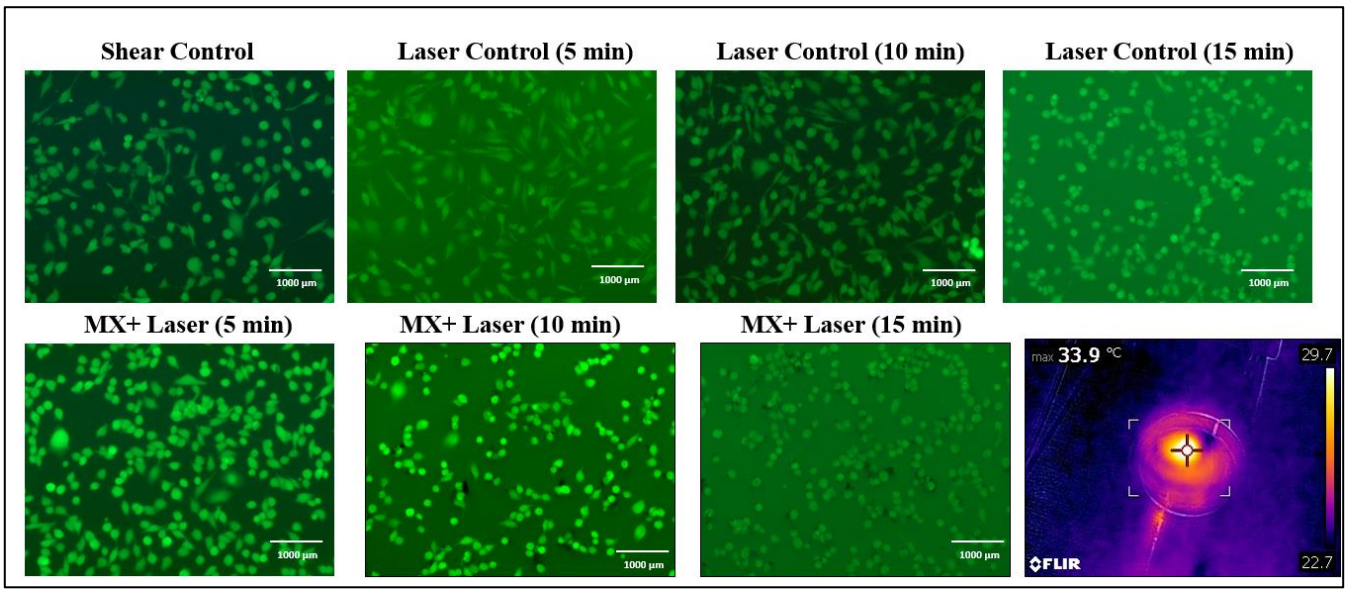

Figure 31: *Live/dead assay for Cell viability assessment after exposure to PD =1W/Cm2 for different durations (5,10 and 15 minutes)- The green color represents live cells.*

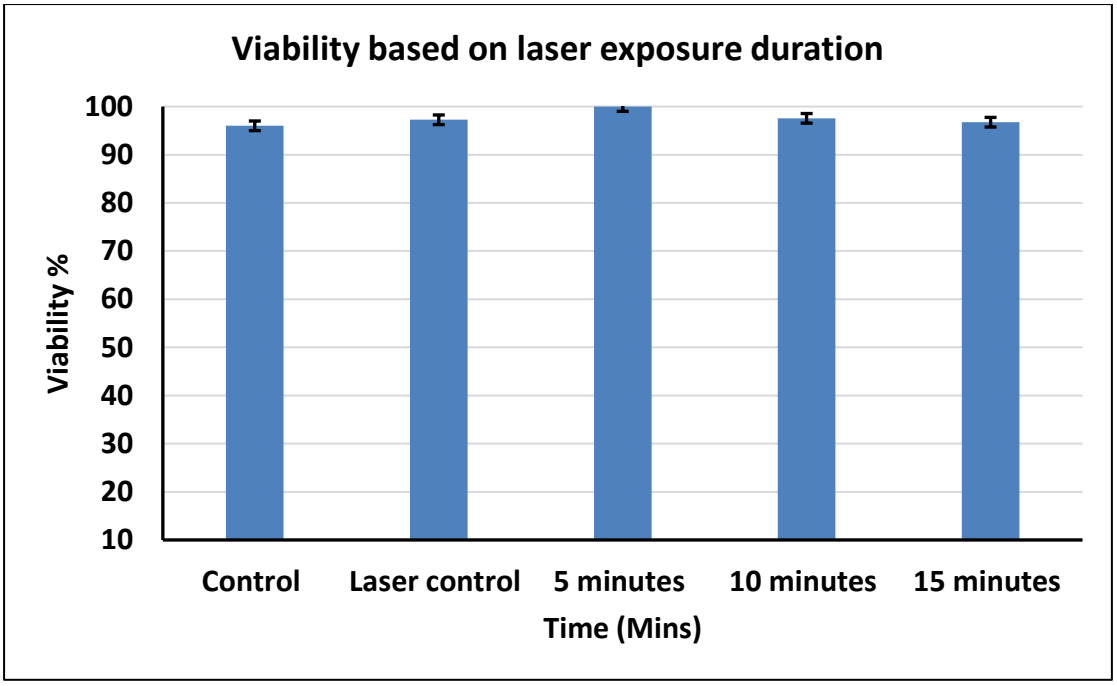

Figure 32:*Cell viability after exposure to PD =3 W/Cm2 for different durations (5,10 and 15 minutes)*

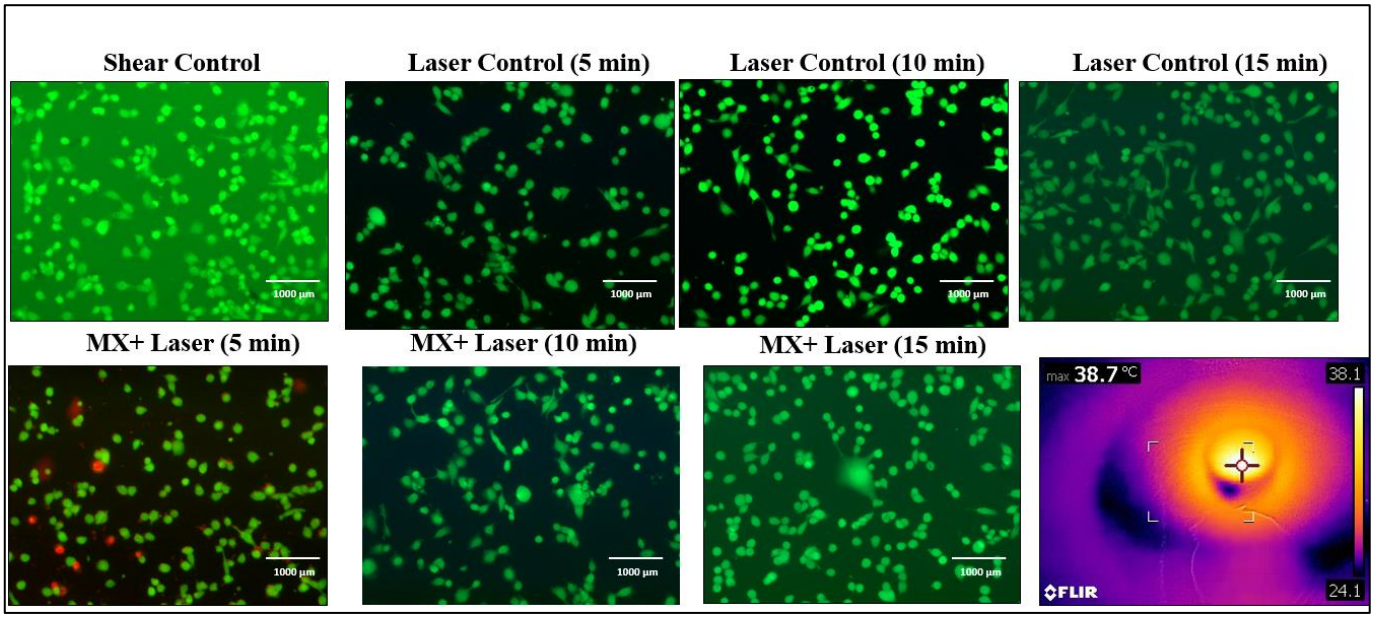

Figure 33:*Live/dead assay for Cell viability assessment after exposure to PD =3 W/Cm2 for different durations (5,10 and 15 minutes)- The green color represents live cells*

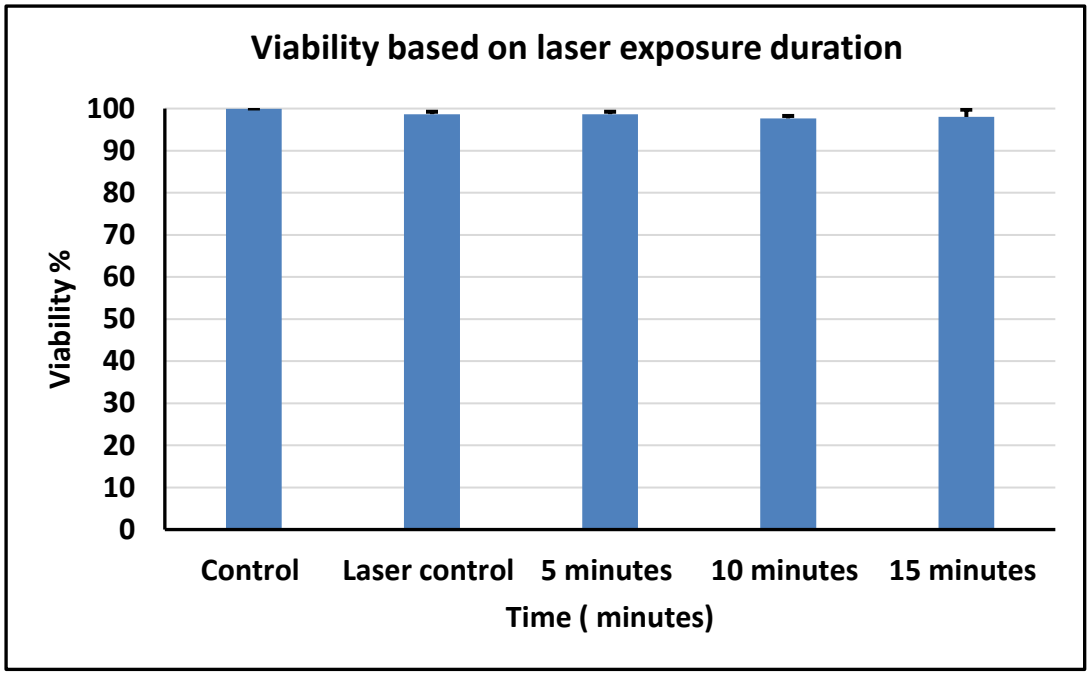

Figure 34:*Cell viability after exposure to PD =5 W/Cm2 for different durations (5,10 and 15 minutes)*

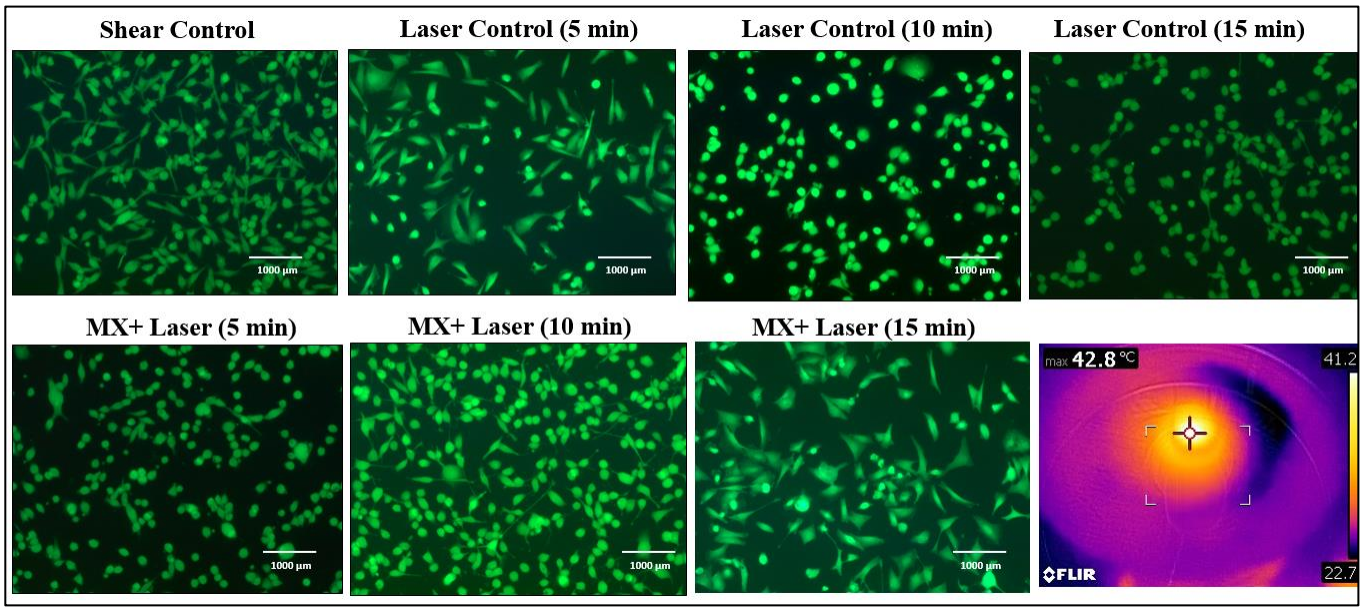

Figure 35: *Live/dead assay for Cell viability assessment after exposure to PD =5 W/Cm2 for different durations (5,10 and 15 minutes)- The green color represents live cells*

3.2.2 The effect of using different flow chamber dimensions

From the previous results, the cells were completely viable, this was attributed to low MXene uptake. Here, the chamber dimensions were changed, the thickness of the silicon gasket was reduced by half (0.5 mm instead of 1 mm). Reducing the thickness will reduce the distance between the particles and cells, thus the interaction will be better. In this experiment, the cells were treated with 100ug/ml MXene under fluid flow for four hours, then exposed to laser PD= 5 W/Cm^2 for 15 minutes.

From **Figure 36**, it is shown that cell viability was not affected by changing the chamber dimensions, which means that the cells are not interacting with the material not due to a technical issue. This lack of interaction is probably due to particle related properties.

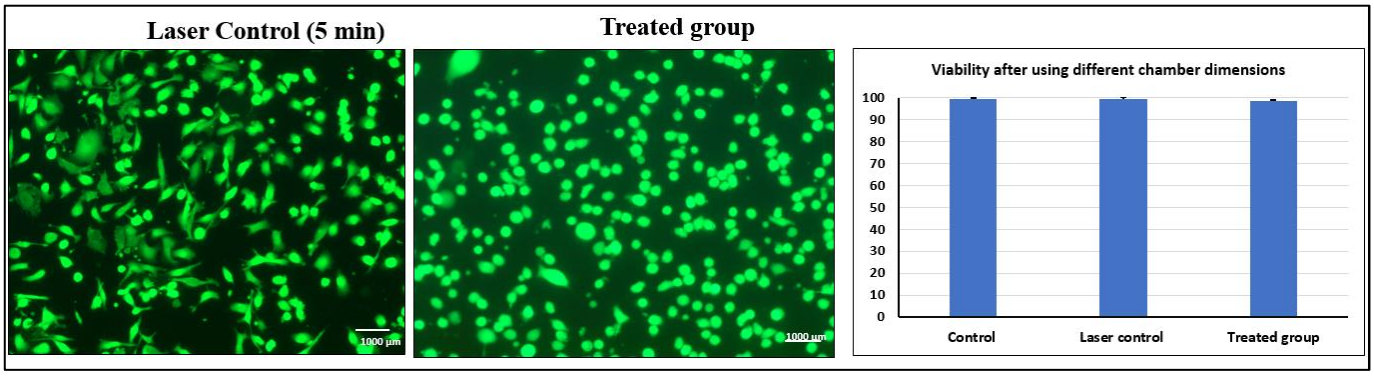

Figure 36:*Live/dead assay for Cell viability assessment after exposure to PD =15 W/Cm2 for 5 minutes- The green color represents live cells.*

3.2.3 The effect of the presence of serum in cell media

In cell culture, the cells are kept in media that have serum for the cells to obtain their necessary nutritional needs. It has been reported in literature that serum proteins tend to interact with nanomaterials if not properly functionalized. When serum proteins interact with nanomaterials, they form what is known as “protein corona”. Protein corona is formed when serum proteins cover the surface of the nanomaterial, which would induce changes in the particles such as size and surface charges. The formation of protein corona will alter many cellular processes, such as cell adhesion and cellular uptake. [114,115,116].

Here, MXene was dispersed in serum-free media, to prevent the formation of protein corona. The cells were treated with MXene for 4 hours under fluid flow, then exposed to laser at PD =5 W/Cm^2 for 15 minutes.

The results in **Figure 37** suggests no difference in viability between control and treated groups. This indicates that, serum proteins are not the main contributors to low MXene uptake by cells.

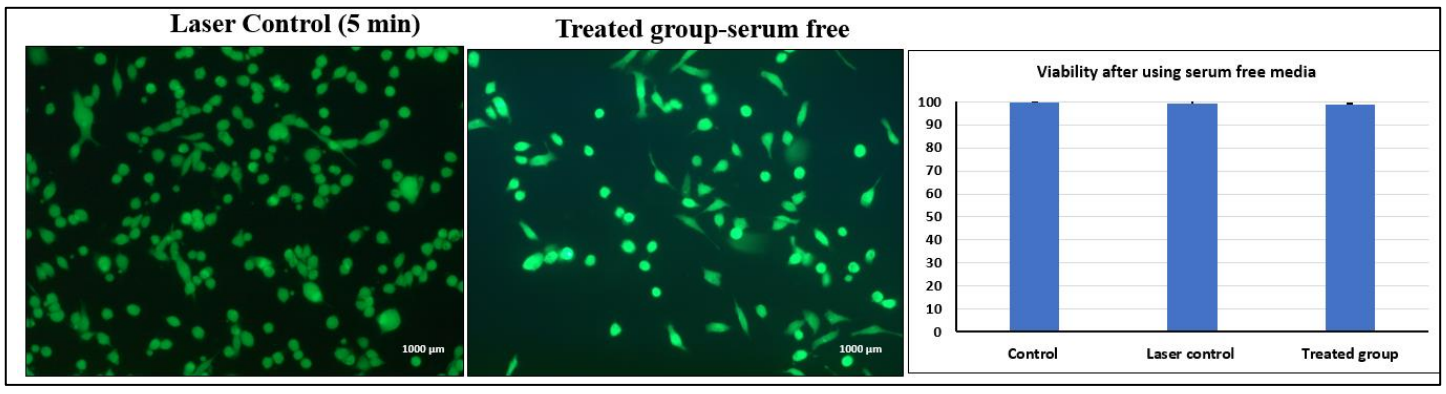

Figure 37:*Live/dead assay for Cell viability assessment after exposure to PD =5 W/Cm2 for 15 minutes- The green color represents live cells.*

3.2.4 The effect of using different MXene concentration

The concentration of nanomaterials plays a role in material uptake by cells, i.e. changing the concentration will influence the way that the cells uptake the materials. As the concentration increases, there is a higher tendency that the material will form aggregates. This aggregate formation will affect the size of the material; thus the uptake route will be different.[117]

To find out the best condition where the cells die due to MXene and laser exposure, the concentration of MXene was doubled. Here, cells were treated with 200ug/ml MXene for 4 hours then exposed to laser PD=5 for 15 minutes.

Even when doubling the concentration, the cell viability was not affected **Figure 38**. Temperature increment was not more than 42 °C which reflects the amount of MXene present inside the cell. We conclude from here, that there is a maximum limit the cell can uptake MXene, which is independent of concentration.

The fewer aggregates formation can be related to the fluid flow in the chamber used; which prevents particles to settle and aggregate. This fluid flow is more realistic and helps to reduce the physiochemical stresses on the cells, by preventing aggerate formation[67].

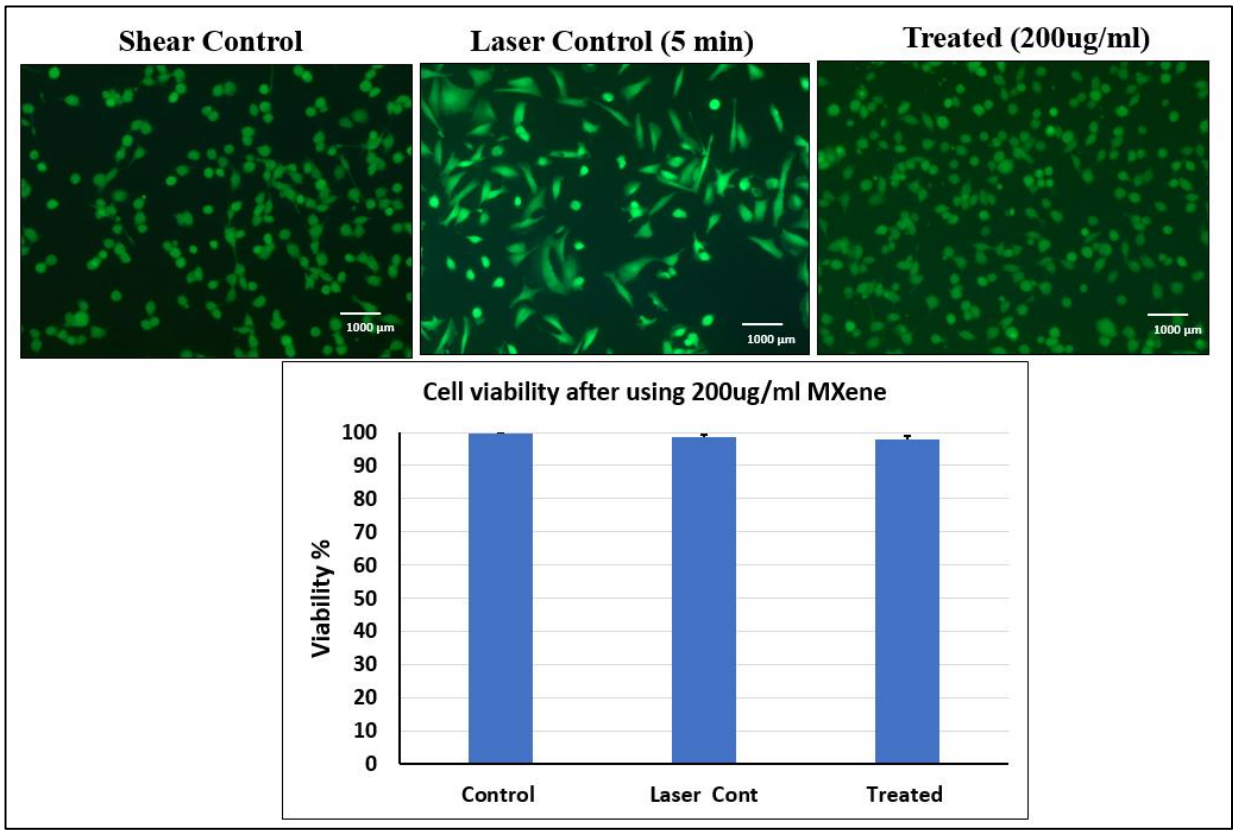

Figure 38: *Live/dead assay for Cell viability assessment after exposure to PD =5 W/Cm2 for 15 minutes- The green color represents live cells*

3.2.5 The effect of using different incubation time

The incubation time might affect the material cell interaction, as there will be more time for the particles to be internalized by the cells. Safi et al. showed that the cellular uptake of quantum dots was directly proportional to increasing the incubation time [118].

To test that,200ug/ml MXene was incubated with the cells under fluid flow for 8 hours (doubling the incubation time) and then was exposed to laser PD=5 for 15 minutes. **Figure 39** shows no difference in cell viability in control groups compared to treated. The temperature range was 39-41 °C in the treated group which is reflective to the amount of MXene internalized by the cells. Correspondingly, this temperature range is not enough to induce cell death for this duration.

3.2.6 The effect of re-incubation the cells after laser treatment

Although there was a mild increment in temperature in pervious results, cell death was not achieved. However, this increment in temperature can cause stress to cells, which might lead to changes in cellular function [119]. To find this effect, cells should be re-incubated after laser treatment for some time, after that viability was assessed.

Cells were treated with 100ug/ml MXene for 4 hours, then exposed to laser PD=5 for 15 minutes. The cells were re-incubated for 1 hour with complete cell media, after that the viability was assessed. The cells were completely viable after re-incubation **Figure 40**. Moreover, cell morphology was not affected which suggests that this mild temperature increment was not enough to damage the cells.

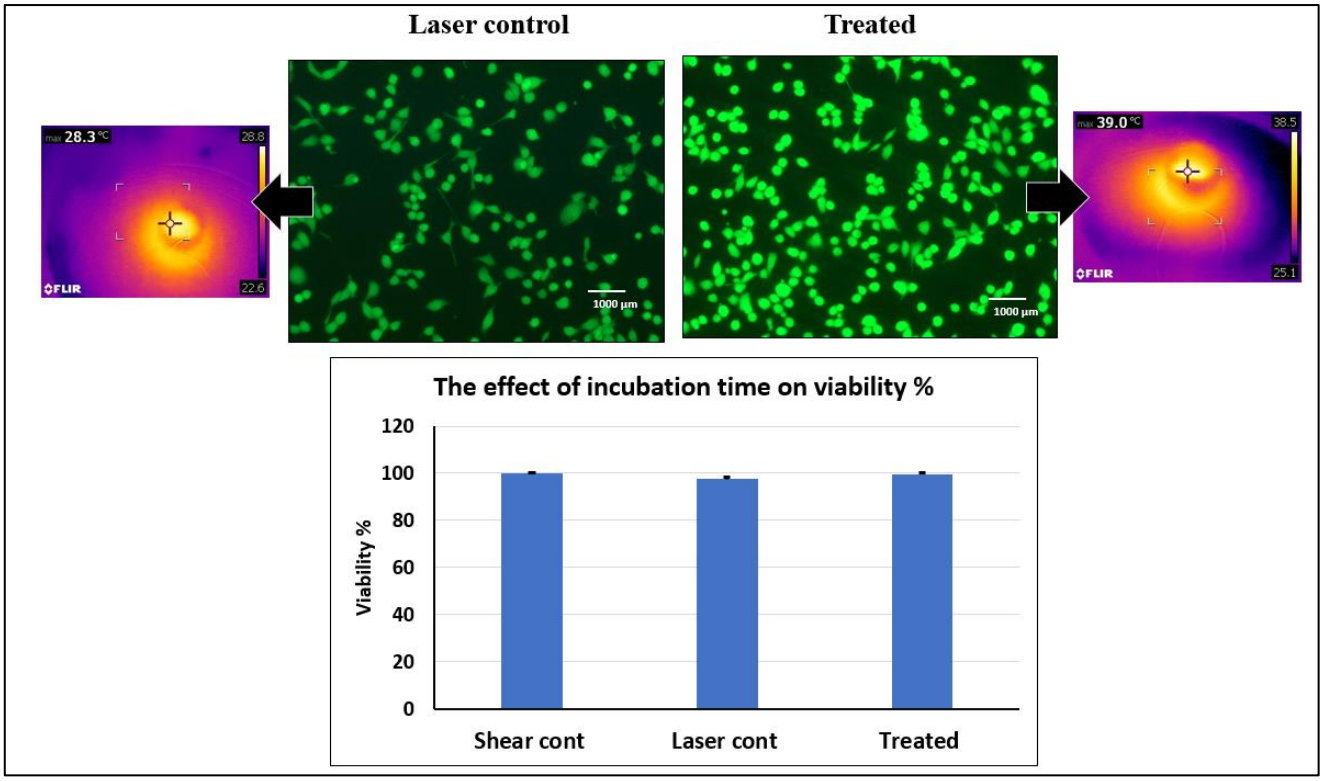

Figure 39:*Live/dead assay for Cell viability assessment after exposure to PD =5 W/Cm2 for 15 minutes- The green color represents live cells*

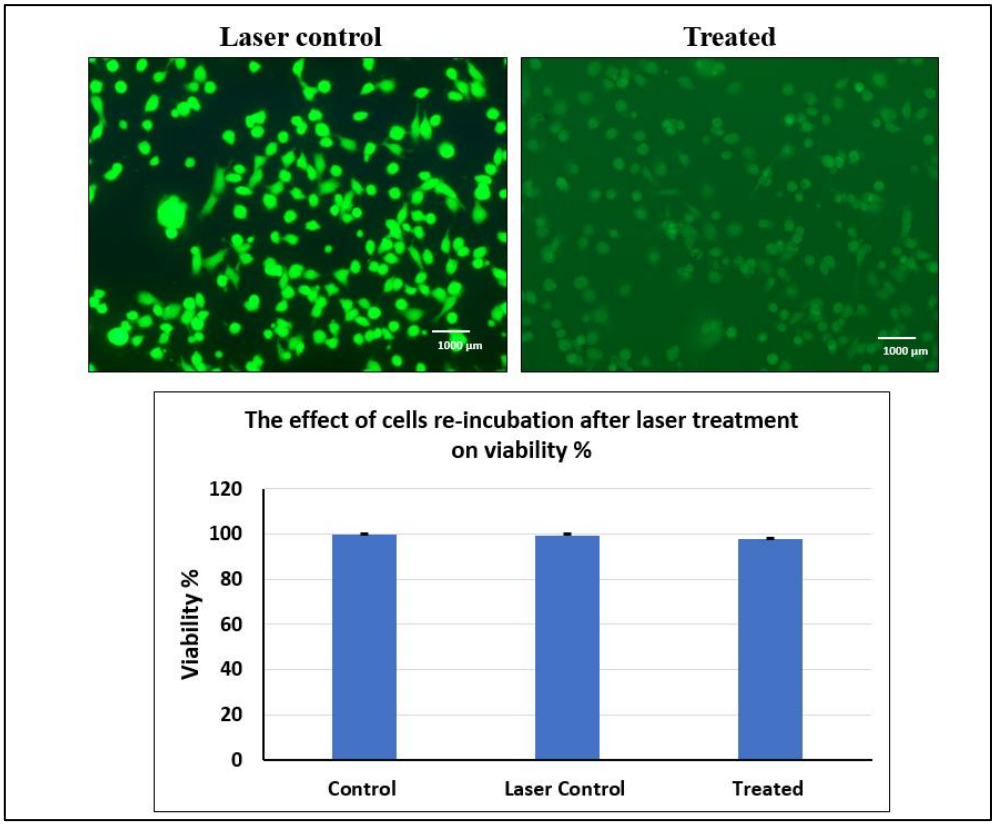

Figure 40:*Live/dead assay for Cell viability assessment after exposure to PD =5 W/Cm2 for 15 minutes- The green color represents live cells*

3.2.7 The effect of shear adaptation

Shear adaptation means, exposing the cells to shear stress before exposing the cells to the drug or nanomaterial. Shear adaptation has shown to influence the internalization of Au NPs by endothelial cells [92].

In this experiment, cells were exposed to shear stress for 4 hours then treated with 100 ug/ml MXene under static conditions. After that, the cells were exposed to a laser of PD=5 for 15 minutes.

The results suggest no difference between treated and control groups **Figure 41.** Which indicates low MXene uptake that results in mild temperature increment which is not satisfactory to kill the cells.

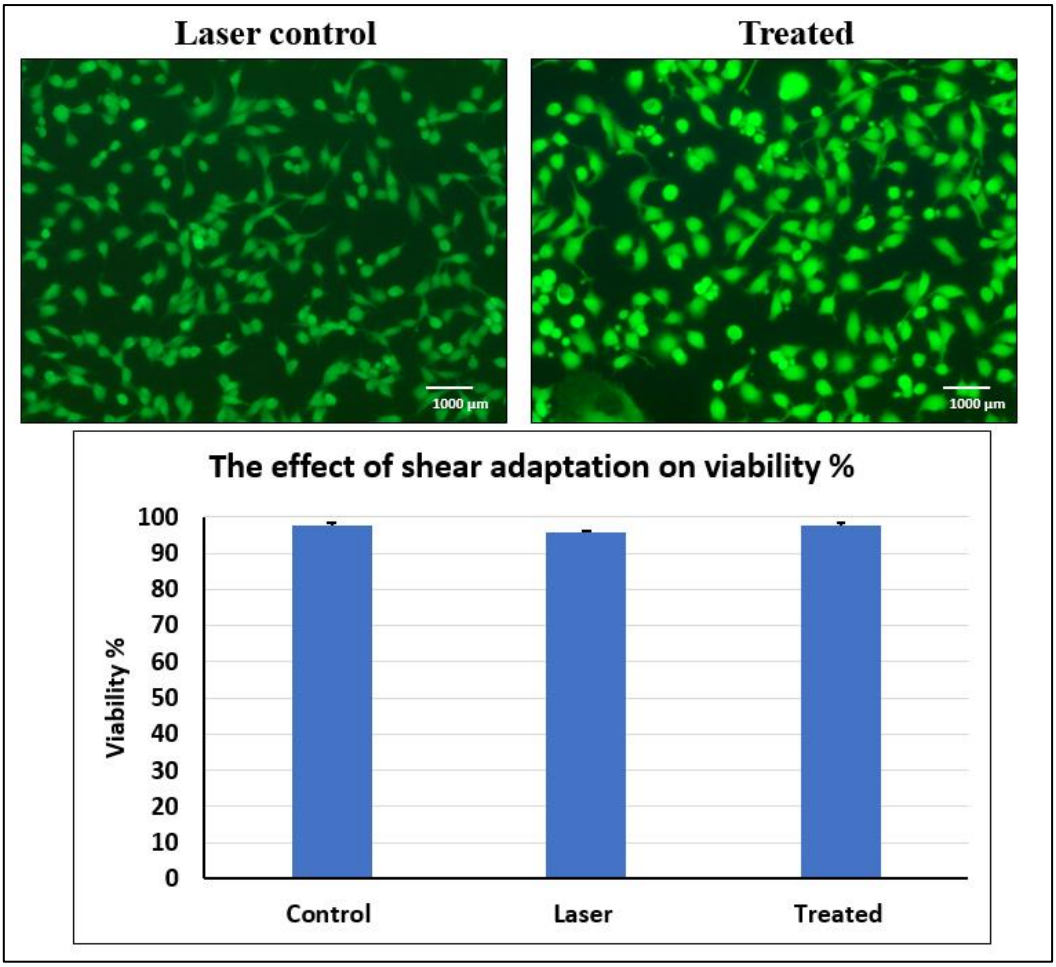

Figure 41:*Live/dead assay for Cell viability assessment after exposure to PD =5 W/Cm2 for 15 minutes- The green color represents live cells*

3.3 Cellular uptake assessment

The uptake of MXene nanosheets was assessed by three different methods, to support the viability data. Confocal microscopy was performed as a preliminary test to make sure that MXene was internalized. SEM and EDS for elemental analysis were carried out to detect Ti in cells, which can give an indication about the weight % of MXene that is present. TEM was used to visualize MXene sheets clearly inside the cells and spot the MXene distribution.

3.3.1 Confocal microscopy

The confocal microscopy analysis allows for taking 3D pictures by stacking multiple images from the same area at different focuses (Z-stacking). We first made a confocal scan for MXene alone, as MXene is not fluorescently labeled. Here, we aimed to find out if Mxene would be visible in treated groups. Then, the cell's cytoplasm was stained green and the nucleus blue to distinguish where MXene is located. **Figure 42** shows that there is few Mxene particles uptaken, in both static and shear exposed cells (sliced 3D volume-arrow). This suggests that the cell can absorb MXene, but quantification and intensity measurement was not possible from Confocal scans as MXene is not fluorescently labeled. To overcome this, EDS analysis was performed to roughly estimate the weight % of MXene in cells.

3.3.2 SEM and EDS analysis

SEM was carried out to find out any morphological changes in cells after the treatment also to check the presence of MXene on the surface. Eight different cases were studied: shear exposed cells with two different durations (4 & 8 hrs) and concentrations (100ug/ml and 200 ug/ml) and static culture with two different durations (4 & 8 hrs) and concentrations (100ug/ml and 200 ug/ml). All the cases were morphologically healthy, and MXene sheets were not detected on the cell's surface (**Figure 43)**.

To measure the weight % of Ti in each of the 8 cases, EDS analysis was performed.

The bar chart in **Figure 44** represents the weight % of Ti in all the cases. Statistical analysis (ANOVA) revealed no significant difference between sample means. This data supports the viability results, where MXene uptake is independent of concentration and duration. Furthermore, fluid flow did not show any effect on MXene uptake compared to static culture. However, fluid flow is essential to get results that are closer to real cases.

3.3.3 TEM imaging

TEM imaging was performed for processed samples, to clearly visualize MXene sheets inside the cells, and, to confirm the results from confocal and EDS. **Figure 45** represents un-treated (control) cells, where all cells look morphologically healthy with clear organelles and internal structures, which suggests successful preparation and imaging.

Figure 46 represents multiple images for MXene treated cells. The MXene distribution in the cell population is not homogenous, as, in some of the cells, MXene is fully internalized. Nevertheless, other cells showed MXene associated with the cell surface (not removed when washed) yet not internalized. These results support the viability data and the mild increment in temperature

The low cellular uptake of MXene can be attributed to many factors, mainly the surface charge. As the cell surface is negatively charged, MXene is also negatively charged (zeta potential) and this charge similarities will prevent a good electrostatic interaction between cells and MXene, leading to low cellular association and uptake [120]. Moreover, MXene was not functionalized or coated with specific ligands that can bind to specific receptors on cells surface. This leads to lower uptake as well as non-homogenous internalization.

In addition to that, Mxene have 2D shape, this might affect the internalization.

Some studies showed better uptake of spherical nanoparticles compared to rod-shaped or 2D nanomaterials [121]. They suggested that the cell membrane wrapping, and internalization of rod-shaped materials is not desirable. The shape- cellular uptake relation was speculated to the area on the cell membrane covered by the particle. As in rod-shaped or 2D material, more area in cell surface would be coved compared to spherical NPs which will block some of the existing surface receptors leading to less particle's interactions and less uptake[122].

Furthermore, cell particle interaction is not limitless. The interaction is governed by thermodynamic rules. When cells reach equilibrium with the solution containing the particles, there won't be any further association or uptake[123].

In all viability and uptake results, it was clear that there is a limit that the particles are uptaken, and no further uptake beyond that limit. Particularly, there was no temperature increment more than 44 ºC in all conditions, additionally, Wt% of Ti was the same in all the cases.

To find out the maximum concentration of MXene internalized, different dilutions of MXene were made and exposed to different power densities. This was done to match the temperatures found from viability data with corresponding dilution **Figure 48.** The MXene concentration that matches the temperature found from viability results was approximately 3 ug/ml. Therefore, we concluded that, 3 ug/ml MXene was internalized by the cells in our experiments, which was not sufficient for the PTT kill the cells.

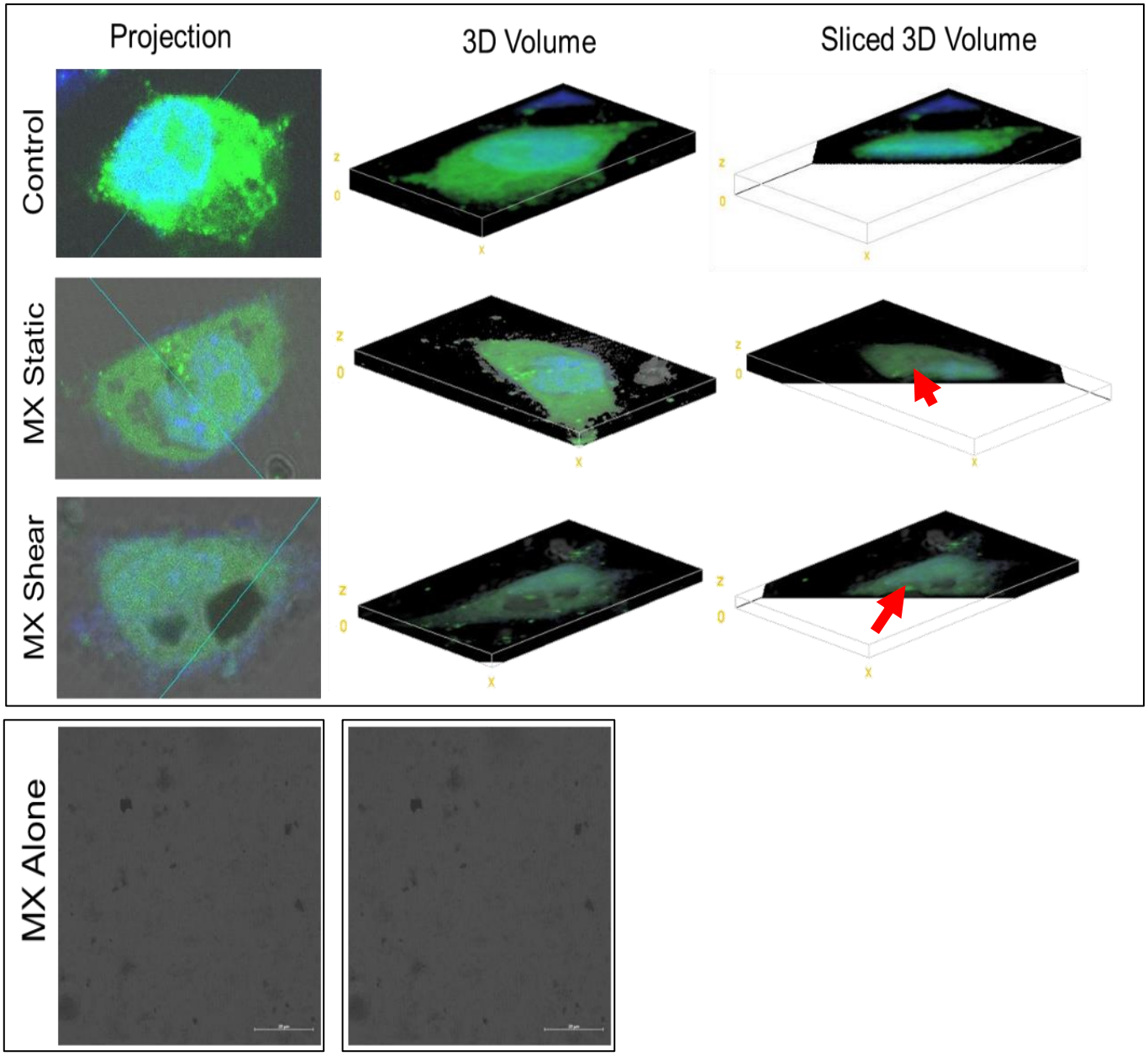

***Figure 42**: Confocal images for MXene treated cells under static and dynamic conditions. The golden arrow represents where MXene is located.*

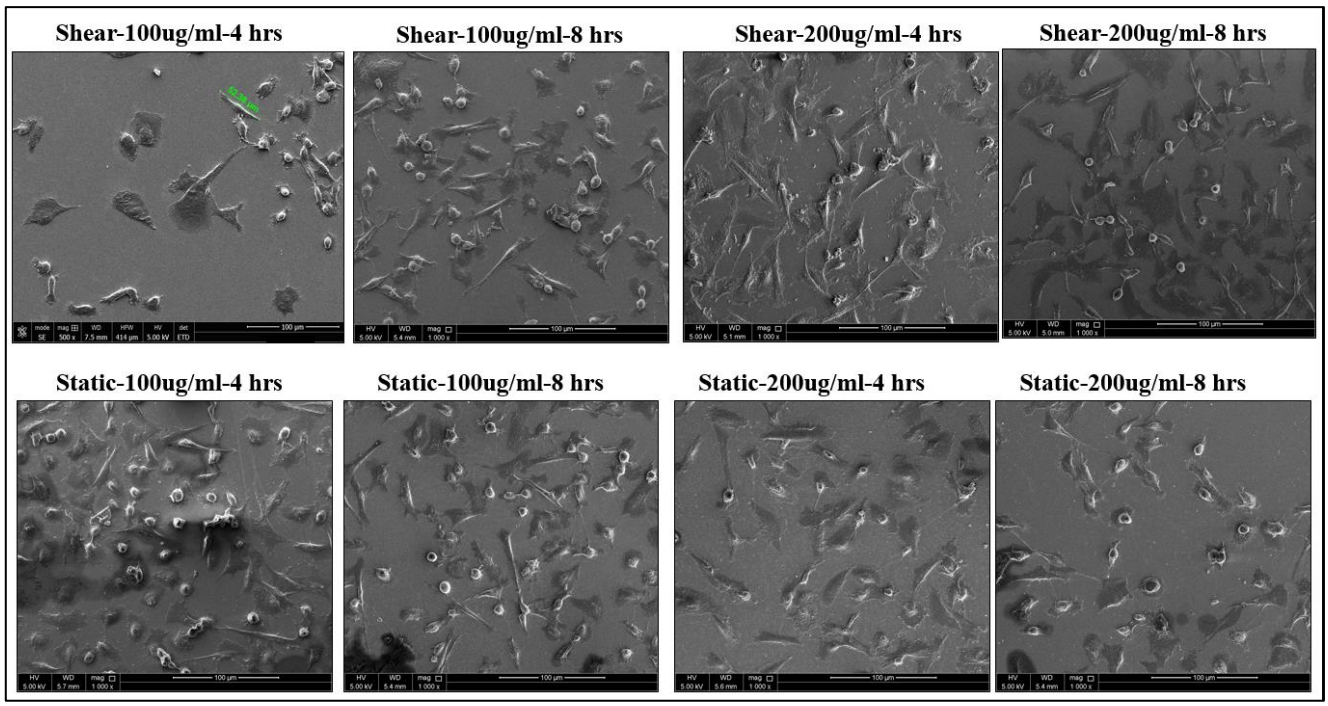

Figure 43:*SEM images for MDA-231 under different conditions*

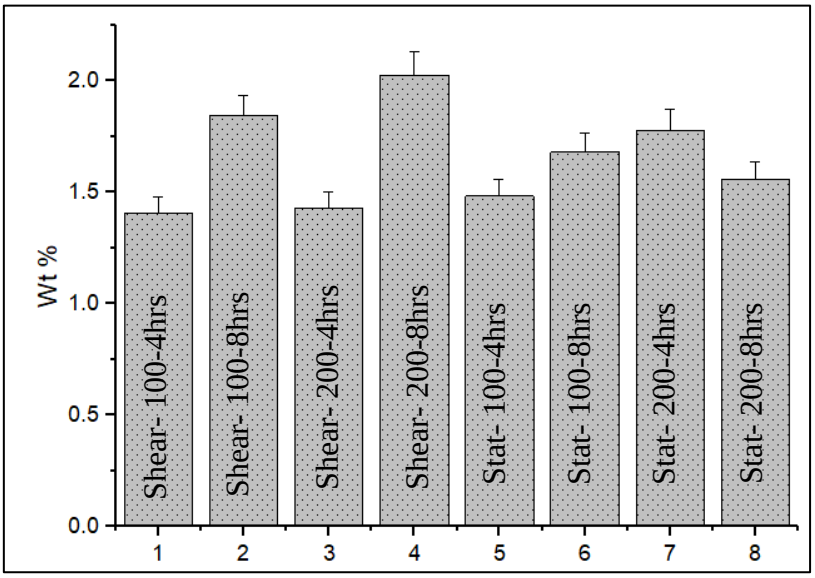

Figure 44:*Bar chart represents wt% for Ti for 8 different cases*

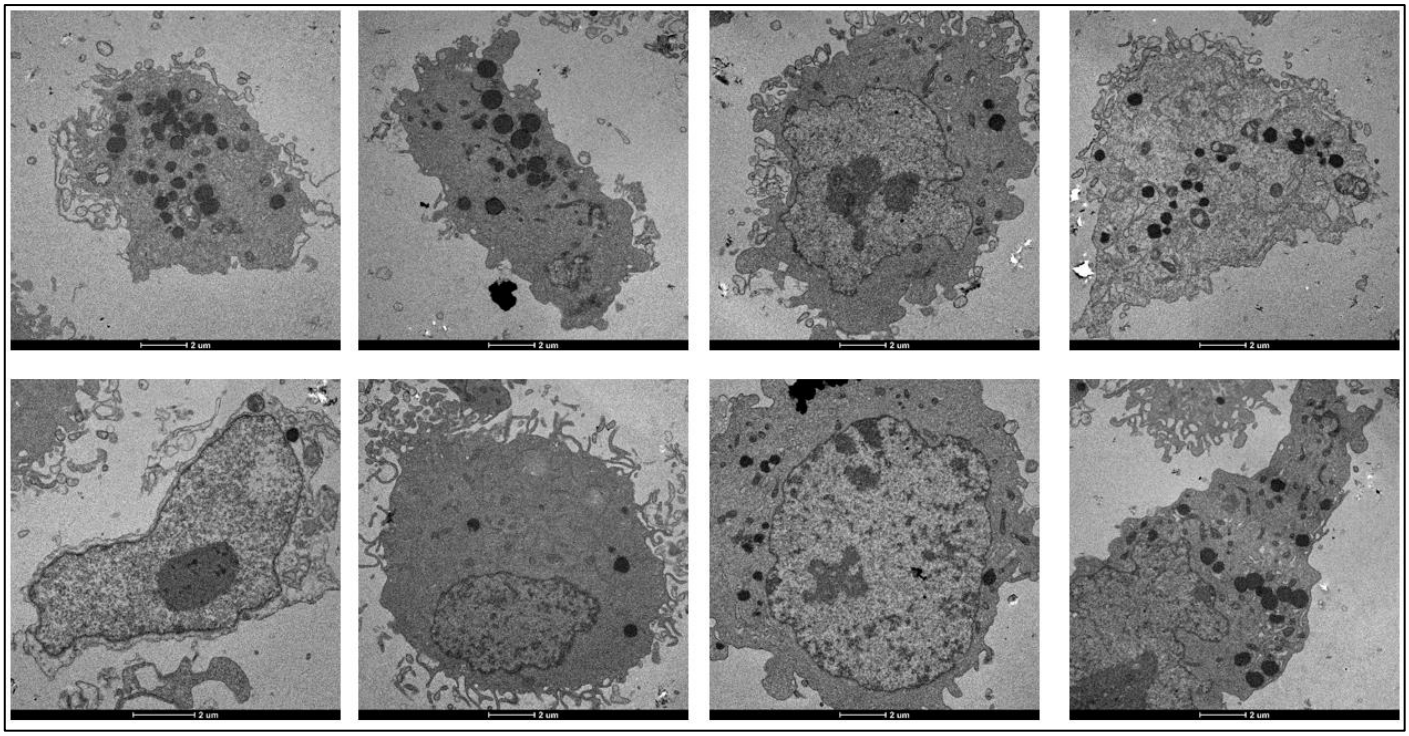

Figure 45: *TEM images for control cells*

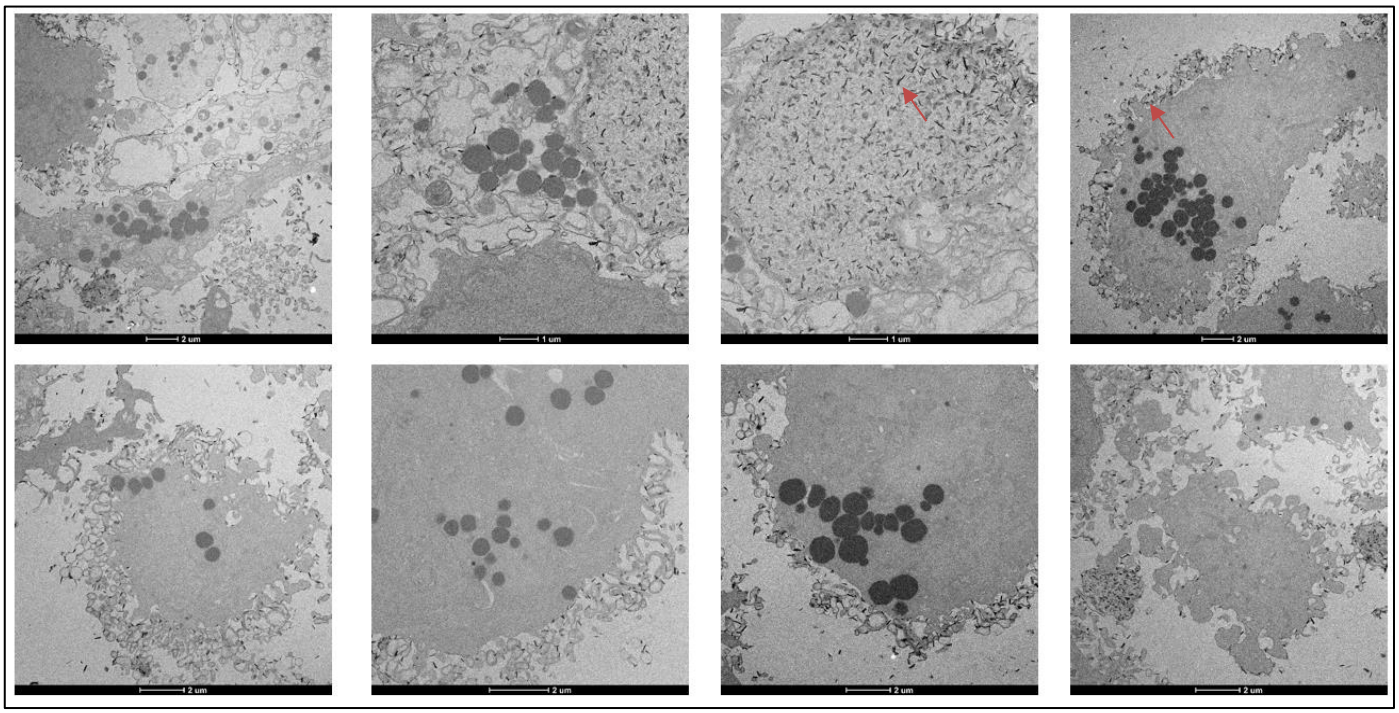

Figure 46: *TEM images for MXene treated cells – Red arrows represent MXene sheets*

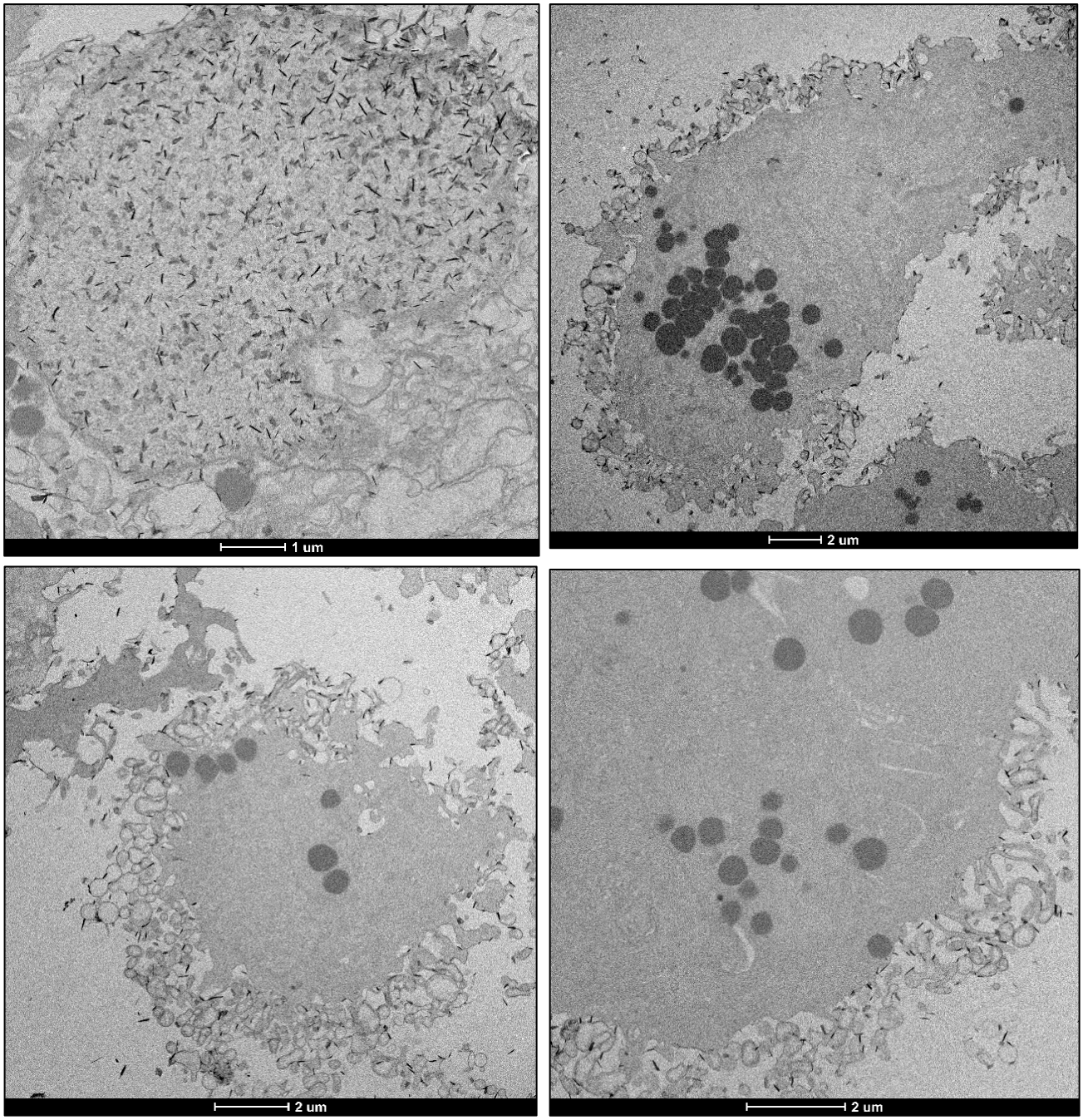

Figure 47: *Zoomed TEM images,the particels are mostly locatde on the cell membrane, only few particels are uptaken by most of the cells.*

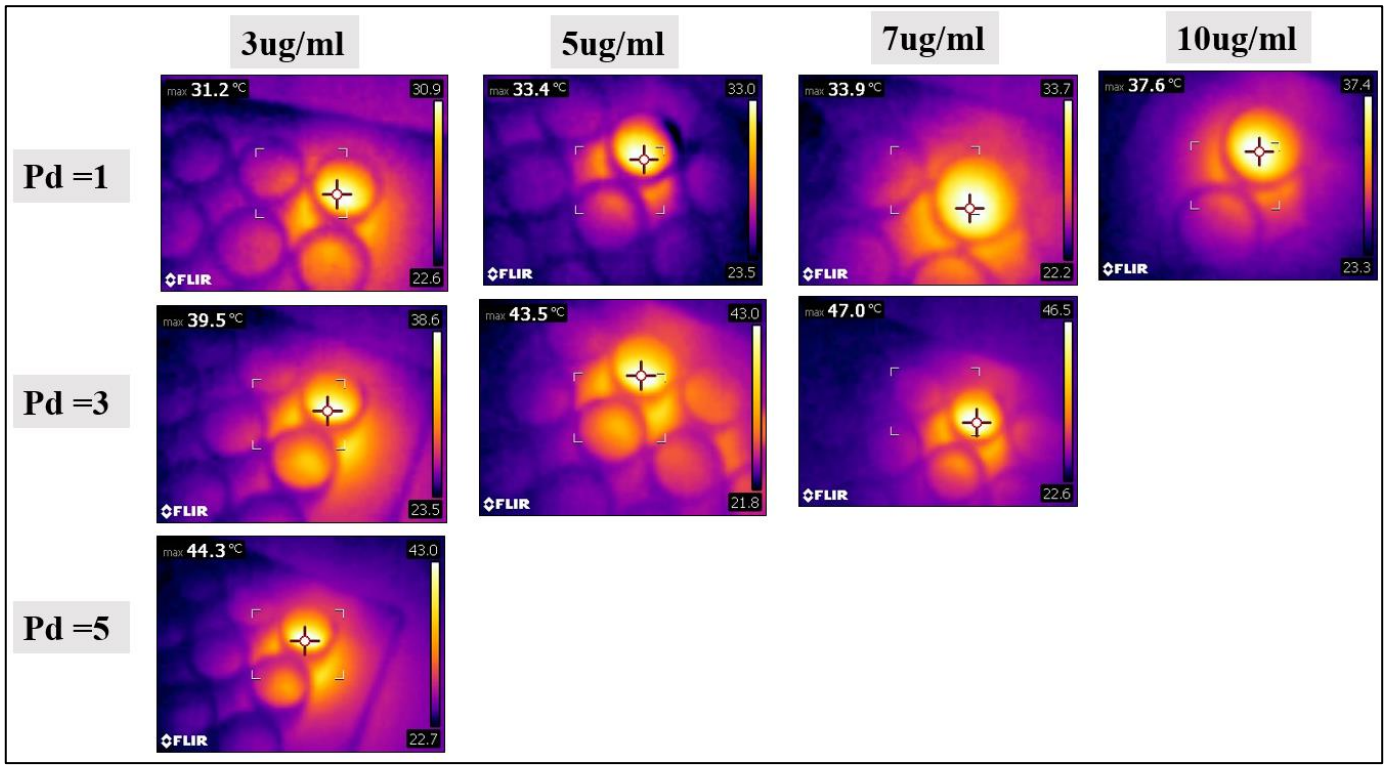

Figure 48: *different dilutions for MXene exposed to different power densities*

Although it was reported in the literature that fluid flow can increase the particle uptake due to formation of cytoskeletal stress fibers and membrane ruffles[124], MXene uptake showed no difference under fluid flow in our experiments. However, stress fibers for the cells exposed to flow were clear when the cytoskeleton was stained (**Figure 49).** This suggests that the uptake, in this case, is not cell or shear stress-related, but particle related.

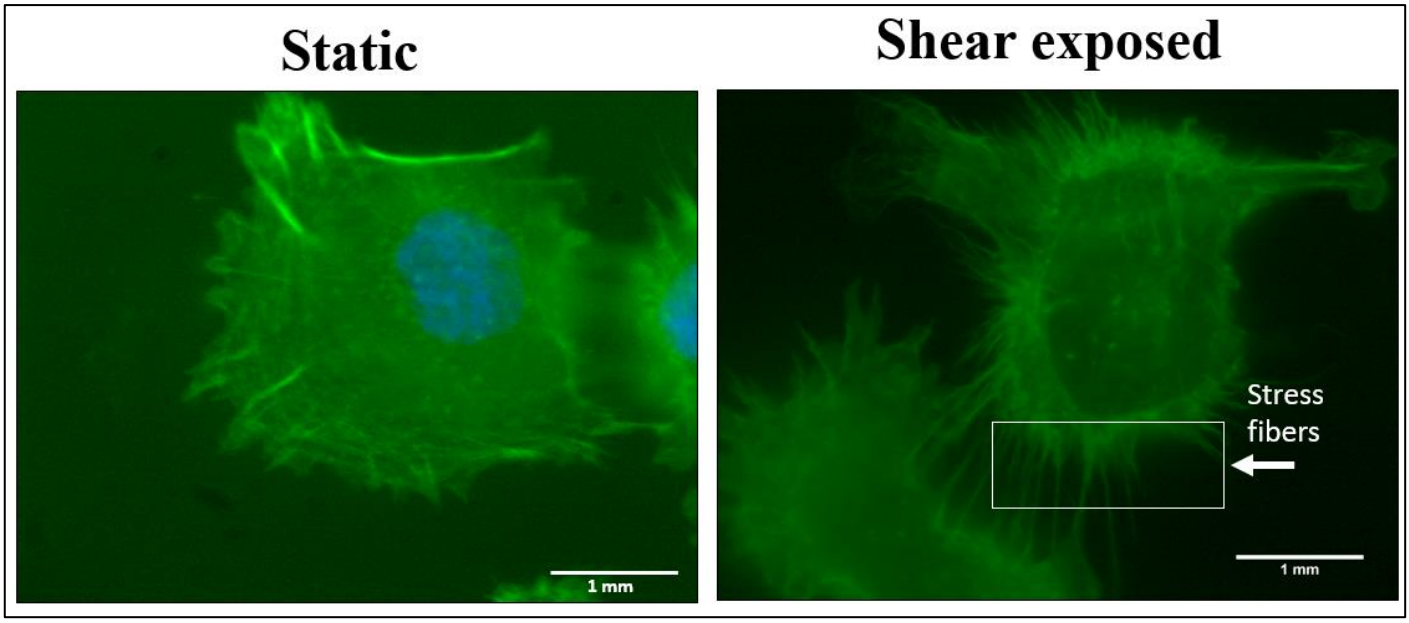

Figure 49: *Cytoskeletal staining for MDA-231 cells under static and fluid flow*

CHAPTER 4

Conclusion

In this work, two 2D materials were prepared: MXene and MXene/Au nanocomposite for photothermal ablation applications. MXene alone showed a good PT efficiency upon laser irradiation whereas, MXene/Au nanocomposite was not as efficient and MXene so it was excluded for further investigation with cells.

Both cellular viability and uptake were determined for MXene and laser exposed cells. Cells under fluid flow were exposed to MXene at different concentrations (100ug/ml and 200ug/ml), durations (4hrs and 8hrs), different laser PDs (1,3 and 5 W/cm^2) and laser exposure durations (5,10 and 15 minutes). None of these conditions showed cell death after MXene treatment and laser exposure, as temperature increment was not sufficient to induce cellular damage. When MXene cellular uptake was assessed, few particles were uptaken with non-homogenous distribution, that some cells could fully internalize the MXene while other cells showed surface association only. Moreover, no difference in cellular uptake was noticed, between static and dynamic culture. This suggests that the cells are unable to uptake the material, probably due to its negatively charged surface that does not form a good electrostatic interaction with the cell's surface that is also negatively charged.

Generally, MXene can be a good candidate for PTT for cancer treatment, but its cellular internalization should be enhanced. This can be achieved by coating the MXene surface and labeling the material with certain ligands that is cancer cell specific.

Future work:

In the future we aim to modify the MXene by either change the cell charge by coating or attach antibodies to its surface that are cancer cell specific. Furthermore, we aim to produce MXene nanocomposites that are absorbance compatible.

REFERENCES

(1) Guimarães, S.; Herlinger, A. L.; Madeira, K. P.; Teixeira, S. F.; Amorim, G. M. Paulo Cilas Morais Lyra Junior ,. **2014**, No. November, 2–36. https://doi.org/10.5772/55282.

(2) Idikio, H. A. Human Cancer Classification : A Systems Biology- Based Model Integrating Morphology , Cancer Stem Cells , Proteomics , and Genomics. **2011**, 107–115.

(3) Radiation, B. C.; Systemic, B. C.; Cancer, B.; Therapy, H.; Targeted, B. C.; Immunotherapy, B. C.; Common, B. C. Treating Breast Cancer. 1–99.

(4) Tohme, S.; Simmons, R. L.; Tsung, A. HHS Public Access. **2018**, *77* (7), 1548–1552. https://doi.org/10.1158/0008-5472.CAN-16-1536.Surgery.

(5) Ou, A.; Louis, H.; Oo, O.; Bi, I.; Pi, A.; Philip, M. Utility of Nanomedicine for Cancer Treatment Nanomedicine & Nanotechnology Utility of Nanomedicine for Cancer Treatment. **2018**, No. March. https://doi.org/10.4172/2157-7439.1000481.

(6) Lin, H.; Chen, Y.; Shi, J. Insights into 2D MXenes for Versatile Biomedical Applications : Current Advances and Challenges Ahead. **2018**, *1800518*. https://doi.org/10.1002/advs.201800518.

(7) Liu, G.; Zou, J.; Tang, Q.; Yang, X.; Zhang, Y. Surface Modified Ti3C2 MXene Nanosheets for Tumor Targeting Photothermal / Photodynamic / Chemo Synergistic Therapy Surface Modified Ti 3 C 2 MXene Nanosheets for Tumor Targeting Photothermal / Photodynamic / Chemo Synergistic Therapy. **2017**. https://doi.org/10.1021/acsami.7b13421.

(8) Liu, Z.; Lin, H.; Zhao, M.; Dai, C.; Zhang, S.; Peng, W.; Chen, Y. T h e r a n o s t i c s 2D Superparamagnetic Tantalum Carbide Composite MXenes for

Efficient Breast-Cancer Theranostics. **2018**, *8* (6). https://doi.org/10.7150/thno.23369.

(9) Xie, Z.; Chen, S.; Liu, Q.; Lin, Z.; Zhao, J.; Fan, T. Biocompatible Two-Dimensional Titanium Nanosheets for Efficient Plasmonic Photothermal Cancer Therapy.

(10) Shen, Z.; Yu, L.; Wei, M.; Ye, H.; Shen, Z.; Yu, L.; Wei, M.; Li, Y. Manipulating Nanoparticle Transport within Blood Flow through External Forces : An Exemplar of Mechanics in Nanomedicine. **2018**.

(11) Ferlin, K. M.; Prendergast, M. E.; Miller, M. L.; Nguyen, B. B.; Kaplan, D. S.; Fisher, J. P. Development of a Dynamic Stem Cell Culture Platform for Mesenchymal Stem Cell Adhesion and Evaluation. **2014**. https://doi.org/10.1021/mp500062n.

(12) Sheng, W.; Seare, W. J.; Almutairi, A. Review of the Progress toward Achieving Heat Confinement — the Holy Grail of Photothermal Therapy Confinement — the Holy Grail of Photothermal Therapy. **2017**, *22* (8). https://doi.org/10.1117/1.JBO.22.8.080901.

(13) Kang, T.; Park, C. Investigation of Biomimetic Shear Stress on Cellular Uptake and Mechanism of Polystyrene Nanoparticles in Various Cancer Cell Lines. *Arch. Pharm. Res.* **2016**, *39* (12), 1663–1670. https://doi.org/10.1007/s12272-016-0847-0.

(14) Mauro, M. Di; Esposito, S.; Naddeo, A. When Physics Meets Biology : A Less Known Feynman. **2011**, *1962* (December 1969).

(15) Conde, J. The Golden Age in Cancer Nanobiotechnology : Quo Vadis ? **2015**, *3* (September 2015), 1–4. https://doi.org/10.3389/fbioe.2015.00142.

(16) Bawa, R. *Handbook of Research on Biomedical Engineering Education and*

Advanced Bioengineering Learning : Interdisciplinary Concepts; 2017. https://doi.org/10.4018/978-1-4666-5125-8.ch003.

(17) Athulya, K.; Anitha, T. Recent Advances in Nano Biotechnology : A Review. **2017**, *2* (3), 15–17.

(18) Das, S.; Mitra, S.; Khurana, S. M. P.; Debnath, N. Frontiers in Life Science Nanomaterials for Biomedical Applications. **2014**, *3769* (2013). https://doi.org/10.1080/21553769.2013.869510.

(19) Hejmadi, M. *Download Free Books At*; 2010.

(20) Sudhakar, A. History of Cancer, Ancient and Modern Treatment Methods. **2009**, *1* (c). https://doi.org/10.4172/1948-5956.100000e2.

(21) Release, P. Latest Global Cancer Data : Cancer Burden Rises to 18 . 1 Million New Cases and 9 . 6 Million Cancer Deaths in 2018 Latest Global Cancer Data : Cancer Burden Rises to 18 . 1 Million New Cases and 9 . 6 Million Cancer Deaths in 2018. **2018**, No. September, 13–15.

(22) Profile, C. M.; Trends, A. C. M.; Incidence, C. Qatar. **2014**, 2–3.

(23) Jain, A.; Jain, A.; Gulbake, A.; Hurkat, P.; Jain, S. K. Solid Tumors : A Review. **2011**, No. May 2014.

(24) Lambert, A. W.; Pattabiraman, D. R.; Weinberg, R. A. Review Emerging Biological Principles of Metastasis. *Cell* **2016**, *168* (4), 670–691. https://doi.org/10.1016/j.cell.2016.11.037.

(25) Urruticoechea, A.; Alemany, R.; Balart, J.; Villanueva, A.; Viñals, F.; Capellá, G. Recent Advances in Cancer Therapy : An Overview. **2010**, 3–10.

(26) Alam, A.; Farooq, U.; Singh, R.; Dubey, V. P.; Kumar, S.; Kumari, R.; Kumar, K. Chemotherapy Treatment and Strategy Schemes : A Review. **2018**, *2* (5). https://doi.org/10.19080/OAJT.2018.02.555600.

(27) American, T.; Society, C. What Is Radiation Therapy ? When Is It Used ? How Does Radiation Therapy Work ?

(28) Maria, G.; Calixto, F.; Bernegossi, J.; Freitas, L. M. De. Nanotechnology-Based Drug Delivery Systems for Photodynamic Therapy of Cancer : A Review. **2016**, No. March. https://doi.org/10.3390/molecules21030342.

(29) Jaque, D.; Maestro, L. M.; Rosal, B. Del. Nanoscale Nanoparticles for Photothermal Therapies. **2014**, No. July. https://doi.org/10.1039/C4NR00708E.

(30) Manuscript, A. NIH Public Access. **2012**, *20* (2), 229–235. https://doi.org/10.1016/j.soc.2010.11.001.The.

(31) Habash, R. W. Y.; Bansal, R.; Krewski, D.; Alhafid, H. T. Thermal Therapy , Part 1 : An Introduction to Thermal Therapy. **2006**, *34* (6), 459–489.

(32) Estelrich, J.; Ant, M. Iron Oxide Nanoparticles in Photothermal Therapy. **2018**. https://doi.org/10.3390/molecules23071567.

(33) Graham, E. G.; Macneill, C. M. REVIEW OF METAL , CARBON AND POLYMER NANOPARTICLES FOR INFRARED PHOTOTHERMAL THERAPY. **2013**, *3* (3), 1–29. https://doi.org/10.1142/S1793984413300021.

(34) Rosal, B.; Haro-gonzalez, P.; Benayas, A. Nanoparticles for Photothermal Therapies. **2014**, 9494–9530. https://doi.org/10.1039/C4NR00708E.

(35) Petryayeva, E.; Krull, U. J. Analytica Chimica Acta Localized Surface Plasmon Resonance : Nanostructures , Bioassays and Biosensing — A Review. *Anal. Chim. Acta* **2011**, *706* (1), 8–24. https://doi.org/10.1016/j.aca.2011.08.020.

(36) Alireza Gharatape , Soodabeh Davaran, R. S.; Hamed Hamishehkar. RSC Advances. **2016**. https://doi.org/10.1039/C6RA18760A.

(37) Jin, Y. Engineering Plasmonic Gold Nanostructures and Metamaterials for Biosensing and Nanomedicine. **2012**, 5153–5165.

https://doi.org/10.1002/adma.201200622.

(38) Huang, X.; El-sayed, M. A. Plasmonic Photo-Thermal Therapy (PPTT). *Alexandria J. Med.* **2011**, *47* (1), 1–9. https://doi.org/10.1016/j.ajme.2011.01.001.

(39) Huang, X.; El-sayed, I. H.; Qian, W.; El-sayed, M. A. Cancer Cell Imaging and Photothermal Therapy in the Near-Infrared Region by Using Gold Nanorods. **2006**, No. 3, 2115–2120. https://doi.org/10.1021/ja057254a.

(40) Willets, K. A.; Duyne, R. P. Van. Localized Surface Plasmon Resonance Spectroscopy and Sensing. **2006**, No. October, 267–297. https://doi.org/10.1146/annurev.physchem.58.032806.104607.

(41) Okuno, T.; Kato, S.; Hatakeyama, Y.; Okajima, J.; Maruyama, S. Photothermal Therapy of Tumors in Lymph Nodes Using Gold Nanorods and Near-Infrared Laser Light. *J. Control. Release* **2013**, *172* (3), 879–884. https://doi.org/10.1016/j.jconrel.2013.10.014.

(42) Alhabeb, M.; Maleski, K.; Anasori, B.; Lelyukh, P.; Clark, L.; Sin, S. Guidelines for Synthesis and Processing of Two-Dimensional Titanium Carbide (Ti 3 C 2 T. **2017**. https://doi.org/10.1021/acs.chemmater.7b02847.

(43) Anasori, B.; Lukatskaya, M.; Gogotsi, Y. 2D Metal Carbides and Nitrides (MXenes) for Energy Storage. **2017**, No. January. https://doi.org/10.1038/natrevmats.2016.98.

(44) Li, Z.; Zhang, H.; Han, J.; Chen, Y.; Lin, H.; Yang, T. Surface Nanopore Engineering of 2D MXenes for Targeted and Synergistic Multitherapies of Hepatocellular Carcinoma. **2018**, *1706981*, 1–11. https://doi.org/10.1002/adma.201706981.

(45) Szuplewska, A.; Kalinowska, D.; Dybko, A.; Jastrzębska, A. M.;

Wojciechowski, T.; Chudy, M.; Grabowska-jadach, I. NU SC. *Mater. Sci. Eng. C* **2019**, #pagerange#. https://doi.org/10.1016/j.msec.2019.01.021.

(46) Li, R.; Zhang, L.; Shi, L.; Wang, P. MXene Ti 3 C 2 : An E Ff Ective 2D Light-to-Heat Conversion Material. **2017**. https://doi.org/10.1021/acsnano.6b08415.

(47) Lin, H.; Chen, Y.; Shi, J. Two-Dimensional Ultrathin MXene Ceramic Nanosheets for Photothermal Conversion. **2016**, No. September 2018. https://doi.org/10.1021/acs.nanolett.6b04339.

(48) Lin, H.; Wang, Y.; Gao, S.; Chen, Y.; Shi, J. Theranostic 2D Tantalum Carbide (MXene). **2017**, *1703284*, 1–11. https://doi.org/10.1002/adma.201703284.

(49) Ling, Z.; Ren, C. E.; Zhao, M.; Yang, J.; Giammarco, J. M.; Qiu, J. Flexible and Conductive MXene Films and Nanocomposites with High Capacitance. **2014**, 1–6. https://doi.org/10.1073/pnas.1414215111.

(50) Rakhi, R. B.; Nayak, P.; Xia, C.; Alshareef, H. N. Novel Amperometric Glucose Biosensor Based on MXene Nanocomposite. *Sci. Rep.* **2016**, *6*, 36422.

(51) Ma, X.; Sun, H.; Wang, Y.; Wu, X.; Zhang, J. Nano Energy Electronic and Optical Properties of Strained Noble Metals : Implications for Applications Based on LSPR. *Nano Energy* **2018**, *53* (September), 932–939. https://doi.org/10.1016/j.nanoen.2018.09.042.

(52) Webb, J. A.; Bardhan, R. Emerging Advances in Nanomedicine with Engineered Gold Nanostructures. **2014**. https://doi.org/10.1039/c3nr05112a.

(53) Buchanan, C. F.; Voigt, E.; Vlachos, P. P.; Nichole, M. SBC2013-14592 TISSUE ENGINEERED TUMOR MICROVESSELS TO STUDY THE ROLE OF FLOW. **2017**, 6–7.

(54) Huo, S.; Liu, J.; Wei, T. Superior Penetration and Retention Behavior of 50 Nm Gold Nanoparticles in Tumors. **2012**, No. May 2014.

https://doi.org/10.1158/0008-5472.CAN-12-2071.

(55) Zhao, M.; Liu, Q.; Gong, Y.; Xu, X.; Zhang, C.; Liu, X.; Zhang, C.; Guo, H.; Zhang, X.; Gong, Y.; et al. GSH-Dependent Antioxidant Defense Contributes to the Acclimation of Colon Cancer Cells to Acidic Microenvironment. *Cell Cycle* **2016**, *15* (8), 1125–1133. https://doi.org/10.1080/15384101.2016.1158374.

(56) Kang, T.; Park, C.; Choi, J.; Cui, J.; Lee, B. Journal of Drug Delivery Science and Technology Effects of Shear Stress on the Cellular Distribution of Polystyrene Nanoparticles in a Biomimetic Micro Fl Uidic System. *J. Drug Deliv. Sci. Technol.* **2016**, *31*, 130–136. https://doi.org/10.1016/j.jddst.2015.12.001.

(57) Huang, Q.; Hu, X.; He, W.; Zhao, Y.; Hao, S.; Wu, Q.; Li, S.; Zhang, S. Fluid Shear Stress and Tumor Metastasis. **2018**, *8* (5), 763–777.

(58) Hyler, A. R.; Baudoin, N. C.; Brown, M. S.; Stremler, M. A.; Cimini, D.; Davalos, R. V; Schmelz, E. M. Fluid Shear Stress Impacts Ovarian Cancer Cell Viability , Subcellular Organization , and Promotes Genomic Instability. **2018**, 1–21.

(59) Labelle, M.; Hynes, R. O. Dissemination. **2013**, *2* (12), 1091–1099. https://doi.org/10.1158/2159-8290.CD-12-0329.The.

(60) Krog, B. L.; Henry, M. D. Biomechanics of the Circulating Tumor Cell Microenvironment. **2018**.

(61) Michor, F.; Liphardt, J.; Ferrari, M.; Widom, J. What Does Physics Have to Do with Cancer ? *Nat. Publ. Gr.* **2011**, *11* (9), 657–670. https://doi.org/10.1038/nrc3092.

(62) Fan, R.; Emery, T.; Zhang, Y.; Xia, Y.; Sun, J.; Wan, J. Circulatory Shear Flow Alters the Viability and Proliferation of Circulating Colon Cancer Cells. *Nat.*

Publ. Gr. **2016**, No. February, 1–8. https://doi.org/10.1038/srep27073.

(63) Lee, H. J.; Diaz, M. F.; Price, K. M.; Ozuna, J. A.; Zhang, S.; Sevick-muraca, E. M.; Hagan, J. P.; Wenzel, P. L. Fluid Shear Stress Activates YAP1 to Promote Cancer Cell Motility. **2017**. https://doi.org/10.1038/ncomms14122.

(64) Munson, J. M.; Shieh, A. C. Interstitial Fluid Flow in Cancer : Implications for Disease Progression and Treatment. **2014**, 317–328.

(65) Yao, W.; Li, Y.; Ding, G. Interstitial Fluid Flow : The Mechanical Environment of Cells and Foundation of Meridians. **2012**, *2012*. https://doi.org/10.1155/2012/853516.

(66) Rutkowski, J. M.; Swartz, M. A. A Driving Force for Change : Interstitial Flow as a Morphoregulator. **2006**, *17* (1). https://doi.org/10.1016/j.tcb.2006.11.007.

(67) Fede, C.; Albertin, G.; Petrelli, L.; Caro, R. De. Influence of Shear Stress and Size on Viability of Endothelial Cells Exposed to Gold Nanoparticles. **2017**. https://doi.org/10.1007/s11051-017-3993-5.

(68) Mahto, S. K.; Charwat, V.; Ertl, P.; Rothen-rutishauser, B.; Rhee, S. W. Microfluidic Platforms for Advanced Risk Assessments of Nanomaterials. **2014**, *5390*, 1–15. https://doi.org/10.3109/17435390.2014.940402.

(69) Wang, Y. X.; Xiang, C.; Liu, B.; Zhu, Y.; Luan, Y.; Liu, S. T.; Qin, K. R. A Multi - Component Parallel - Plate Flow Chamber System for Studying the Effect of Exercise - Induced Wall Shear Stress on Endothelial Cells. *Biomed. Eng. Online* **2016**, *15* (s2), 659–672. https://doi.org/10.1186/s12938-016-0273-z.

(70) Han, J.; Shuvaev, V. V; Davies, P. F.; Eckmann, D. M.; Muro, S.; Muzykantov, V. R. Flow Shear Stress Differentially Regulates Endothelial Uptake of Nanocarriers Targeted to Distinct Epitopes of PECAM-1. *J. Control. Release*

2015, *210*, 39–47. https://doi.org/10.1016/j.jconrel.2015.05.006.

(71) Rinkenauer, A. C.; Press, A. T.; Raasch, M.; Pietsch, C.; Schweizer, S.; Schwörer, S.; Rudolph, K. L.; Mosig, A.; Bauer, M.; Traeger, A.; et al. Comparison of the Uptake of Methacrylate-Based Nanoparticles in Static and Dynamic in Vitro Systems as Well as in Vivo. *J. Control. Release* **2015**, *216*, 158–168. https://doi.org/10.1016/j.jconrel.2015.08.008.

(72) Development_of_a_Parallel_Plate_Flow_Chamber_for.11.Pdf.

(73) Lane, W. O.; Jantzen, A. E.; Carlon, T. A.; Jamiolkowski, R. M.; Grenet, J. E.; Ley, M. M.; Haseltine, J. M.; Galinat, J.; Lin, F.; Allen, J. D.; et al. Parallel-Plate Flow Chamber and Continuous Flow Circuit to Evaluate Endothelial Progenitor Cells under Laminar Flow Shear Stress. **2012**, No. January, 1–11. https://doi.org/10.3791/3349.

(74) Björnmalm, M.; Yan, Y.; Caruso, F. Engineering and Evaluating Drug Delivery Particles in Microfluidic Devices. *J. Control. Release* **2014**. https://doi.org/10.1016/j.jconrel.2014.04.030.

(75) Mahto, S. K.; Yoon, T. H.; Rhee, S. W. A New Perspective on in Vitro Assessment Method for Evaluating Quantum Dot Toxicity by Using Microfluidics. **2010**, 1–8. https://doi.org/10.1063/1.3486610.

(76) Huefner, A.; Septiadi, D.; Wilts, B. D.; Patel, I. I.; Kuan, W.; Fragniere, A.; Barker, R. A.; Mahajan, S. Gold Nanoparticles Explore Cells : Cellular Uptake and Their Use as Intracellular Probes. *Methods* **2014**, *68* (2), 354–363. https://doi.org/10.1016/j.ymeth.2014.02.006.

(77) Salatin, S.; Yari Khosroushahi, A. Overviews on the Cellular Uptake Mechanism of Polysaccharide Colloidal Nanoparticles. *J. Cell. Mol. Med.* **2017**, *21* (9), 1668–1686. https://doi.org/10.1111/jcmm.13110.

(78) Ek, P. K.; Jansman, M. M. T.; Wohl, B. M. Interaction between Drug Delivery Vehicles and Cells under the Effect of Shear Stress. **2015**, *052605*, 1–19. https://doi.org/10.1063/1.4923324.

(79) Forest, V.; Cottier, M.; Pourchez, J. Electrostatic Interactions Favor the Binding of Positive Nanoparticles on Cells : A Reductive Theory. *Nano Today* **2015**, *10* (6), 677–680. https://doi.org/10.1016/j.nantod.2015.07.002.

(80) Geng, Y. A. N.; Dalhaimer, P.; Cai, S.; Tsai, R.; Minko, T.; Discher, D. E. NIH Public Access. **2009**, *2* (4), 249–255. https://doi.org/10.1038/nnano.2007.70.Shape.

(81) Chachisvilis, M.; Zhang, Y.-L.; Frangos, J. A. G Protein-Coupled Receptors Sense Fluid Shear Stress in Endothelial Cells. *Proc. Natl. Acad. Sci.* **2006**, *103* (42), 15463–15468. https://doi.org/10.1073/pnas.0607224103.

(82) Holme, M. N.; Fedotenko, I. A.; Abegg, D.; Althaus, J.; Babel, L.; Favarger, F.; Reiter, R.; Tanasescu, R.; Zaffalon, P.-L.; Ziegler, A.; et al. Shear-Stress Sensitive Lenticular Vesicles for Targeted Drug Delivery. *Nat. Nanotechnol.* **2012**, *7*, 536.

(83) Korin, N.; Kanapathipillai, M.; Matthews, B. D.; Crescente, M.; Brill, A.; Mammoto, T.; Ghosh, K.; Jurek, S.; Bencherif, S. A.; Bhatta, D.; et al. Shear-Activated Nanotherapeutics for Drug Targeting to Obstructed Blood Vessels. *Science (80-.).* **2012**, *337* (6095), 738–742. https://doi.org/10.1126/science.1217815.

(84) Kim, D.; Lin, Y.; Haynes, C. L. On-Chip Evaluation of Shear Stress Effect on Cytotoxicity of Mesoporous Silica Nanoparticles. **2011**, 8377–8382.

(85) Han, J.; Zern, B. J.; Shuvaev, V. V; Davies, P. F.; Muro, S.; Muzykantov, V. Acute and Chronic Shear Stress Differently Regulate Endothelial Internalization

of Nanocarriers Targeted to Platelet-Endothelial Cell Adhesion Molecule-1. *ACS Nano* **2012**, *6* (10), 8824–8836. https://doi.org/10.1021/nn302687n.

(86) Samuel, S. P.; Jain, N.; Dowd, F. O.; Paul, T.; Gerard, V. A.; Gun, Y. K.; Prina-mello, A. Multifactorial Determinants That Govern Nanoparticle Uptake by Human Endothelial Cells under Flow. **2012**, 2943–2956.

(87) Hosta-Rigau, L.; Städler, B. Shear Stress and Its Effect on the Interaction of Myoblast Cells with Nanosized Drug Delivery Vehicles. *Mol. Pharm.* **2013**, *10* (7), 2707–2712. https://doi.org/10.1021/mp4001298.

(88) Teo, B. M.; van der Westen, R.; Hosta-Rigau, L.; Städler, B. Cell Response to PEGylated Poly(Dopamine) Coated Liposomes Considering Shear Stress. *Biochim. Biophys. Acta - Gen. Subj.* **2013**, *1830* (10), 4838–4847. https://doi.org/https://doi.org/10.1016/j.bbagen.2013.06.022.

(89) Kona, S.; Dong, J.-F.; Liu, Y.; Tan, J.; Nguyen, K. T. Biodegradable Nanoparticles Mimicking Platelet Binding as a Targeted and Controlled Drug Delivery System. *Int. J. Pharm.* **2012**, *423* (2), 516–524. https://doi.org/https://doi.org/10.1016/j.ijpharm.2011.11.043.

(90) Blackwell, J. E.; Dagia, N. M.; Dickerson, J. B.; Berg, E. L.; Goetz, D. J. Ligand Coated Nanosphere Adhesion to E- and P-Selectin under Static and Flow Conditions. *Ann. Biomed. Eng.* **2001**, *29* (6), 523–533. https://doi.org/10.1114/1.1376697.

(91) Lin, A.; Sabnis, A.; Kona, S.; Nattama, S.; Patel, H.; Dong, J.; Nguyen, K. T.; Al, L. I. N. E. T. Shear-Regulated Uptake of Nanoparticles by Endothelial Cells and Development of Endothelial-Targeting Nanoparticles. *J. Biomed. Mater. Res. Part A* **2009**, *93* (3), 833–842. https://doi.org/10.1002/jbm.a.32592.

(92) Klingberg, H.; Oddershede, L. B. The in Fl Uence of Fl Ow, Shear Stress and

Adhesion Molecule Targeting on Gold Nanoparticle Uptake in Human Endothelial Cells †. **2015**. https://doi.org/10.1039/c5nr01467k.

(93) Yazdimamaghani, Barber, Moghaddam, and G. In Fl Uence of Silica Nanoparticle Density and Flow Conditions on Sedimentation, Cell Uptake, and Cytotoxicity. **2018**. https://doi.org/10.1021/acs.molpharmaceut.8b00213.

(94) Jurney, P.; Agarwal, R.; Singh, V.; Choi, D.; Roy, K.; Sreenivasan, S. V; Shi, L. Unique Size and Shape-Dependent Uptake Behaviors of Non-Spherical Nanoparticles by Endothelial Cells Due to a Shearing Fl Ow. *J. Control. Release* **2017**, *245*, 170–176. https://doi.org/10.1016/j.jconrel.2016.11.033.

(95) Palchetti, S.; Pozzi, D.; Laura, A.; La, G.; Zenezini, R.; Digiacomo, L.; Peruzzi, G.; Caracciolo, G.; Laganà, A. Colloids and Surfaces B : Biointerfaces Influence of Dynamic Flow Environment on Nanoparticle-Protein Corona : From Protein Patterns to Uptake in Cancer Cells. *Colloids Surfaces B Biointerfaces* **2017**, *153*, 263–271. https://doi.org/10.1016/j.colsurfb.2017.02.037.

(96) Berdiyorov, G. R. Optical Properties of Functionalized Ti3C2T2 (T = F , O , OH) MXene : First-Principles Calculations. **2016**, *2* (May). https://doi.org/10.1063/1.4948799.

(97) Lynn, D. E. *Cell Culture*, Second Edition.; Elsevier Inc., 1972. https://doi.org/10.1016/B978-0-12-374144-8.00048-5.

(98) CELL CULTURE BASICS Handbook.

(99) Mda-mb-, T.; Triple-negative, A. Cell Line Profile MDA-MB-231 (ECACC Catalogue No . 92020424). *231* (92020424), 6–8.

(100) Sheet, P. Mda-mb-231 (Atcc ® Htb- 26 ™). 3–5.

(101) Press, D. The Effect of Nanoparticle Uptake on Cellular Behavior : Disrupting or Enabling Functions ? **2012**, 87–100.

(102) Alhabeb, M.; Maleski, K.; Anasori, B.; Lelyukh, P.; Clark, L.; Sin, S. Guidelines for Synthesis and Processing of Two-Dimensional Titanium Carbide (Ti3C2Tx MXene). **2017**. https://doi.org/10.1021/acs.chemmater.7b02847.

(103) Tang, Y.; Yang, C.; Que, W. A Novel Two-Dimensional Accordion-like Titanium Carbide (MXene) for Adsorption of Cr (VI) from Aqueous Solution. **2018**, *8* (5), 1–5. https://doi.org/10.1142/S2010135X18500352.

(104) Lin, H.; Gao, S.; Dai, C.; Chen, Y.; Shi, J. A Two-Dimensional Biodegradable Niobium Carbide (MXene) for Photothermal Tumor Eradication in NIR - I and NIR-II Biowindows. **2017**, 16235–16247. https://doi.org/10.1021/jacs.7b07818.

(105) Li, J.; Gu, M.; Member, S. Gold-Nanoparticle-Enhanced Cancer Photothermal Therapy. **2010**, *16* (4), 989–996.

(106) Naguib, M.; Kurtoglu, M.; Presser, V.; Lu, J.; Niu, J.; Heon, M.; Hultman, L.; Gogotsi, Y.; Barsoum, M. W. Two-Dimensional Nanocrystals Produced by Exfoliation of Ti 3 AlC 2. **2011**, 4248–4253. https://doi.org/10.1002/adma.201102306.

(107) C, T. R. Chemical Stability of Ti 3 C 2 MXene with Al in The. **2018**, 1–9. https://doi.org/10.3390/ma11101979.

(108) Tian, W.; Vahidmohammadi, A.; Hamedi, M. M. Layer-by-Layer Self-Assembly of Pillared Two-Dimensional Multilayers. *Nat. Commun.* No. 2019, 1–10. https://doi.org/10.1038/s41467-019-10631-0.

(109) Zagho, M. M.; Rizeq, B. R.; Pintus, G.; Mahmoud, K. A.; Nasrallah, G. K.; Elzatahry, A. A. Plasmonic MXene-Based Nanocomposites Exhibiting Photothermal Therapeutic Effects with Lower Acute Toxicity than Pure MXene. **2019**.

(110) Biotechnol, A. M. Comparison of the Optimal Culture Conditions for Cell

Growth and Tissue Plasminogen Activator Production by Human Embryo Lung Cells on Microcarriers. **1994**, 565–570.

(111) Xie, X.; Shao, X.; Gao, F.; Jin, H.; Zhou, J.; Du, L.; Zhang, Y.; Ouyang, W.; Wang, X.; Zhao, L.; et al. Effect of Hyperthermia on Invasion Ability and TGF-ß 1 Expression of Breast Carcinoma MCF-7 Cells. **2011**, No. 10, 1573–1579. https://doi.org/10.3892/or.2011.1240.

(112) Doughty, A. C. V; Hoover, A. R.; Layton, E.; Murray, C. K.; Howard, E. W.; Chen, W. R. Nanomaterial Applications in Photothermal Therapy for Cancer. **2019**. https://doi.org/10.3390/ma12050779.

(113) Nagashima, K.; Takagi, R. Effect of Local Hyperthermia on Metastases in Oral Squamous Cell Carcinoma. **2002**, 84–89. https://doi.org/10.1054/ijom.2001.0176.

(114) Shannahan, J. H.; Lai, X.; Ke, P. C.; Podila, R.; Brown, J. M.; Witzmann, F. A. Silver Nanoparticle Protein Corona Composition in Cell Culture Media. **2013**, *8* (9). https://doi.org/10.1371/journal.pone.0074001.

(115) Abdelkhaliq, A.; Zande, M. Van Der; Punt, A.; Helsdingen, R.; Boeren, S. Impact of Nanoparticle Surface Functionalization on the Protein Corona and Cellular Adhesion , Uptake and Transport. *J. Nanobiotechnology* **2018**, 1–13. https://doi.org/10.1186/s12951-018-0394-6.

(116) Lee, B. Protein Corona : A New Approach for Nanomedicine Design. **2017**, 3137–3151.

(117) Mustafa, T.; Watanabe, F.; Monroe, W.; Mahmood, M.; Xu, Y.; Saeed, L. M.; Karmakar, A. Impact of Gold Nanoparticle Concentration on Their Cellular Uptake by MC3T3-E1 Mouse Osteoblastic Cells as Analyzed by Transmission Electron Microscopy Nanomedicine & Nanotechnology. **2011**, *2* (6).

https://doi.org/10.4172/2157-7439.1000118.

(118) Safi, M.; Domitrovic, T.; Kapur, A.; Aldeek, F.; Johnson, J. E.; Mattoussi, H. Intracellular Delivery of Luminescent Quantum Dots Mediated by a Virus-Derived Lytic Peptide Intracellular Delivery of Luminescent Quantum Dots Mediated by a Virus- Derived Lytic Peptide * Correspondence Author : **2016**. https://doi.org/10.1021/acs.bioconjchem.6b00609.

(119) Lepock, J. R. How Do Cells Respond to Their Thermal Environment ? **2011**, *6736* (May). https://doi.org/10.1080/02656730500307298.

(120) Fröhlich, E. The Role of Surface Charge in Cellular Uptake and Cytotoxicity of Medical Nanoparticles. **2012**, 5577–5591.

(121) Foroozandeh, P.; Aziz, A. A. Insight into Cellular Uptake and Intracellular Trafficking of Nanoparticles. **2018**, *6*.

(122) Toit, L. C. Parameters and Characteristics Governing Cellular Internalization and Trans-Barrier Trafficking of Nanostructures. **2015**, 2191–2206.

(123) Zhang, S.; Gao, H.; Bao, G. Physical Principles of Nanoparticle Cellular Endocytosis. **2017**, *9* (9), 8655–8671. https://doi.org/10.1021/acsnano.5b03184.Physical.

(124) Ispanixtlahuatl-meráz, O.; Schins, R. P. F.; Chirino, Y. I. Environmental Science Nano Cell Type Specific Cytoskeleton Disruption Induced by Engineered Nanoparticles. *Environ. Sci. Nano* **2017**. https://doi.org/10.1039/C7EN00704C.